Modular Skeletal Evolution in Sticklebacks Is Controlled by Additive and Clustered Quantitative Trait Loci

Craig T. Miller,*,†,1,2 Andrew M. Glazer,*,1 Brian R. Summers,† Benjamin K. Blackman,†,3 Andrew R. Norman,†,4 Michael D. Shapiro,†,5 Bonnie L. Cole,†,6 Catherine L. Peichel,†,7 Dolph Schluter,‡ and David M. Kingsley†,2

*Molecular and Cell Biology Department, University of California, Berkeley, California 94720, †Department of Developmental Biology and Howard Hughes Medical Institute, Stanford University, Stanford, California 94305, and ‡Department of Zoology, University of British Columbia, Vancouver, British Columbia V6T 1Z4, Canada

ABSTRACT Understanding the genetic architecture of evolutionary change remains a long-standing goal in biology. In vertebrates, skeletal evolution has contributed greatly to adaptation in body form and function in response to changing ecological variables like diet and predation. Here we use genome-wide linkage mapping in threespine stickleback fish to investigate the genetic architecture of evolved changes in many armor and trophic traits. We identify >100 quantitative trait loci (QTL) controlling the pattern of serially repeating skeletal elements, including gill rakers, teeth, branchial bones, jaws, median fin spines, and vertebrae. We use this large collection of QTL to address long-standing questions about the anatomical specificity, genetic dominance, and genomic clustering of loci controlling skeletal differences in evolving populations. We find that most QTL (76%) that influence serially repeating skeletal elements have anatomically regional effects. In addition, most QTL (71%) have at least partially additive effects, regardless of whether the QTL controls evolved loss or gain of skeletal elements. Finally, many QTL with high LOD scores cluster on chromosomes 4, 20, and 21. These results identify a modular system that can control highly specific aspects of skeletal form. Because of the general additivity and genomic clustering of major QTL, concerted changes in both protective armor and trophic traits may occur when sticklebacks inherit either marine or freshwater alleles at linked or possible "supergene" regions of the stickleback genome. Further study of these regions will help identify the molecular basis of both modular and coordinated changes in the vertebrate skeleton.

UNDERSTANDING the quantitative genetic architecture underlying evolutionary change in nature remains a major goal in genetics. The past two decades have seen a rapid increase in experimental data from various model systems, generating vigorous debate over the relative importance of coding *vs.* regulatory alleles, the prevalence of pleiotropy, and the role of large-effect mutations during adaptation to new environments (Stern and Orgogozo 2008; Streisfeld and Rausher 2011; Rockman 2012).

One particularly interesting genetic architecture found in several natural systems is close linkage of loci controlling multiple, often coadaptive, phenotypes. Such trait clusters, sometimes called "supergenes," have been observed in primroses (Darwin 1877; Mather 1950; Li *et al.* 2011), butterflies (Clarke *et al.* 1968; Mallet 1989; Joron *et al.* 2006), snails (Murray and Clarke 1976), and fish (Winge 1927; Protas *et al.* 2008; Roberts *et al.* 2009; Tripathi *et al.* 2009). Trait clusters could result from recombination suppression (Noor *et al.* 2001), for example through chromosomal inversions (Lowry and Willis 2010; Joron *et al.* 2011; Fishman *et al.* 2013). Alternatively, trait clusters could result from tightly linked loci or pleiotropic effects of individual genes (Mallet 1989; Studer and Doebley 2011). Having

doi: 10.1534/genetics.114.162420
Manuscript received January 31, 2014; accepted for publication February 22, 2014; published Early Online March 19, 2014.
Supporting information is available online at http://www.genetics.org/lookup/suppl/doi:10.1534/genetics.114.162420/-/DC1.
[1]These authors contributed equally to this work.
[2]Corresponding authors: Department of Molecular and Cell Biology, 142 Life Sciences Addition, University of California, Berkeley, CA 94720. E-mail: ctmiller@berkeley.edu; and Department of Developmental Biology, 279 Campus Dr., Howard Hughes Medical Institute and Stanford University School of Medicine, Stanford, CA 94305. E-mail: kingsley@stanford.edu
[3]Present address: Department of Biology, University of Virginia, Charlottesville, VA 22904.
[4]Present address: Department of Biochemistry, University of California, San Francisco, CA 94158.
[5]Present address: Department of Biology, University of Utah, Salt Lake City, UT 84112.
[6]Present address: Department of Anatomic Pathology, University of Washington, and Department of Laboratories, Seattle Children's Hospital, Seattle, WA 98105.
[7]Present address: Divisions of Human Biology and Basic Sciences, Fred Hutchinson Cancer Research Center, Seattle, WA 98109.

multiple different phenotypes controlled by the same genomic region could greatly facilitate rapid adaptive evolution (Kirkpatrick and Barton 2006; Feder *et al.* 2011; Yeaman and Whitlock 2011).

Adaptive mutations may arise *de novo* or be selected from preexisting standing variants that become favorable following environmental change. When selection acts on newly arising mutations, dominant alleles should have a higher probability of fixation than recessive alleles (Haldane 1927). However, if previously unfavorable standing variant alleles become advantageous following environmental change, there is little bias in the likelihood of alleles of different dominances to sweep to fixation (Orr and Betancourt 2001). Therefore in systems where selection from standing variation predominates, the observed distribution of dominances should largely reflect the underlying distribution of dominances of advantageous mutations. Although most new mutations are recessive (Fisher 1928; Orr 1991), advantageous mutations may have a different distribution of dominances than all mutations. Dominance distributions of adaptive mutations are still poorly characterized, particularly for alleles underlying morphological traits in natural vertebrate populations.

Cis-regulatory changes may predominate during morphological evolution because of the highly pleiotropic effects of developmental regulatory genes (Stern 2000; Carroll 2008). Protein-coding changes in such genes will alter the gene's function at all sites of expression. In contrast, *cis*-regulatory changes can alter expression at highly specific times or locations, limiting phenotypic effects to subdomains of a gene's function. This idea predicts that quantitative trait loci (QTL) controlling adaptive morphological changes may typically act in subsets of anatomical regions. Although this idea can be tested by looking for regional *vs.* global effects among evolutionary QTL that influence serially repeating morphology, few studies have examined large numbers of traits to test the prevalence of modular genetic effects in naturally evolved species (Wagner *et al.* 2007).

The threespine stickleback (*Gasterosteus aculeatus*) species complex provides a powerful system for forward genetic dissection of repeated evolution in nature. Migratory marine sticklebacks colonized thousands of new freshwater lakes and streams following the last Ice Age. Newly established freshwater populations evolved similar phenotypes in response to similar ecological conditions, providing strong evidence that the corresponding traits evolve by natural selection (Schluter 2000). Despite dramatic morphological and physiological differences among sticklebacks, intercrosses between populations produce viable and fertile offspring, making it possible to study the genetic and genomic mechanisms that underlie adaptive evolution in new environments (reviewed in Kingsley and Peichel 2007; Schluter *et al.* 2010). The remarkably compact genome size (~460 Mb) has facilitated a high-quality genome assembly and resequencing of fish from 20 different populations, revealing abundant reuse of standing variants as one of several mechanisms underlying evolutionary differences in this system (Jones *et al.* 2012b).

Previous studies have identified many trophic and defensive armor traits that evolve repeatedly in freshwater (Bell and Foster 1994). A classic case of ecology-driven natural selection is the reduction in number of gill raker bones (Schluter 2000) in countless freshwater stickleback populations throughout the northern hemisphere (Hagen and Gilbertson 1972; Gross and Anderson 1984). Oceanic fish primarily feed on tiny zooplankton in the water column, while freshwater fish adapted to the benthic zone (bottom of lake) have shifted to a diet of larger invertebrates living in sediments or attached to vegetation (Kislalioglu and Gibson 1977; Gross and Anderson 1984). Both reduced gill raker number and larger jaw gape are found in benthic-adapted species (Schluter and McPhail 1992). While large jaws and low gill raker counts correlate with more successful benthos foraging (Lavin and McPhail 1986), small jaws and high gill raker counts correlate with more successful foraging of small prey from the water column (Bentzen and McPhail 1984). Benthic-adapted stickleback forms also display changes in skull morphology that distinguish them from forms adapted to eat smaller prey items (Willacker *et al.* 2010; McGee *et al.* 2013). Collectively, these studies suggest that a concerted set of craniofacial changes allows freshwater populations to forage more efficiently on new diets in freshwater habitats. In addition to head skeletal traits, aspects of the median fin and vertebral skeleton are known to vary and be under selection in stickleback populations. These include dorsal spine lengths (Gross 1978; Bell *et al.* 2006; Hunt *et al.* 2008), the number and position of dorsal and anal fin rays and their supporting pterygiophores, and vertebral number and positioning (Swain 1992a,b; Ahn and Gibson 1999).

Here we apply genome-wide linkage mapping to investigate the genetic architecture of >100 trophic, armor, and serially repeating skeletal traits in sticklebacks. Using a large set of newly identified QTL, we address several general questions in evolutionary genetics, including the extent to which loci are clustered in the genome, the dominance distribution of evolutionary alleles, and the proportion of loci that have anatomically regional effects. Our results show that loci controlling both regressive (loss) and constructive (gain) traits are clustered in the stickleback genome, making it possible to shape multiple aspects of both trophic and defensive morphology by co-inheritance of marine or freshwater alleles at linked loci.

Materials and Methods

Ethics statement

All animal work was approved by University of British Columbia and Stanford University Institutional Animal Care and Use Committees (protocols A97-0298 and 13834).

QTL mapping

A family of 370 full-sibling F_2 fish derived from a Japanese Pacific marine grandmother and a Paxton Lake (British Columbia, Canada) benthic freshwater grandfather (Colosimo *et al.* 2004) was genotyped with 275 microsatellite markers

and phenotyped for 110 skeletal traits across eight trait classes. Linkage map construction, skeletal phenotype analyses, trait transformations, significance threshold determinations, and QTL mapping using R/qtl (Broman and Sen 2009) are described in Supporting Information, File S1. New microsatellite markers are listed in Table S1. QTL within the same trait class with overlapping 1.5-LOD intervals were filtered, keeping the QTL with the highest LOD and removing lesser-effect QTL to avoid redundant QTL sampling. This filtered QTL set was used for all dominance and clustering analyses. All raw phenotype, adjusted phenotype (see Table S2), and genotype data used for QTL mapping are presented in File S2. Details on the genetic positions, effect sizes, and dominances of all QTL are presented in File S3 and File S4.

Anatomical specificity of QTL

For investigating the anatomical specificity of QTL, the subset of QTL with clearly or likely serially homologous domains (QTL controlling gill raker number, pharyngeal tooth number, branchial bone length, upper and lower jaw size, and dorsal spine lengths) was considered. QTL were considered regional if they affected a subset of domains and global if they affected all domains.

Dominance analyses

To calculate the dominance of each QTL, *Z*-scored residual phenotypes were first calculated from a linear regression of the phenotype against all other peak marker genotypes affecting that phenotype. For calculating dominance, the equation d/a (Falconer 1989) was used, with a representing the additive effect of one additional benthic allele (*i.e.*, half the phenotypic difference between the homozygous benthic and homozygous marine genotypic classes). d represents the dominance effect: the difference between the heterozygous phenotype and the midpoint between homozygous parental phenotypes. Similar to a sunflower domestication QTL study (Burke *et al.* 2002), we used the following d/a ranges to classify the dominance effect of benthic alleles: < -1.25 for underdominant, -1.25 to -0.75 for recessive, -0.75 to -0.25 for partially recessive, -0.25 to 0.25 for additive, 0.25 to 0.75 for partially dominant, 0.75 to 1.25 for dominant, and >1.25 for overdominant. For each QTL, one value of a and two values of d were calculated by Haley–Knott regression, as two classes of heterozygous F_2 animals were present. For 2 of 342 QTL, the chromosome had only one heterozygous genotypic class (because F_1 parents had same heterozygous genotypes across this chromosome). For these 2 QTL, the single value of d was counted twice. For the other 340 QTL, d for both the M_1B_1 and M_2B_2 (M, marine; B, benthic) heterozygous genotypic classes was calculated. Simulations investigating dominance bias in detection, *i.e.*, whether additive QTL were less likely to be detected than recessive or dominant QTL, are described in File S1.

Tests of trait clustering

To determine whether QTL were significantly clustered in the genome, we took the observed number of QTL per trait class for (1) all QTL or (2) large-effect QTL, defined as the top quartile of QTL by LOD score (LOD $>$ 8.95, see File S1). We then simulated 1000 random placements of peak markers in the genome, allowing only one QTL per trait class per chromosome (similar to the QTL filtering method described above). For each simulation, we determined the number of QTL with peak markers $<$5 cM away. We calculated *P*-values by comparing the observed number of QTL having peak markers within 5 cM to this null distribution. To determine whether the number of QTL on a single chromosome was significantly enriched relative to a null hypothesis of independent and evenly distributed QTL, simulations were also performed with all of the QTL or the top quartile of QTL by LOD score. For each simulation, the observed total number of trait classes with QTL on each chromosome was determined. This observed set of QTL for each trait class was distributed randomly to chromosomes without replacement with probability in proportion to (1) the genetic length of the chromosome, (2) the physical length of the chromosome (Jones *et al.* 2012b), or (3) the number of Ensembl-predicted genes (Jones *et al.* 2012b) within the chromosome. For each case, 10,000 simulations were performed to calculate a null distribution of QTL per chromosome as well as a mean number of "expected" QTL. For every chromosome, the true number of QTL was compared to the null distribution to calculate a *P*-value. Since sexually dimorphic traits represent a genetic effect of the sex chromosome (chromosome 19) and this effect was largely statistically removed prior to QTL mapping, chromosome 19 was excluded from the clustering simulations and analysis.

Results

Major skeletal differences between marine and freshwater fish

The skeletons of Paxton benthic freshwater (PAXB) sticklebacks show multiple obvious reductions in external bones compared to Japanese Pacific marine (JAMA) animals, including reduced size and number of armor plates, loss of pelvic fins, and reduced length of dorsal spines (Figure 1, A and B). In addition, computerized tomography (Figure 1, C–H) revealed a mixture of both regressive ("loss") and constructive ("gain") traits in the skull and internal branchial skeleton of PAXB sticklebacks. The derived freshwater fish show dramatic reductions in the number and length of gill rakers (Figure 1, C and D), as expected based on previous studies (McPhail 1992; Kitano *et al.* 2007). However, PAXB branchial bones, especially the first epibranchial, have increased in length compared to their marine counterparts (arrowheads in Figure 1, C and D). In addition, PAXB fish have roughly twice the number of ventral pharyngeal teeth seen in JAMA animals (Figure 1, E and F). Compared to marine animals, PAXB fish also show a longer and thinner supraoccipital crest, a posterior process on the supraoccipital bone at the back of the skull that serves as the insertion point for muscles involved in buccal cavity opening (Figure 1, G

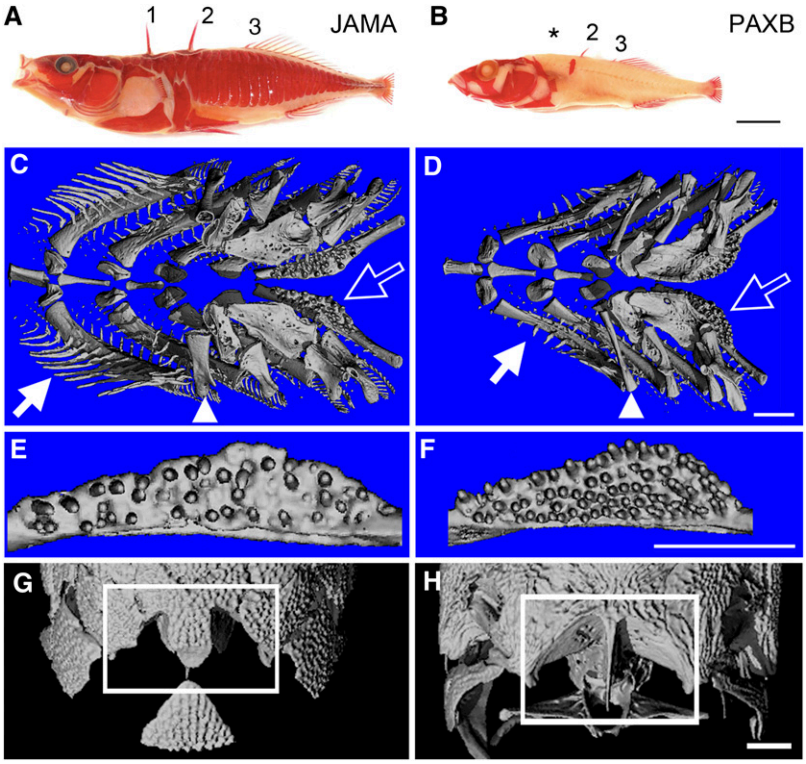

Figure 1 Evolved skeletal differences between marine and benthic sticklebacks. Skeletal morphology was revealed by Alizarin red staining (A and B) or microcomputerized tomography (C–H) of adult Japanese Pacific marine (JAMA) (A, C, E, and G) and Paxton benthic freshwater (PAXB) (B, D, F, and H) fish. (A and B) Lateral views of bone-stained adults reveal differences in dorsal spine lengths. Three dorsal spines are numbered in A. The first dorsal spine is missing (asterisk) in this PAXB fish. (C and D) Dorsal views of branchial skeletons reveal fewer and less densely spaced gill rakers (white arrows) and longer branchial bones (white arrowheads) in PAXB. (E and F) Ventral pharyngeal toothplates (labeled with open white arrow in C and D) reveal higher tooth number in PAXB. (G and H) Dorsal views of skulls reveal differences in the size and shape of the supraoccipital crest (white boxes). The JAMA supraoccipital crest is shorter and wider but larger in area, while the PAXB supraoccipital crest is longer and narrower, smaller in area, and flanked by more robust insertion points for the epaxial muscles. Bars, 1 mm.

and H). Increased size of these muscles is a characteristic feature of PAXB fish, and is thought to increase force generation and suction pressure for feeding on attached littoral prey items (McGee *et al.* 2013).

To investigate the genetic architecture underlying the evolution of these trophic, armor, and other skeletal traits, we used genome-wide linkage mapping in a large marine × benthic F_2 genetic cross previously studied for lateral plate, pelvic spine, and pigmentation patterning (Colosimo *et al.* 2004, 2005; Shapiro *et al.* 2004; Miller *et al.* 2007). We phenotyped 370 full-sibling F_2 fish from this cross and then mapped QTL influencing 110 different skeletal phenotypes (Table S2), including a large number of traits in the branchial skeleton (Figure 2, A–I); multiple aspects of jaw, skull, and opercle morphology (Figure 2, J–O); dorsal and anal spine lengths and degree of spine serrations (Figure 2, P and Q); and several median fin and vertebral traits (Ahn and Gibson 1999) proposed to be important for freshwater adaptation (Figure 2Q).

Most traits are sexually dimorphic

As most traits (93 of 110) are size and/or sex dependent, we systematically corrected for size and/or sex (Table S2). In total, 72 traits showed significant differences between the sexes (Table S3). The traits that show dimorphism, and the direction of dimorphism, were largely consistent with previous reports. For example, males had bigger jaws, more oral teeth, more vertebrae, fewer abdominal vertebrae, more dorsal and anal fin rays, more pterygiophores, and dorsal spines with more serrations both in the current study and in previous studies (Lindsey 1962; Reimchen and Nelson 1987; McPhail 1992; Caldecutt *et al.* 2001; Kitano *et al.* 2007, 2009).

Most QTL are anatomically specific

Raw or corrected trait values (Table S2) and a genome-wide linkage map (Figure S1) were used to map QTL with a multiple-QTL mapping approach in R/qtl (Broman and Sen 2009). This analysis (described in File S1) identified 342 total QTL for 92 of the 110 traits (File S3). Based on segmental homology and likely embryonic origin, we divided the 110 skeletal traits into eight trait classes: rakers, teeth, branchial bones, jaw, skull, opercle, median fin, and vertebrae (Figure 3). In cases where a particular chromosome region had an effect on multiple phenotypes within the same trait class, it is parsimonious to assume that a single underlying QTL affected the trait across several domains. Thus, for our analysis of the properties of these QTL, we conservatively considered such QTL only once. To define a minimally nonredundant set of QTL by trait class, we included only QTL whose 1.5-LOD intervals [an ~95% confidence interval (Dupuis and Siegmund 1999)] did not overlap. This filtering defined a set of 118 QTL across the eight trait classes (Table S4, Figure 3). The overall distribution of percentage of variance explained (PVE) of these QTL consisted of many small-effect QTL and few large-effect QTL (Figure S2), similar to that in a previous stickleback shape QTL study (Albert *et al.* 2008). For trait classes that had multiple serially homologous anatomical domains or elements (raker number, teeth, branchial, jaw, and spine classes), we asked whether QTL controlling these

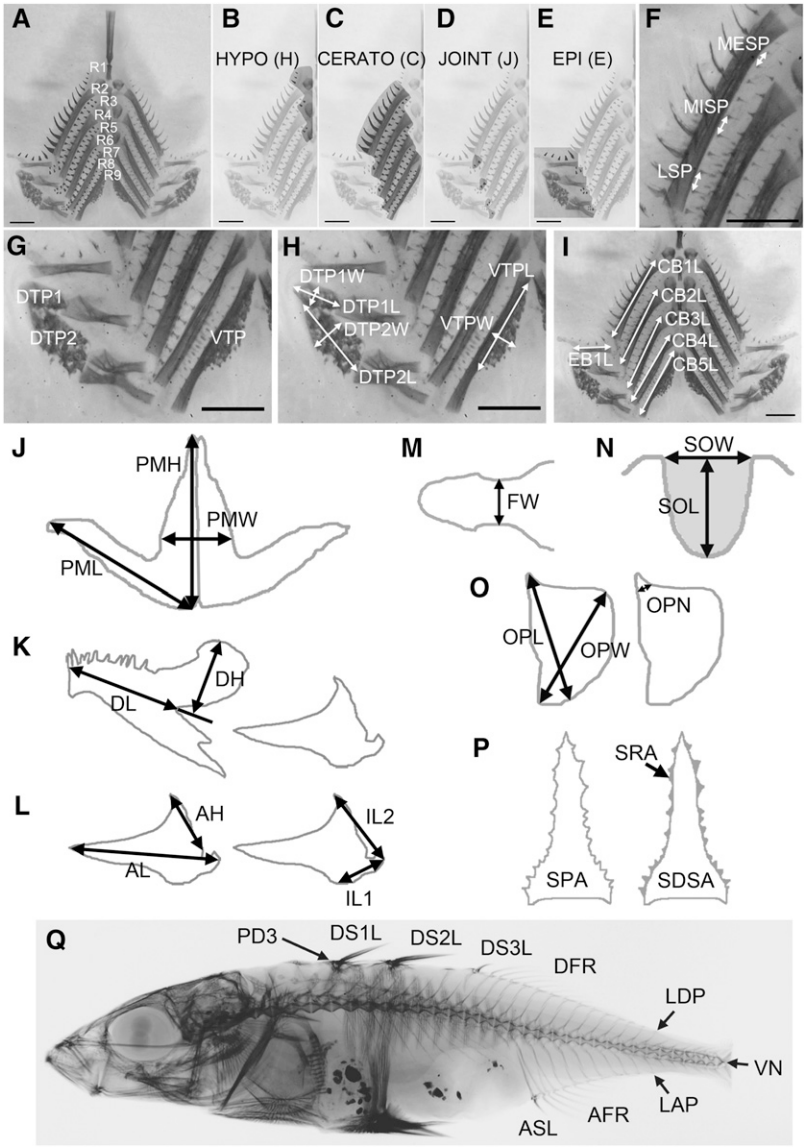

Figure 2 Raker, tooth, branchial bone, jaw, skull, opercle, median fin, and vertebral skeletal phenotypes. (A–I) Branchial skeleton from Alizarin red-stained F_2 fish, dissected and flattened into two-dimensional preparation by single incision along the dorsal midline. All branchial bones, including pharyngeal toothplates and gill rakers, are readily visible. Bars, 1 mm. (A) Nine rows of gill rakers (R1–R9), pseudocolored black on left half, line the anterior and posterior faces of each segment, except for the last segment, which lacks gill rakers on its posterior side. (B–E) Dorsal–ventral domains of gill rakers, defined by edges of branchial bones (see File S1) from ventromedial to dorsal: hypo (B), cerato (C), joint (D), and epi (E) gill raker domains. (F) Three interraker spacing measurements in lateral (LSP), middle (MISP), and medial (MESP) regions of row 2 cerato rakers. (G) Three pharyngeal toothplates (two dorsal and one ventral) are present on each side. (H) Pharyngeal toothplate lengths and widths. (I) Branchial bone lengths. (J) Dorsal view of premaxilla bone (upper jaw) traits. (K) Lateral view of dentary bone (lower jaw, shown with articular posteriorly). (L) Lateral view of articular bone traits. (M) Dorsal view of frontal bone width (or interorbital distance). (N) Dorsal view of caudal end of supraoccipital bone, with supraoccipital crest area shaded gray (also see Figure 1, G and H). (O) Lateral view of opercle bone traits. (P) Second dorsal spine area and serration traits. (Q) X ray showing spine, median fin ray, and vertebral position landmarks. Abbreviations (defined in Table S2): AFR, number of anal fin rays; AH, articular height; AL, articular length; ASL, anal spine length; CB1L, ceratobranchial 1 length; CB2L, ceratobranchial 2 length; CB3L, ceratobranchial 3 length; CB4L, ceratobranchial 4 length; CB5L, ceratobranchial 5 length; DFR, dorsal fin ray number; DH, dentary height; DL, dentary length; DS1L, dorsal spine 1 length; DS2L, dorsal spine 2 length; DS3L, dorsal spine 3 length; DTP1, dorsal toothplate 1; DTP1L, dorsal toothplate 1 length; DTP1W, dorsal toothplate 1 width; DTP2, dorsal toothplate 2; DTP2L, dorsal toothplate 2 length; DTP2W, dorsal toothplate 2 width; EB1L, epibranchial 1 length; FW, frontal width; IL1, in-lever 1 of the articular; IL2, in-lever 2 of the articular; LAP, vertebrae number of last anal pterygiophore; LDP, vertebrae number of last dorsal pterygiophore; LSP, lateral row 2 raker spacing; MESP, medial row 2 raker spacing; MISP, middle row 2 raker spacing; OPL, opercle length; OPN, opercle neck width; OPW, opercle width; PD3, vertebrae number of third predorsal pterygiophore; PMH, premaxilla height; PML, premaxilla length; PMW, premaxilla width; R1–R9, rows 1–9 of gill rakers; SDSA, smoothened dorsal spine 2 area; SOL, supraoccipital crest length; SOW, supraoccipital crest width; SPA, dorsal spine 2 area; SRA, spine 2 serration area; VN, total vertebrae number; VTP, ventral toothplate; VTPL, ventral toothplate length; VTPW, ventral toothplate width.

traits had anatomically regional or global effects. Of this set of QTL, a large majority (76%) affected only a subset of the possible domains while 24% affected all domains (Figure 4, Figure S3, Figure S4, Figure S5, Figure S6, Figure S7, Table S5).

Gill rakers: Gill rakers are present in nine rows from anterior to posterior and in four regions from dorsal to ventral (Figure 2, A–E). Given well-established regional developmental genetic control of pharyngeal segments along the anterior/posterior (A/P) and dorsal/ventral (D/V) axes (*e.g.*, *Hox* gene control of segmental identity and *Dlx* gene control of D/V patterning, reviewed in Minoux and Rijli 2010), we scored and mapped gill raker number separately for each individual A/P and D/V domain, as well as composite phenotypes that represented putative developmental domains [*e.g.*, all ventral (cerato) rakers]. Overall, we found 23 QTL controlling gill raker number or spacing. The raker QTL displayed a high degree of regional specificity, with no QTL having significant effects in all possible domains (Table S5, Figure 4). For example, the largest-effect gill raker QTL mapped to chromosome 20 and had strictly ventral (cerato)-specific effects on raker number, while chromosomes 10 and 7 had regional effects on joint and hypo rakers, respectively (Figure 4 and Figure S3). Additionally, on chromosome 4, the second-largest-effect raker QTL mapped to one end of the chromosome and was largely ventral (cerato)-specific, whereas a nonoverlapping region more centrally located on chromosome 4 had a dorsal (epi)-specific effect on raker number (see below). Both chromosome 4 and chromosome 20 large-effect gill raker number QTL controlled gill raker number at least in

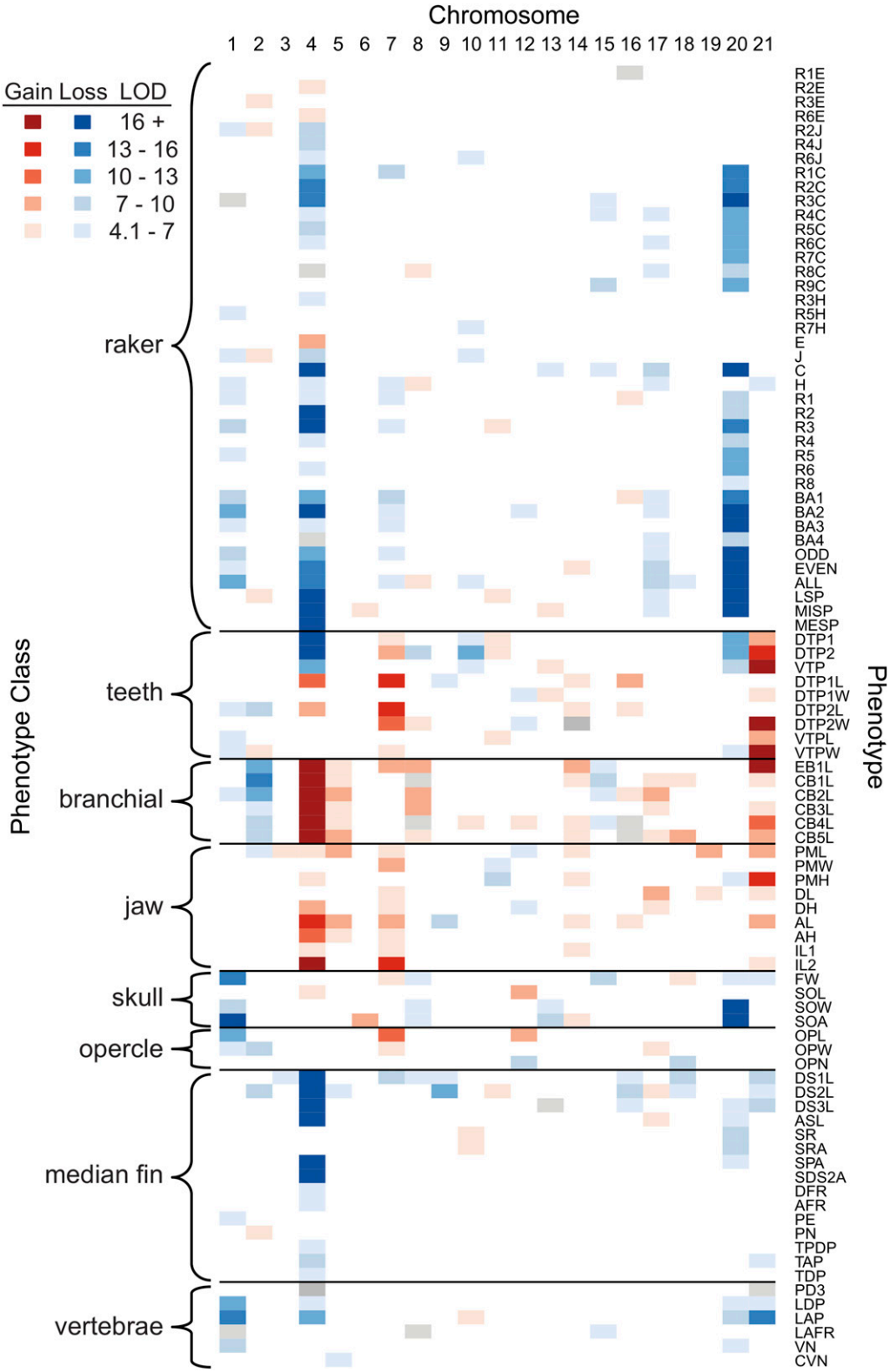

Figure 3 Genome-wide overview of detected skeletal QTL. Classes of traits are grouped on the left and individual traits listed on the right. Abbreviations are defined in Figure 2 legend and in Table S2. For each trait, the LOD score for each QTL on each chromosome is indicated by the heat map shown at the top left, with "gain" traits (benthic allele confers more or bigger bones) colored red and "loss" traits (benthic allele confers fewer or smaller bones) colored blue. Heterotic QTL (homozygous marine and benthic F_2 fish do not differ significantly in phenotype by two-tailed *t*-test) and vertebral position QTL (trait is neither loss nor gain) are shaded gray.

part through controlling gill raker spacing, as row 2 interraker spacing mapped strongly to an overlapping region of chromosomes 4 and 20. Four raker QTL (right chromosome 4 and chromosomes 6, 11, and 13) had a raker spacing measurement map more strongly than any raker number trait.

Teeth: We identified 20 QTL on 14 chromosomes controlling tooth number or toothplate size (Figure 2, G and H), including two QTL with large effects on tooth number (Table S4). A QTL on chromosome 21 explained nearly a third of the variance in ventral pharyngeal tooth number, while

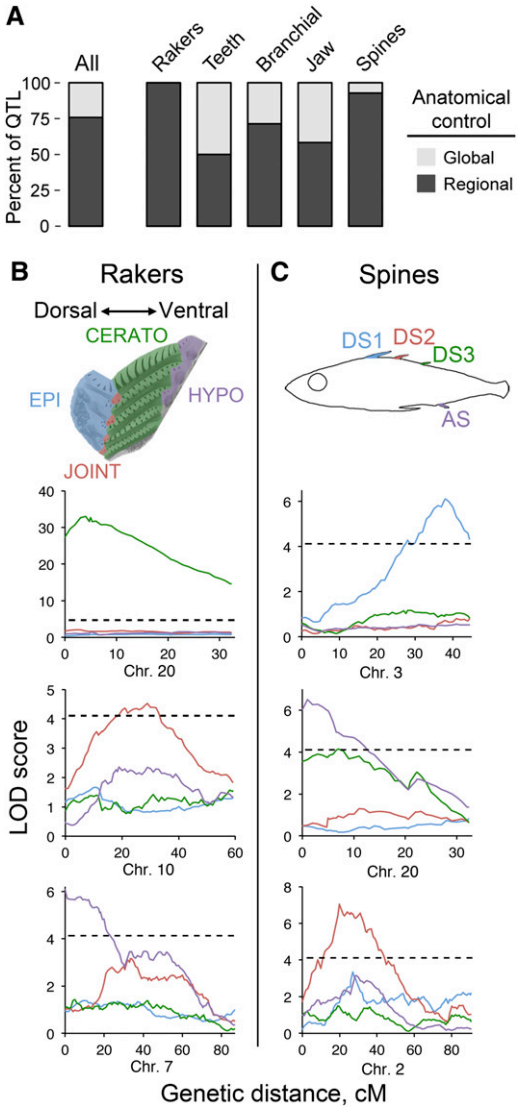

Figure 4 Skeletal QTL with anatomically regional effects. (A) Proportion of QTL with regional *vs.* global effects. For trait classes containing multiple serial or developmental homologous elements or domains, percentages of QTL controlling some (black) or all (gray) elements or domains within the trait class are shown. (B and C) Gill raker (B) and median fin spine (C) morphologies are controlled mainly by QTL with highly regional effects. (B, top) Color-coded dorsal–ventral domains of gill rakers. From dorsal to the ventral midline, rakers are present in EPI (dorsal, blue), JOINT (intermediate, red), CERATO (ventral, green), and HYPO (ventromedial, purple) domains. Below, examples of three gill raker QTL with regional effects in these dorsal–ventral domains are shown, from top to bottom: chromosomes 20, 10, and 7 have regional cerato (ventral), joint, and hypo-specific domains, respectively. Raker totals in each domain are mapped separately and results are color coded as in the raker schematic. (C, top) Three dorsal spines (DS1–DS3) and one anal spine are color coded in the spine schematic. Below are examples of three spine QTL on chromosomes 3, 2, and 20 having regional effects on DS1, DS3 + AS, and DS2 respectively. In each QTL plot, genetic distance in centimorgans is on the *x*-axis and LOD score on the *y*-axis. Dashed lines are significance thresholds.

a QTL on chromosome 4 had large effects on dorsal pharyngeal tooth number. All tooth number QTL had stronger effects (>2 LOD units difference) on either dorsal or ventral pharyngeal tooth number (Figure S4). Genetic control of oral and pharyngeal tooth variation appeared largely independent. Although oral tooth number in the upper jaw was sexually dimorphic (Table S3) as previously reported for several wild stickleback populations (Caldecutt *et al.* 2001), no autosomal QTL for oral tooth number were detected (Table S2).

Branchial bones: We measured the lengths of all five ceratobranchials (large ventral bones in the branchial skeleton), as well as the first epibranchial, a dorsal branchial bone (Figure 2I). We identified 16 QTL on 14 chromosomes controlling branchial bone length, including two QTL on chromosomes 4 and 21 that had large effects on ventral and dorsal bones, respectively (Table S4, Figure S5). QTL with anatomically regional or broad effects were both detected in the cross: four QTL (chromosomes 1, 7, 10, and 12) had significant effects on only one of six bones analyzed, while 4 other QTL (chromosomes 2, 4, 5, and 8) had significant effects on all six branchial bones analyzed.

Jaw: Unlike the branchial bones, which ossify endochondrally, the premaxilla and dentary, the major bones of the fish upper and lower jaw (Figure 2, J–L), respectively, are dermal bones that form without a cartilage intermediate (Anker 1974; Cubbage and Mabee 1996). We detected 15 QTL on 14 chromosomes controlling jaw morphology (Table S4, Figure S6). Eleven QTL influenced the size of the premaxilla, with the largest-effect QTL on chromosome 21. Ten QTL influenced the size of the dentary and the associated articular bone, with the largest-effect QTL mapping to chromosome 4. Three QTL (chromosomes 2, 3, and 20) controlled upper but not lower jaw size and 3 other QTL (chromosomes 9, 16, and 17) controlled lower but not upper jaw size (Figure S6). In contrast, 7 QTL (chromosomes 4, 5, 7, 12, 14, 19, and 21) had significant effects on both the upper and lower jaw.

Skull: In the posterior skull, the supraoccipital crest is longer and thinner in benthic fish than in marine fish (Figure 1, G and H, and Figure 2, M and N). The supraoccipital crest serves as the attachment points of the epaxial muscles that generate force during suction feeding. These muscles are larger in Paxton benthic fish, contributing to a derived increase in suction index (McGee and Wainwright 2013). We hypothesized that these differences in supraoccipital crest morphology are adaptive for benthic feeding and have a heritable genetic component. We measured supraoccipital crest length, width, and area and a fourth skull trait, frontal width (interorbital distance). We identified 12 QTL that affect these skull traits (Table S4), including a large-effect QTL on chromosome 20 that significantly influenced supraoccipital crest width and area.

Opercle: The shape of the opercle bone (Figure 2O) also varies between marine and freshwater populations, which might reflect differences in feeding and/or respiration (Kimmel *et al.* 2005, 2012). Opercle size in this cross was strongly sexually dimorphic (Table S3) and was also controlled by seven autosomal QTL controlling opercle length, width, or neck width (Table S4).

Spines and median fins: We mapped QTL on 16 chromosomes controlling dorsal or anal spine length (Table S4). A QTL on chromosome 4 affecting the length of the second dorsal spine was the most significant QTL in our entire data set, with a LOD of 51. Chromosome 4 also had large effects on the lengths of the other two dorsal spines and the anal spine (Figure S7). In contrast, QTL on 7 chromosomes (2, 3, 5, 7, 8, 11, and 13) had regional effects with significant effects restricted to only one of the four spines measured. Chromosomes 3 and 2 had specific effects on dorsal spines 1 and 2, respectively, while chromosome 20 had regional effects on dorsal spine 3 and the anal spine (Figure 4). QTL controlling the number and area of serrations on the second dorsal spine (Figure 2P) mapped independently of the QTL controlling the length of the second spine, consistent with previous studies showing that presence or absence of serrations varies substantially among stickleback populations, even among populations with prominent second dorsal spines (Gross 1978).

Vertebrae traits: We found vertebrae number to be sexually dimorphic (Table S3), consistent with previous studies (Reimchen and Nelson 1987). Vertebrae number and position of axial landmarks were also under autosomal control, mapping to eight QTL. Although caudal vertebrae number mapped to one significant QTL, the caudal to abdominal vertebrae ratio, proposed to be important for larval fitness (Swain 1992b), had no detected QTL.

Covariance of traits and multivariate analysis of covariance

We analyzed patterns of trait covariance across all trait classes and found that in general, traits within a trait class tended to covary (Figure S8). As expected, traits that mapped strongly to the same chromosome (*e.g.*, gill raker and dorsal spine reduction, which both map strongly to chromosome 4) also tended to covary (Figure S8). The mean absolute correlations were 0.30 and 0.12 for traits within and between trait classes, respectively. We performed principal components analysis with all traits quantified in this study and mapped the first five principal components (Figure S9, Figure S10). The first principal component maps strongly to chromosomes 4 and 21 (Figure S9), and as expected, traits that map strongly to these two chromosomes (*e.g.*, branchial bone length, jaw size, and ventral pharyngeal tooth gain) load heavily onto this component (Figure S10). The second principal component maps strongly to chromosome 20 (Figure S9), and traits that map strongly to this chromosome (*e.g.*, gill raker reduction and supraoccipital crest shape) load heavily onto this component (Figure S10). Four of the top five principal components map significantly to chromosome 4 (Figure S9), suggesting that the patterns of trait covariance and integration are complex, but frequently involve particular stickleback chromosomes.

The genomic regions underlying trait clusters on chromosomes 4, 20, and 21 contain 48, 35, and 11 genes, respectively, that have Gene Ontology annotations suggesting key roles in early developmental patterning and signaling (see File S1). Changes in such genes may contribute to the multiple traits and covariances that map to particular stickleback chromosomes.

Most QTL are additive or partially additive

We estimated the dominance of each QTL using the formula d/a (Falconer 1989), where benthic alleles with strictly recessive, additive, and dominant effects have d/a values of -1, 0, and 1, respectively. Across all trait classes, there was a tendency for QTL to act additively, with the distribution of dominance values centered around 0 (Figure 5A). We defined dominance classes using d/a ranges as in a large sunflower domestication QTL study (Burke *et al.* 2002). Using these ranges, 28% of QTL are additive, 22% partially recessive, 21% partially dominant, 11% recessive, 5% dominant, 6% underdominant, and 6% overdominant (Table S6, Figure S11, Figure S12, Figure S13, Figure S14). QTL in different trait classes had similar patterns of dominance, with a consistent bias toward additive and partially recessive/dominant QTL (Table S6). We also observed an apparent relationship between effect size and dominance, with larger-effect QTL having more of an additive effect (Figure 5B, Figure S15), which simulations show is at least in part driven by a lower precision of dominance estimates of small-effect QTL (data not shown). To investigate possible bias in the detection of QTL differing in dominance, we carried out a simulation to determine the detection probability of additive and dominant QTL. Since more variance is present among the mean phenotypes of genotypic classes of a completely dominant or recessive QTL than an additive QTL, we predicted that additive QTL would be harder to detect than dominant QTL by interval mapping. As expected, the probability of detection was slightly higher for a dominant QTL than for an additive QTL (Figure S16). Thus, the detection of more QTL with additive effects does not result from a detection bias.

Although many different types of mutations can lead to loss or gain of structures during development, we tested the hypothesis that regressive or loss QTL (where the freshwater benthic allele contributes to smaller or fewer bones) might more often be recessive, while constructive or gain QTL (where the benthic allele contributes to larger or additional bones) might show more dominance. However, the sets of loss and gain QTL contained similar proportions of dominant QTL (5%), and the set of gain QTL actually showed a higher percentage of recessive QTL (16% *vs.* 7%, Table S6).

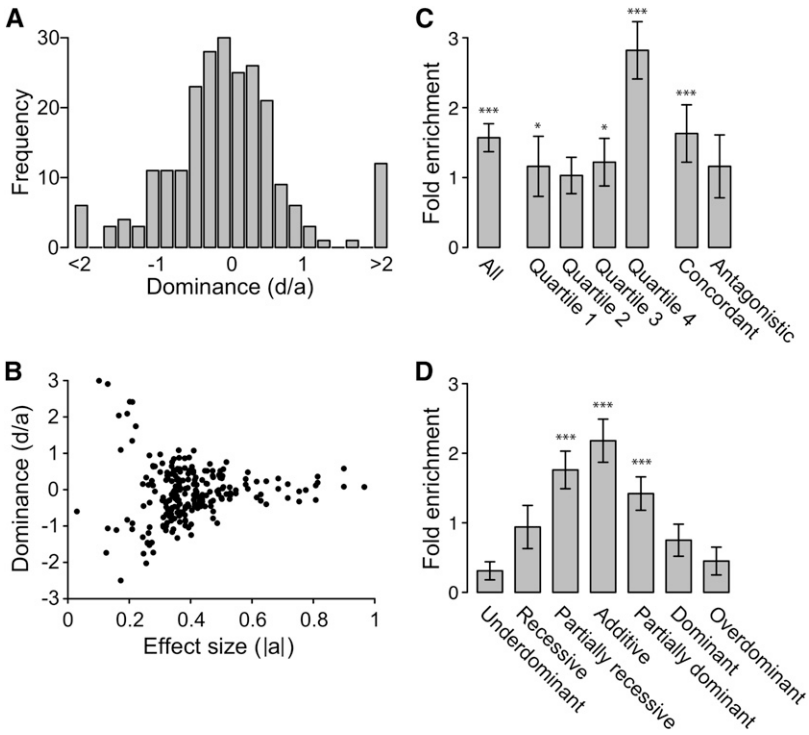

Figure 5 QTL dominance patterns and overlap with genomic intervals repeatedly selected during global marine–freshwater stickleback divergence. (A) Histogram of dominance values (*d*/*a*) of QTL reveals a tendency toward additive QTL (*d*/*a* = 0). (B) Dominance values for each QTL plotted against effect size (absolute value of *a*). Ten outlier dominance values that were either >3 or < −3 (File S3) are not shown. As effect size increases, QTL tend to be more additive. (C) Fold enrichment of QTL 1.5-LOD interval overlaps with genomic regions showing parallel marine–freshwater divergence in whole-genome sequence comparisons (Jones *et al.* 2012b) for all QTL, quartiles of QTL by LOD score, and concordant or antagonistic QTL. Highly significant enrichment is seen for all QTL, highest-LOD QTL (quartile 4), and concordant QTL. (D) Fold enrichment of QTL 1.5-LOD interval overlaps with signals of selection (Jones *et al.* 2012b) by dominance class. Highly significant enrichment is seen for partially recessive, additive, and partially dominant QTL, but not for other dominance classes. $*P < 0.05$, $***P < 0.001$.

For both sets of QTL, most loci were at least partially additive (69% for gain and 74% for loss, Table S6), and there was no significant difference ($P = 0.46$, Mann–Whitney *U*-test) between the distributions of dominances of loss and gain QTL.

QTL can also be classified into sets whose effects are either concordant or antagonistic to the overall direction of evolutionary change, (*i.e.*, where substitution of a benthic allele confers a more benthic-like or a more marine-like phenotype, respectively). Most (66%) QTL with a predicted evolutionary direction (based on known phenotypes from the grandparental populations) were in the concordant direction. Although we hypothesized that concordant and antagonistic QTL might show different dominance distributions, we observed no significant differences for the QTL identified in this study ($P = 0.61$, Mann–Whitney *U*-test).

Recent whole-genome resequencing studies in sticklebacks have identified a genome-wide set of regions that are consistently differentiated between marine and freshwater fish populations around the world and have likely been selected repeatedly to produce marine–freshwater differences (Jones *et al.* 2012b). The 1.5-LOD genetic intervals controlling skeletal traits in this QTL study were significantly enriched for the genomic regions that show consistent marine–freshwater sequence differences ($P < 0.001$, Figure 5C). The biggest enrichment was found for the genetic intervals that had the most significant effects on morphology, with a 2.8-fold enrichment ($P < 0.001$) observed for QTL in the top quartile of the LOD score (quartile 4, Figure 5C). Interestingly, we also observed significant enrichment for the set of concordant QTL that act in the same direction as overall evolutionary change (1.6-fold enriched, $P < 0.001$), but no significant enrichment for the set of antagonistic QTL (Figure 5C), as expected if marine–freshwater differentiated regions represent genomic intervals that are repeatedly selected to produce the consistent morphological differences observed in marine and freshwater environments. However, there was a trend toward enrichment for discordant QTL, and the difference in fold enrichment between concordant and antagonistic QTL was not significant ($P = 0.44$, two-tailed Student's *t*-test).

Some variants controlling freshwater stickleback phenotypes are carried at low frequency in marine populations (Colosimo *et al.* 2005; Miller *et al.* 2007), and the dominance of such variants may affect their carrier frequency in marine populations or the rate at which they increase in frequency following colonization of new freshwater environments. We therefore tested whether QTL in different dominance classes were differentially enriched for the marine–freshwater genomic regions that show evidence of repeated selection. Neither recessive nor dominant QTL were enriched for overlap with the genomic regions identified in the Jones *et al.* (2012b) study (Figure 5D). In contrast, partially recessive, additive, and partially dominant QTL were all strongly enriched for overlap with signals of repeated genomic selection ($P < 0.001$, Figure 5D).

Trait clusters on chromosomes 4, 20, and 21

As detailed above, inspection of QTL results revealed many complex and nonoverlapping patterns of genetic control within and among trait classes (Figure 3). However, certain chromosomes appeared enriched for QTL, especially QTL with high LOD scores, spanning multiple trait classes (Figure 3 and Table S4). To examine possible clustering in greater

detail, we first tested whether detected QTL were more likely to have peak markers within 5 cM of each other, compared to randomly distributed QTL (Protas *et al.* 2008). For both (1) all QTL and (2) large-effect QTL (defined as being in the top quartile by LOD), peak markers were significantly clustered ($P = 0.01$ and $P < 0.001$ for all QTL and large-effect QTL, respectively). In the entire set of filtered QTL, as expected, LOD score and PVE were highly correlated (Pearson's correlation coefficient = 0.95).

To ask whether specific chromosomes were significantly enriched for QTL, we used simulations to ask whether (1) all QTL or (2) large-effect QTL were overrepresented on any autosome. Relative to a null prediction where QTL are distributed in the genome in proportion to the genetic lengths of autosomes, large-effect QTL were significantly enriched on chromosomes 4, 20, and 21 (Figure 6). In contrast, only chromosome 21 was statistically enriched when we analyzed all QTL, not just those of large effect (Table S7). Since we statistically corrected for the effect of sexual dimorphism for each trait, we did not include the sex chromosome (chromosome 19) in these calculations.

Given that QTL are more likely to be detected in regions of low recombination ["the Noor effect" (Noor *et al.* 2001)], a low recombination rate on a particular chromosome could contribute to an enrichment of detected QTL on that chromosome. We therefore asked whether trait clustering was significant even when considering physical distance or gene number of each chromosome in the recently published stickleback genome assembly (Jones *et al.* 2012b). The enrichment of large-effect QTL on chromosomes 4 and 21 remains significant when compared to a null distribution of QTL generated in proportion to either chromosome length or gene number (Table S7), while the enrichment of QTL on chromosome 20 is suggestive, but not significant ($P = 0.14$ after correcting for either chromosome length or gene number).

For chromosomes 4 and 21, clustered traits included both loss and gain QTL, with benthic alleles in the same trait cluster contributing to bone loss for some traits and bone gain for others (Figure 7). For example, chromosome 4 had large effects on gill raker and dorsal spine loss, but also on jaw size gain. Chromosome 21 had large effects on tooth and branchial bone gain, but also on dorsal spine loss (Figure 7). In contrast, QTL mapping to chromosome 20 were in the direction where the benthic allele conferred loss or reduction of bone size across multiple trait classes.

Finally, we asked whether the three trait clusters on chromosomes 4, 20, and 21 are enriched for the genome-wide set of regions that are consistently differentiated between marine and freshwater stickleback populations (Jones *et al.* 2012b). These trait clusters on chromosomes 4, 20, and 21 overlapped 70, 26, and 6 marine–freshwater divergent regions from this set, respectively. Compared to the genome-wide average for an equivalently sized chromosome segment, the chromosome 4 and 20 trait clusters are significantly enriched ($P <$ 0.001 for both), with a 4.5-fold and 3.4-fold enrichment, respectively. The chromosome 21 trait cluster, in contrast, has only a 1.1-fold enrichment for these marine–freshwater divergent regions, which is not significant ($P = 0.28$). Thus, two of the three trait clusters are significantly associated with characteristic marine–freshwater divergent genomic regions.

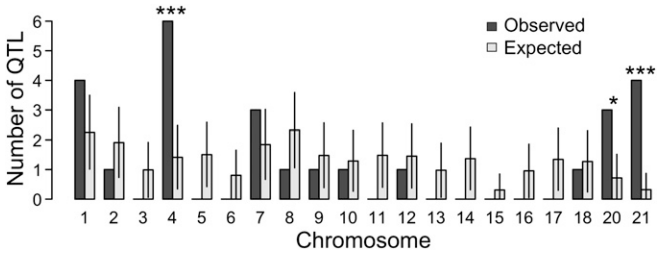

Figure 6 Large-effect QTL are enriched on chromosomes 4, 20, and 21. Observed (solid bars) and expected (open bars) numbers of large-effect QTL (top quartile by LOD) per chromosome are shown. Data for the expected values represent the mean and standard deviation of values generated from 10,000 simulations. This analysis excluded the sex chromosome (chromosome 19). $*P < 0.05$, $***P < 0.001$.

Discussion

Regional control of skeletal anatomy

A main finding of this study is that the genetic control of evolved skeletal morphology in sticklebacks involves both differential genetic control between trait classes and highly specific control of individual skeletal elements within a trait class. It is not surprising to find differential genetic control between trait classes, given the likely different embryonic origins of skeletal elements in different trait classes. Perhaps more surprising is the extent of highly specific anatomical control among skeletal elements thought to be serially homologous.

Consider, for example, the genetic mapping data for gill raker number. Gill rakers form throughout the pharynx, projecting from dorsal, joint, and ventral regions of branchial arches. The reduction in gill raker number in derived freshwater fish occurs in each branchial segment (Gross and Anderson 1984) and is typically described by summing all anterior-facing rakers on the first branchial segment [row 1 (*e.g.*, Hagen and Gilbertson 1972)]. Our mapping data revealed that in the Paxton benthic population, gill raker reduction was accomplished genetically in a piecemeal fashion by at least 23 QTL with specific effects in particular dorsal/ventral domains. Both of the large-effect gill raker QTL had regionally specific effects, the QTL on right chromosome 4 controlling anterior ventral gill raker number and spacing and the chromosome 20 raker QTL controlling strictly ventral gill raker number (Figure 4 and Figure S2). This decoupling of the genetic control of dorsal and ventral gill rakers is also consistent with a previous ecological study that found ventral, but not dorsal, gill raker number to have predictive value in discriminating different wild freshwater populations, perhaps reflecting population-specific diets (Reimchen *et al.* 1985). The anatomical specificity of QTL

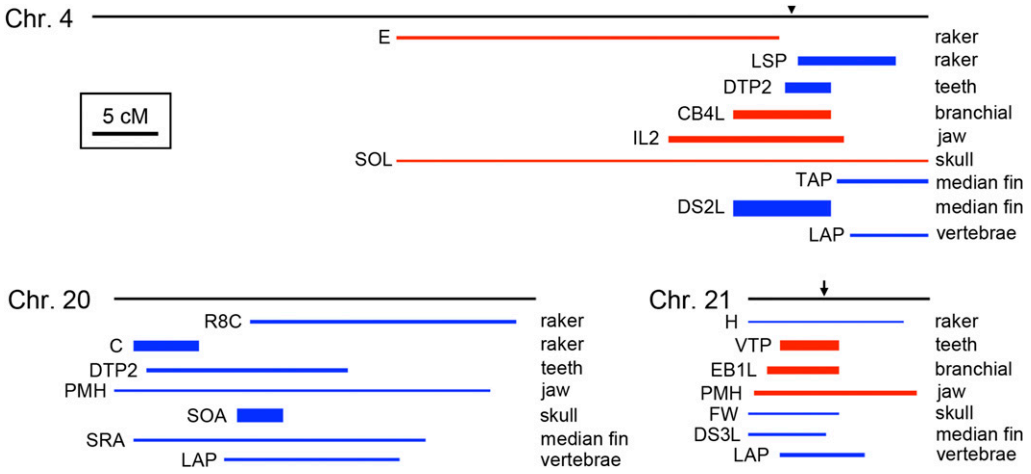

Figure 7 Trait clusters on chromosomes 4, 20, and 21. For each chromosome, the genetic length of the chromosome is shown as the black line at the top of each panel. (Bar, 5 cM.) Each blue, red, or gray bar represents a QTL, with the length of the bar denoting the 1.5-LOD interval. Trait abbreviations (Table S2) are listed to the right of each bar. The height of each bar is proportional to the LOD score of the QTL. For each QTL, direction of effect is indicated by red (benthic allele confers more or bigger bones) or blue (benthic allele confers fewer or smaller bones). The position of *Ectodysplasin* on chromosome 4 is marked with an arrowhead. A 1.7-Mb inversion on chromosome 21 (arrow), with different orientations typical in marine and freshwater fish (Jones *et al.* 2012b), mapped within the 1.5-LOD interval of all seven QTL on this chromosome, although the peak markers for each QTL (Table S4) mapped left of the inversion. See Figure 3, Figure S3, Figure S4, Figure S5, Figure S6, Figure S7, and File S3 for more details on traits controlled by these three chromosomes. Abbreviations (see Figure 2 and Table S2): C, total cerato (ventral) gill raker number; CB4L, ceratobranchial 4 length; DS2L, dorsal spine 2 length; DS3L, dorsal spine 3 length; DTP2, dorsal toothplate 2 tooth number; E, epi (dorsal) gill raker number; EB1L, epibranchial 1 length; FW, frontal width; H, total hypo gill raker number; IL2, in-lever 2 of the articular; LAP, vertebrae number of last anal pterygiophore; LSP, lateral row 2 raker spacing; PMH, premaxilla height; R8C, row 8 cerato (ventral) gill raker number; SOL, supraoccipital crest length; SOA, supraoccipital crest area; SRA, spine 2 serration area; TAP, total postanal pterygiophore number; VTP, ventral toothplate tooth number.

might be even more complex; even within the ventral domain, the chromosome 20 raker QTL had regional effects, controlling only lateral and middle, but not medial spacing (Figure S2).

Another example of highly specific anatomical effects within a trait class is the genetic control of dorsal spine development. Nine of 14 QTL controlling dorsal spine lengths were specific to one of the three dorsal spines. Additional QTL controlled the number and area of barb-like serrations along the surface of the second dorsal spine, and these QTL mapped to different genomic regions than QTL that control length of the second dorsal spine. Previous studies have shown that natural populations of sticklebacks differ in the number of spines, the length of particular spines, and the degree of barb development along spines, likely reflecting the key roles of dorsal spine morphology in defense against different types of predators, as well as possible functions in display and dorsal pricking interactions during stickleback courtship (Hoogland *et al.* 1957; Gross 1978; Reimchen 1980; Kitano *et al.* 2009). Across larger phylogenetic distances, many other fish groups show striking changes in the length or morphology of individual spines, for example, the specific elongation of the first dorsal spine in trigger fish and angler fish. These dramatic species-specific modifications also likely depend on precise anatomical control of spine growth by genetic mechanisms that do not cause comparable changes in all members of a developmentally related series.

The high degree of regional control for skeletal QTL in sticklebacks is consistent with the idea that anatomically specific changes may avoid negative pleiotropy during development and will therefore predominate during morphological evolution in natural populations (Stern 2000; Carroll 2008). Highly specific skeletal effects may be controlled by genes whose expression patterns are themselves highly restricted along developmental axes (*e.g.*, *Hox* and *Dlx* genes) or by *cis*-regulatory changes that alter a particular subset of the expression domains of more broadly expressed genes. Further molecular dissection of the QTL mapped in this study, using genetic fine mapping and transgenic methods similar to those that have been successfully applied to other stickleback traits (Colosimo *et al.* 2005; Miller *et al.* 2007; Chan *et al.* 2010), should help illuminate the detailed mechanisms that vertebrates use to shape the size and number of individual skeletal elements as they evolve in different environments.

Most QTL had additive or partially additive effects

A second major conclusion from this study is that the majority of the detected evolutionary QTL had additive or partially additive effects, regardless of skeletal trait class and regardless of the overall direction of their effects on the skeleton (either gain or loss of bone in the derived freshwater form; Table S6). Our simulations indicated that detection bias does not explain the enrichment in additive QTL; instead it might contribute to an underdetection of additive QTL (Figure S16). The strong tendency toward additivity across trait classes suggests that this trend may be a general feature of evolved stickleback traits. Previous studies have shown that repressive genetic interactions tend to be as common as activating genetic mechanisms during development (Davidson and Levine 2008). Since constructive traits could be due to either loss of repressors or gain of activators, and regressive traits could arise by either loss of activators or gain of repressors, it is perhaps not surprising that a range of skeletal traits, including both increases and decreases of bony tissue, tend to show similar genetic architectures.

Two main models have been proposed for the effect of the dominance of a mutation on its likelihood of fixation during adaptation. "Haldane's sieve" predicts that new advantageous mutations are more likely to increase in frequency if they are not recessive (Haldane 1927). In contrast, Orr and Betancourt (2001) showed that if standing variants preexist in populations at mutation–selection balance and are disadvantageous prior to, but favored after, an environmental change, then probability of fixation in the new selective regime is largely independent of dominance. In the stickleback system, detailed case histories of the specific variants underlying armor and pigment traits (Colosimo *et al.* 2005; Miller *et al.* 2007) and more recent genome-wide surveys of parallel evolving freshwater populations (Hohenlohe *et al.* 2010; Jones *et al.* 2012b) show that repeated selection of ancient standing variants plays a substantial, but not exclusive (Chan *et al.* 2010), role in repeated marine–freshwater divergence. The overall distribution of dominance we observe for skeletal QTL in sticklebacks is thus likely based on a mixture of *de novo* mutations that have arisen during the divergence of the particular populations studied and older standing variants that likely exist at selection–migration balance in ocean populations, which become favorable when introduced into new freshwater environments. We observe a strong tendency toward additivity for QTL, which cannot be simply explained by either Haldane's sieve or the Orr/Betancourt model. However, the Haldane and Orr/Betancourt predictions are for fitness, and it is possible that the dominance for the skeletal traits studied here does not reflect the dominances for fitness, as previously seen in the dominances of *Eda* and chromosome 4 genotype on lateral plate morphology and fitness (Barrett *et al.* 2008).

Similar trends toward additivity of QTL have been observed in genetic studies of traits under artificial selection in mice and outbreeding plants (deVicente and Tanksley 1993; Burke *et al.* 2002; Kenney-Hunt *et al.* 2008; Ronfort and Glemin 2013), as well as in naturally evolved differences between surface and cave-adapted fish (Protas *et al.* 2008). This trend toward additivity for evolutionary QTL could result at least in part from a bias in the dominance distribution of the types of mutations favored by selection. For example, segregating *cis*-regulatory alleles have been found to be additive more often than *trans*-regulatory alleles (Lemos *et al.* 2008; McManus *et al.* 2010; Gruber *et al.* 2012). If selection favors *cis*-regulatory mutations, then additive QTL are expected to be common. Furthermore, the Orr/Betancourt model assumes that standing variation is at mutation–selection balance, whereas much of the standing variation reused by stickleback populations may be at migration–selection balance (Barrett and Schluter 2008), maintained in the ancestral marine population by introgression from freshwater populations. Such variation has already been filtered by selection: to be present in the sea it likely had increased in frequency already in freshwater populations. As a result, standing variation should be biased toward the kinds of mutations that selection favors in freshwater, which we hypothesize to be *cis*-regulatory mutations due to their low pleiotropy and a tendency to be additive.

Although we observed a strong tendency toward additivity of QTL, the 12% of overdominant and underdominant QTL observed likely indicates that some of the genetic effects observed in this cross result from complex interactions between the divergent grandparental genomes used for the cross, some of which may not be typical for very recent divergence between more closely related populations. Furthermore, although the extant Japanese Pacific marine population was used in this study as a living proxy for the marine ancestor of Pacific basin-derived freshwater fish including Paxton benthics, modern day marine fish cannot be equated with the ancestor of Paxton Lake fish. Given that genetic effects including dominance of QTL are likely context (*e.g.*, genetic background and environment) dependent, additional crosses will be needed to test general patterns of evolved genetic effects in this system.

Overall, the QTL identified in this study show significant enrichment for overlap with the previously identified haplotypes that are consistently differentiated between marine and freshwater fish populations around the world (Jones *et al.* 2012b). This enrichment suggests that a subset of the genomic regions repeatedly used for freshwater adaptation is selected for their effects on skeletal morphology. Large-effect QTL and additive QTL display the strongest enrichment, while small-effect, recessive, or dominant QTL show no or less enrichment for overlap with these haplotypes. These enrichment differences could at least partly result from a higher proportion of false positives in the set of small-effect QTL, which are more likely to be recessive or dominant. In addition, small-effect, recessive, and dominant classes might be enriched for new mutations (rather than standing genetic variation), which have a lower probability of detection by the method used in the Jones *et al.* (2012b) study. Further analysis of the QTL intervals identified in this study will test the hypothesis that the enrichment of these signals of selection in the QTL intervals is driven by particular genomic regions that act to control specific skeletal traits mapped in this study. Future population genetic studies in marine and Paxton benthic populations can also test whether haplotypes inside the QTL intervals identified here are outliers for metrics such as F_{st}.

Clustering of QTL on chromosomes 4, 20, and 21

A third major finding of this study is that multiple trophic and armor traits map strongly to chromosomes 4, 20, and 21. We found that QTL from six (chromosome 20) or seven (chromosomes 4 and 21) of the eight trait classes mapped to each trait cluster (Figure 3). Although all QTL were enriched only on chromosome 21, large-effect (top quartile of QTL by LOD) QTL were enriched on chromosomes 4, 20, and 21 (Figure 6). All three trait clusters controlled specific subsets of skeletal traits and are thus unlikely to represent loci generally involved in bone formation. For example,

some skeletal traits, such as opercle size, mapped strongly to multiple genomic locations but were not significantly controlled by any of the three large-effect trait clusters.

The trait clusters could result from single genes with pleiotropic effects or from the combined effects of multiple linked genes. Several QTL studies have identified loci that are thought to have pleiotropic consequences (Kimura *et al.* 2007; Albert *et al.* 2008; Studer and Doebley 2011), including a large-scale study of QTL controlling skeletal differences between mice artificially selected for large or small body size (Kenney-Hunt *et al.* 2008). In contrast, genetic studies in butterflies, pinthrum, and *Petunia* have reported some trait clusters that are due to closely linked but separable loci, rather than to pleiotropic effects of a single gene (Kurian and Richards 1997; Joron *et al.* 2006; Ferguson *et al.* 2010; Hermann *et al.* 2013). As the degree of pleiotropy of a QTL increases, the relative frequency of antagonistic effects (effect in the opposite direction of the direction of evolutionary change) is predicted to increase during selection (Griswold and Whitlock 2003), which perhaps at least partially explains our observation that a significant fraction (34%) of QTL are antagonistic. However, antagonistic effects could also result from stabilizing selection, from genetic drift (Rieseberg *et al.* 2002; Griswold and Whitlock 2003), or from pleiotropic mutations that overshoot the optimum phenotype.

For two of the stickleback trait clusters presented here, genetic resolution of linked traits argues against pleiotropy. For example, two of the linked raker QTL on chromosome 4, as well as two linked raker and supraoccipital crest QTL on chromosome 20, appear spatially distinct from each other, with nonoverlapping 1.5-LOD intervals (Figure 7). In addition, for the trait clusters on chromosomes 4 and 21, benthic alleles do not act in a consistent phenotypic direction (Figure 7). For example, chromosome 4 benthic alleles reduce gill raker number, pharyngeal tooth number, and dorsal and anal spine lengths, but also increase upper and lower jaw sizes, branchial bone sizes, and the length of the supraoccipital crest. Given the opposite directions of phenotypic effects and the genetic resolution separating some of the linked QTL, we favor a model where several individual, linked QTL exist, possibly including a supergene complex with multiple effects on both armor and trophic phenotypes. Increased genetic resolution of these overlapping QTL is needed to test whether the QTL are separable and whether some of the overlapping traits might resolve to a supergene complex. In cases where loss and gain QTL overlap, it is possible these traits share developmental interactions (*e.g.*, the genetically encoded loss of a trait might result indirectly in the gain of another).

In cases of multiple linked QTL, trait clustering may be due to genomic intervals of decreased recombination. For example, inversions suppress recombination and in *Mimulus* and *Heliconius* appear to lock in a suite of coadaptive polymorphisms (Lowry and Willis 2010; Joron *et al.* 2011; Fishman *et al.* 2013). Recent stickleback genome sequencing revealed a 1.7-Mb inversion on chromosome 21 that displays strong signals of selection, whereby marine and freshwater populations have high and low allele frequencies, respectively, of the inversion (Jones *et al.* 2012b). Jones *et al.* (2012b) proposed that this inversion may hold several distinct adaptive loci together, and both the current study of skeletal QTL and another recent study of lateral line QTL (Wark *et al.* 2012) confirm that many QTL map to chromosome 21, with confidence intervals that overlap the position of the inversion. Although this study identifies a large number of new traits that may be controlled by an inversion/supergene complex in sticklebacks, we note that the peak markers for each of the chromosome 21 QTL map left of the inversion. Ongoing fine-mapping studies using crosses that generate recombination events in and around the inversion will provide useful information on both the position and the identity of the genes and mutations that underlie one of the most distinctive trait clusters in the stickleback genome.

Previous studies have identified multiple QTL mapping to chromosome 4 in sticklebacks, including QTL for lateral plate number and lateral plate size (Colosimo *et al.* 2004; Cresko *et al.* 2004), pelvic spine length (Shapiro *et al.* 2004), and multiple aspects of body shape (Albert *et al.* 2008; Rogers *et al.* 2012). The data presented here reveal that a surprisingly large number of additional traits also map to chromosome 4, including gill raker number, pharyngeal tooth number, branchial bone size, premaxilla size, dentary and articular size, supraoccipital crest length, dorsal and anal spine length, and aspects of vertebral positioning. Many of these traits, including larger jaws and fewer gill rakers, shorter dorsal and pelvic spine lengths, reductions in lateral plate number, and changes in overall body shape, appear to have adaptive significance in benthic environments, as multiple benthic species independently evolve these morphological changes in recurrent stickleback species pairs (Schluter and McPhail 1992). Linkage of large-effect QTL controlling multiple aspects of both trophic morphology and antipredator defense may preserve combinations of traits that function together in different ecological environments. For example, fish foraging in open water environments not only specialize on different food sources, but also tend to encounter different predators. Thus, tight linkage of genes controlling feeding and armor traits may provide a fitness advantage to offspring of contrasting ecotypes, and theory predicts that such linked assemblages will evolve under conditions where strongly contrasting forms sometimes meet and hybridize (Kirkpatrick and Barton 2006), as frequently occurs in marine–stream and benthic–limnetic stickleback species pairs.

Parallel evolution of polygenic traits

Large-effect QTL for armor plate, pigment, and pelvic development that were previously mapped in this cross do not appear to be specific to this cross. Instead the same major loci (Colosimo *et al.* 2004; Cresko *et al.* 2004; Shapiro *et al.* 2004; Coyle *et al.* 2007), the same underlying genes

(Chan *et al.* 2010), and sometimes even the same freshwater alleles (Colosimo *et al.* 2005; Miller *et al.* 2007) are used repeatedly in other populations that have evolved similar phenotypes (Jones *et al.* 2012a). All of these well-studied examples involve QTL that control half or more of the variance in the corresponding trait, and it remains unclear whether QTL with smaller effects, like many of those identified here, will also be used in parallel in other populations. Previous studies have mapped two gill raker number and four dorsal spine length QTL in a Priest Lake benthic × limnetic cross (Peichel *et al.* 2001). Both of the Priest Lake raker QTL overlap raker QTL found in this study, although anatomical domains affected by these QTL differ. In contrast, only one of the four Priest Lake dorsal spine QTL overlaps any of the spine QTL presented here. Although the Priest Lake cross also used benthic forms, it was a backcross to freshwater limnetic fish, and trophic and armor selective pressures likely differ on limnetic *vs.* marine fish. It is also likely that some genetic variation is not fixed within a population and that the spectrum of QTL observed in a genetic cross could be different if different individuals from the same population were used. Additional crosses are needed to test whether similar genetic loci underlie repeated evolution of similar trophic and armor phenotypes in many benthic lake and stream forms that have evolved from marine ancestors.

Acknowledgments

We thank Steve Arnott, Anne Knecht, and Joy Yang for helpful discussions. This work was supported in part by a Jane Coffin Childs Fund Fellowship, a March of Dimes Basil O'Connor award, a Pew Scholar in Biomedical Sciences award supported by the Pew Charitable Trusts, and National Institutes of Health (NIH) grant DE021475 (to C.T.M.); National Science Foundation Graduate Research Fellowships (to A.M.G. and B.R.S.); a Helen Hay Whitney Foundation fellowship (to M.D.S.); Burroughs Wellcome Fund Career Awards in the Biomedical Sciences (to M.D.S. and C.L.P.); a Canada Research Chair and grants from the National Sciences and Engineering Research Council and the Canada Foundation for Innovation (to D.S.); and an NIH Center for Excellence in Genomic Studies grant (5P50HG002568) and investigator position at the Howard Hughes Medical Institute (to D.M.K.).

Literature Cited

Ahn, D. G., and G. Gibson, 1999 Axial variation in the three-spine stickleback: genetic and environmental factors. Evol. Dev. 1: 100–112.

Albert, A. Y., S. Sawaya, T. H. Vines, A. K. Knecht, C. T. Miller *et al.*, 2008 The genetics of adaptive shape shift in stickleback: pleiotropy and effect size. Evolution 62: 76–85.

Anker, G. C., 1974 Morphology and kinetics of the head of the stickleback, *Gasterosteus aculeatus*. Trans. Zool. Soc. Lond. 32: 311–416.

Barrett, R. D. H., and D. Schluter, 2008 Adaptation from standing genetic variation. Trends Ecol. Evol. 23: 38–44.

Barrett, R. D. H., S. M. Rogers, and D. Schluter, 2008 Natural selection on a major armor gene in threespine stickleback. Science 322: 255–257.

Bell, M. A., and S. A. Foster, 1994 *The Evolutionary Biology of the Threespine Stickleback*. Oxford University Press, New York.

Bell, M. A., M. P. Travis, and D. M. Blouw, 2006 Inferring natural selection in a fossil threespine stickleback. Paleobiology 32: 562–577.

Bentzen, P., and J. D. McPhail, 1984 Ecology and evolution of sympatric sticklebacks (*Gasterosteus*): specialization for alternative trophic niches in the Enos Lake species pair. Can. J. Zool. 62: 2280–2286.

Broman, K. W., and S. Sen, 2009 *A Guide to QTL Mapping with R/qtl*. Springer, Dordrecht, The Netherlands.

Burke, J. M., S. Tang, S. J. Knapp, and L. H. Rieseberg, 2002 Genetic analysis of sunflower domestication. Genetics 161: 1257–1267.

Caldecutt, W. J., M. A. Bell, and J. A. Buckland-Nicks, 2001 Sexual dimorphism and geographic variation in dentition of threespine stickleback, *Gasterosteus aculeatus*. Copeia 2001: 936–944.

Carroll, S. B., 2008 Evo-devo and an expanding evolutionary synthesis: a genetic theory of morphological evolution. Cell 134: 25–36.

Chan, Y. F., M. E. Marks, F. C. Jones, G. Villarreal, Jr., M. D. Shapiro *et al.*, 2010 Adaptive evolution of pelvic reduction in sticklebacks by recurrent deletion of a Pitx1 enhancer. Science 327: 302–305.

Clarke, C. A., P. M. Sheppard, and I. W. Thornton, 1968 Genetics of mimetic butterfly *Papilio Memnon* L. Philos. Trans. R. Soc. Lond. B Biol. Sci. 254: 37–89.

Colosimo, P. F., C. L. Peichel, K. Nereng, B. K. Blackman, M. D. Shapiro *et al.*, 2004 The genetic architecture of parallel armor plate reduction in threespine sticklebacks. PLoS Biol. 2: e109.

Colosimo, P. F., K. E. Hosemann, S. Balabhadra, G. Villarreal, Jr., M. Dickson *et al.*, 2005 Widespread parallel evolution in sticklebacks by repeated fixation of *Ectodysplasin* alleles. Science 307: 1928–1933.

Coyle, S. M., F. A. Huntingford, and C. L. Peichel, 2007 Parallel evolution of *Pitx1* underlies pelvic reduction in Scottish threespine stickleback (*Gasterosteus aculeatus*). J. Hered. 98: 581–586.

Cresko, W. A., A. Amores, C. Wilson, J. Murphy, M. Currey *et al.*, 2004 Parallel genetic basis for repeated evolution of armor loss in Alaskan threespine stickleback populations. Proc. Natl. Acad. Sci. USA 101: 6050–6055.

Cubbage, C. C., and P. M. Mabee, 1996 Development of the cranium and paired fins in the zebrafish *Danio rerio* (*Ostariophysi*, *cyprinidae*). J. Morphol. 229: 121–160.

Darwin, C., 1877 *The Different Forms of Flowers on Plants of the Same Species*. J. Murray, London.

Davidson, E. H., and M. S. Levine, 2008 Properties of developmental gene regulatory networks. Proc. Natl. Acad. Sci. USA 105: 20063–20066.

deVicente, M. C., and S. D. Tanksley, 1993 QTL analysis of transgressive segregation in an interspecific tomato cross. Genetics 134: 585–596.

Dupuis, J., and D. Siegmund, 1999 Statistical methods for mapping quantitative trait loci from a dense set of markers. Genetics 151: 373–386.

Falconer, D. S., 1989 *Introduction to Quantitative Genetics*. Pearson, New York.

Feder, J. L., R. Gejji, T. H. Powell, and P. Nosil, 2011 Adaptive chromosomal divergence driven by mixed geographic mode of evolution. Evolution 65: 2157–2170.

Ferguson, L., S. F. Lee, N. Chamberlain, N. Nadeau, M. Joron *et al.*, 2010 Characterization of a hotspot for mimicry: assembly of a butterfly wing transcriptome to genomic sequence at the *HmYb/Sb* locus. Mol. Ecol. 19(Suppl 1): 240–254.

Fisher, R. A., 1928 The possible modification of the response of the wild type to recurrent mutations. Am. Nat. 62: 115–126.

Fishman, L., A. Stathos, P. M. Beardsley, C. F. Williams, and J. P. Hill, 2013 Chromosomal rearrangements and the genetics of reproductive barriers in *Mimulus* (monkeyflowers). Evolution 67: 2547–2560.

Griswold, C. K., and M. C. Whitlock, 2003 The genetics of adaptation: the roles of pleiotropy, stabilizing selection and drift in shaping the distribution of bidirectional fixed mutational effects. Genetics 165: 2181–2192.

Gross, H. P., 1978 Natural selection by predators on the defensive apparatus of the three-spined stickleback, *Gasterosteus aculeatus* L. Can. J. Zool. 56: 398–413.

Gross, H. P., and J. M. Anderson, 1984 Geographic variation in the gillrakers and diet of European threespine sticklebacks, *Gasterosteus aculeatus*. Copeia 1984: 87–97.

Gruber, J. D., K. Vogel, G. Kalay, and P. J. Wittkopp, 2012 Contrasting properties of gene-specific regulatory, coding, and copy number mutations in *Saccharomyces cerevisiae*: frequency, effects, and dominance. PLoS Genet. 8: e1002497.

Hagen, D. W., and L. G. Gilbertson, 1972 Geographic variation and environmental selection in *Gasterosteus aculeatus* L. in the Pacific Northwest, America. Evolution 26: 32–51.

Haldane, J. B. S., 1927 A mathematical theory of natural and artificial selection, part V: selection and mutation. Proc. Camb. Philos. Soc. 23: 838–844.

Hermann, K., U. Klahre, M. Moser, H. Sheehan, T. Mandel *et al.*, 2013 Tight genetic linkage of prezygotic barrier loci creates a multifunctional speciation island in petunia. Curr. Biol. 23: 873–877.

Hohenlohe, P. A., S. Bassham, P. D. Etter, N. Stiffler, E. A. Johnson *et al.*, 2010 Population genomics of parallel adaptation in threespine stickleback using sequenced RAD tags. PLoS Genet. 6: e1000862.

Hoogland, R. D., D. Morris, and N. Tinbergen, 1957 The spines of sticklebacks (*Gasterosteus* and *Pygosteus*) as means of defense against predators (*Perca* and *Esox*). Behaviour 10: 205–230.

Hunt, G., M. A. Bell, and M. P. Travis, 2008 Evolution toward a new adaptive optimum: phenotypic evolution in a fossil stickleback lineage. Evolution 62: 700–710.

Jones, F. C., Y. F. Chan, J. Schmutz, J. Grimwood, S. D. Brady *et al.*, 2012a A genome-wide SNP genotyping array reveals patterns of global and repeated species-pair divergence in sticklebacks. Curr. Biol. 22: 83–90.

Jones, F. C., M. G. Grabherr, Y. F. Chan, P. Russell, E. Mauceli *et al.*, 2012b The genomic basis of adaptive evolution in threespine sticklebacks. Nature 484: 55–61.

Joron, M., R. Papa, M. Beltran, N. Chamberlain, J. Mavarez *et al.*, 2006 A conserved supergene locus controls colour pattern diversity in *Heliconius* butterflies. PLoS Biol. 4: 1831–1840.

Joron, M., L. Frezal, R. T. Jones, N. L. Chamberlain, S. F. Lee *et al.*, 2011 Chromosomal rearrangements maintain a polymorphic supergene controlling butterfly mimicry. Nature 477: 203–206.

Kenney-Hunt, J. P., B. Wang, E. A. Norgard, G. Fawcett, D. Falk *et al.*, 2008 Pleiotropic patterns of quantitative trait loci for 70 murine skeletal traits. Genetics 178: 2275–2288.

Kimmel, C. B., B. Ullmann, C. Walker, C. Wilson, M. Currey *et al.*, 2005 Evolution and development of facial bone morphology in threespine sticklebacks. Proc. Natl. Acad. Sci. USA 102: 5791–5796.

Kimmel, C. B., W. A. Cresko, P. C. Phillips, B. Ullmann, M. Currey *et al.*, 2012 Independent axes of genetic variation and parallel evolutionary divergence of opercle bone shape in threespine stickleback. Evolution 66: 419–434.

Kimura, T., A. Shimada, N. Sakai, H. Mitani, K. Naruse *et al.*, 2007 Genetic analysis of craniofacial traits in the medaka. Genetics 177: 2379–2388.

Kingsley, D. M., and C. L. Peichel, 2007 The molecular genetics of evolutionary change in sticklebacks, pp. 41–81 in *Biology of the Three-Spine Stickleback*, edited by S. Ostlund-Nilsson, I. Mayer, and F. A. Huntingford. CRC Press, Boca Raton, FL.

Kirkpatrick, M., and N. Barton, 2006 Chromosome inversions, local adaptation and speciation. Genetics 173: 419–434.

Kislalioglu, M., and R. N. Gibson, 1977 Feeding relationship of shallow water fishes in a Scottish sea loch. J. Fish Biol. 11: 257–266.

Kitano, J., S. Mori, and C. L. Peichel, 2007 Sexual dimorphism in the external morphology of the threespine stickleback (*Gasterosteus aculeatus*). Copeia 2007: 336–349.

Kitano, J., J. A. Ross, S. Mori, M. Kume, F. C. Jones *et al.*, 2009 A role for a neo-sex chromosome in stickleback speciation. Nature 461: 1079–1083.

Kurian, V., and A. J. Richards, 1997 A new recombinant in the heteromorphy '*S*' supergene in *Primula*. Heredity 78: 383–390.

Lavin, P. A., and J. D. McPhail, 1986 Adaptive divergence of trophic phenotype among freshwater populations of the threespine stickleback (*Gasterosteus aculeatus*). Can. J. Fish. Aquat. Sci. 43: 2455–2463.

Lemos, B., L. O. Araripe, P. Fontanillas, and D. L. Hartl, 2008 Dominance and the evolutionary accumulation of *cis*- and *trans*-effects on gene expression. Proc. Natl. Acad. Sci. USA 105: 14471–14476.

Li, J., M. A. Webster, M. C. Smith, and P. M. Gilmartin, 2011 Floral heteromorphy in *Primula vulgaris*: progress towards isolation and characterization of the *S* locus. Ann. Bot. 108: 715–726.

Lindsey, C. C., 1962 Experimental study of meristic variation in a population of threespine stickleback, *Gasterosteus aculeatus*. Can. J. Zool. 40: 271–312.

Lowry, D. B., and J. H. Willis, 2010 A widespread chromosomal inversion polymorphism contributes to a major life-history transition, local adaptation, and reproductive isolation. PLoS Biol. 8: e1000500.

Mallet, J., 1989 The genetics of warning colour in Peruvian hybrid zones of *Heliconius Erato* and *H. Melpomene*. Proc. R. Soc. Lond. B Biol. Sci. 236: 163–185.

Mather, K., 1950 The genetical architecture of heterostyly in *Primula sinensis*. Evolution 4: 340–352.

McGee, M. D., and P. C. Wainwright, 2013 Convergent evolution as a generator of phenotypic diversity in threespine stickleback. Evolution 67: 1204–1208.

McGee, M. D., D. Schluter, and P. C. Wainwright, 2013 Functional basis of ecological divergence in sympatric stickleback. BMC Evol. Biol. 13: 277.

McManus, C. J., J. D. Coolon, M. O. Duff, J. Eipper-Mains, B. R. Graveley *et al.*, 2010 Regulatory divergence in Drosophila revealed by mRNA-seq. Genome Res. 20: 816–825.

McPhail, J. D., 1992 Ecology and evolution of sympatric sticklebacks (*Gasterosteus*): evidence for a species pair in Paxton Lake, Texada Island, British Columbia. Can. J. Zool. 70: 361–369.

Miller, C. T., S. Beleza, A. A. Pollen, D. Schluter, R. A. Kittles *et al.*, 2007 *cis*-Regulatory changes in *Kit ligand* expression and parallel evolution of pigmentation in sticklebacks and humans. Cell 131: 1179–1189.

Minoux, M., and F. M. Rijli, 2010 Molecular mechanisms of cranial neural crest cell migration and patterning in craniofacial development. Development 137: 2605–2621.

Murray, J., and B. Clarke, 1976 Supergenes in polymorphic land snails I. *Partula taeniata*. Heredity 37: 253–269.

Noor, M. A., A. L. Cunningham, and J. C. Larkin, 2001 Consequences of recombination rate variation on quantitative trait locus mapping studies: simulations based on the *Drosophila melanogaster* genome. Genetics 159: 581–588.

Orr, H. A., 1991 A test of Fisher's theory of dominance. Proc. Natl. Acad. Sci. USA 88: 11413–11415.

Orr, H. A., and A. J. Betancourt, 2001 Haldane's sieve and adaptation from the standing genetic variation. Genetics 157: 875–884.

Peichel, C. L., K. S. Nereng, K. A. Ohgi, B. L. Cole, P. F. Colosimo *et al.*, 2001 The genetic architecture of divergence between threespine stickleback species. Nature 414: 901–905.

Protas, M., I. Tabansky, M. Conrad, J. B. Gross, O. Vidal *et al.*, 2008 Multi-trait evolution in a cave fish, *Astyanax mexicanus*. Evol. Dev. 10: 196–209.

Reimchen, T. E., 1980 Spine deficiency and polymorphism in a population of *Gasterosteus aculeatus*—an adaptation to predators. Can. J. Zool. 58: 1232–1244.

Reimchen, T. E., and J. S. Nelson, 1987 Habitat and morphological correlates to vertebral number as shown in a teleost, *Gasterosteus aculeatus*. Copeia 1987: 868–874.

Reimchen, T. E., E. M. Stinson, and J. S. Nelson, 1985 Multivariate differentiation of parapatric and allopatric populations of threespine stickleback in the Sangan River Watershed, Queen Charlotte Islands. Can. J. Zool. 63: 2944–2951.

Rieseberg, L. H., A. Widmer, A. M. Arntz, and J. M. Burke, 2002 Directional selection is the primary cause of phenotypic diversification. Proc. Natl. Acad. Sci. USA 99: 12242–12245.

Roberts, R. B., J. R. Ser, and T. D. Kocher, 2009 Sexual conflict resolved by invasion of a novel sex determiner in Lake Malawi cichlid fishes. Science 326: 998–1001.

Rockman, M. V., 2012 The QTN program and the alleles that matter for evolution: all that's gold does not glitter. Evolution 66: 1–17.

Rogers, S. M., P. Tamkee, B. Summers, S. Balabahadra, M. Marks *et al.*, 2012 Genetic signature of adaptive peak shift in threespine stickleback. Evolution 66: 2439–2450.

Ronfort, J., and S. Glemin, 2013 Mating system, Haldane's sieve, and the domestication process. Evolution 67: 1518–1526.

Schluter, D., 2000 *The Ecology of Adaptive Radiation*. Oxford University Press, Oxford.

Schluter, D., and J. D. McPhail, 1992 Ecological character displacement and speciation in sticklebacks. Am. Nat. 140: 85–108.

Schluter, D., K. B. Marchinko, R. D. H. Barrett, and S. M. Rogers, 2010 Natural selection and the genetics of adaptation in threespine stickleback. Philos. Trans. R. Soc. Lond. B Biol. Sci. 365: 2479–2486.

Shapiro, M. D., M. E. Marks, C. L. Peichel, B. K. Blackman, K. S. Nereng *et al.*, 2004 Genetic and developmental basis of evolutionary pelvic reduction in threespine sticklebacks. Nature 428: 717–723.

Stern, D. L., 2000 Evolutionary developmental biology and the problem of variation. Evolution 54: 1079–1091.

Stern, D. L., and V. Orgogozo, 2008 The loci of evolution: How predictable is genetic evolution? Evolution 62: 2155–2177.

Streisfeld, M. A., and M. D. Rausher, 2011 Population genetics, pleiotropy, and the preferential fixation of mutations during adaptive evolution. Evolution 65: 629–642.

Studer, A. J., and J. F. Doebley, 2011 Do large effect QTL fractionate? A case study at the maize domestication QTL *teosinte branched1*. Genetics 188: 673–681.

Swain, D. P., 1992a The functional basis of natural selection for vertebral traits of larvae in the stickleback *Gasterosteus aculeatus*. Evolution 46: 987–997.

Swain, D. P., 1992b Selective predation for vertebral phenotype in *Gasterosteus aculeatus*: reversal in the direction of selection at different larval sizes. Evolution 46: 998–1013.

Tripathi, N., M. Hoffmann, E. M. Willing, C. Lanz, D. Weigel *et al.*, 2009 Genetic linkage map of the guppy, *Poecilia reticulata*, and quantitative trait loci analysis of male size and colour variation. Proc. Biol. Sci. 276: 2195–2208.

Wagner, G. P., M. Pavlicev, and J. M. Cheverud, 2007 The road to modularity. Nat. Rev. Genet. 8: 921–931.

Wark, A. R., M. G. Mills, L. H. Dang, Y. F. Chan, F. C. Jones *et al.*, 2012 Genetic architecture of variation in the lateral line sensory system of threespine sticklebacks. G3 2: 1047–1056.

Willacker, J. J., F. A. von Hippel, P. R. Wilton, and K. M. Walton, 2010 Classification of threespine stickleback along the benthic-limnetic axis. Biol. J. Linn. Soc. Lond. 101: 595–608.

Winge, O., 1927 The location of eighteen genes in *Lebistes reticulatus*. J. Genet. 18: 1–43.

Yeaman, S., and M. C. Whitlock, 2011 The genetic architecture of adaptation under migration-selection balance. Evolution 65: 1897–1911.

Communicating editor: C. D. Jones

GENETICS

Supporting Information
http://www.genetics.org/lookup/suppl/doi:10.1534/genetics.114.162420/-/DC1

Modular Skeletal Evolution in Sticklebacks Is Controlled by Additive and Clustered Quantitative Trait Loci

Craig T. Miller, Andrew M. Glazer, Brian R. Summers, Benjamin K. Blackman, Andrew R. Norman, Michael D. Shapiro, Bonnie L. Cole, Catherine L. Peichel, Dolph Schluter, and David M. Kingsley

DOI: 10.1534/genetics.114.162420

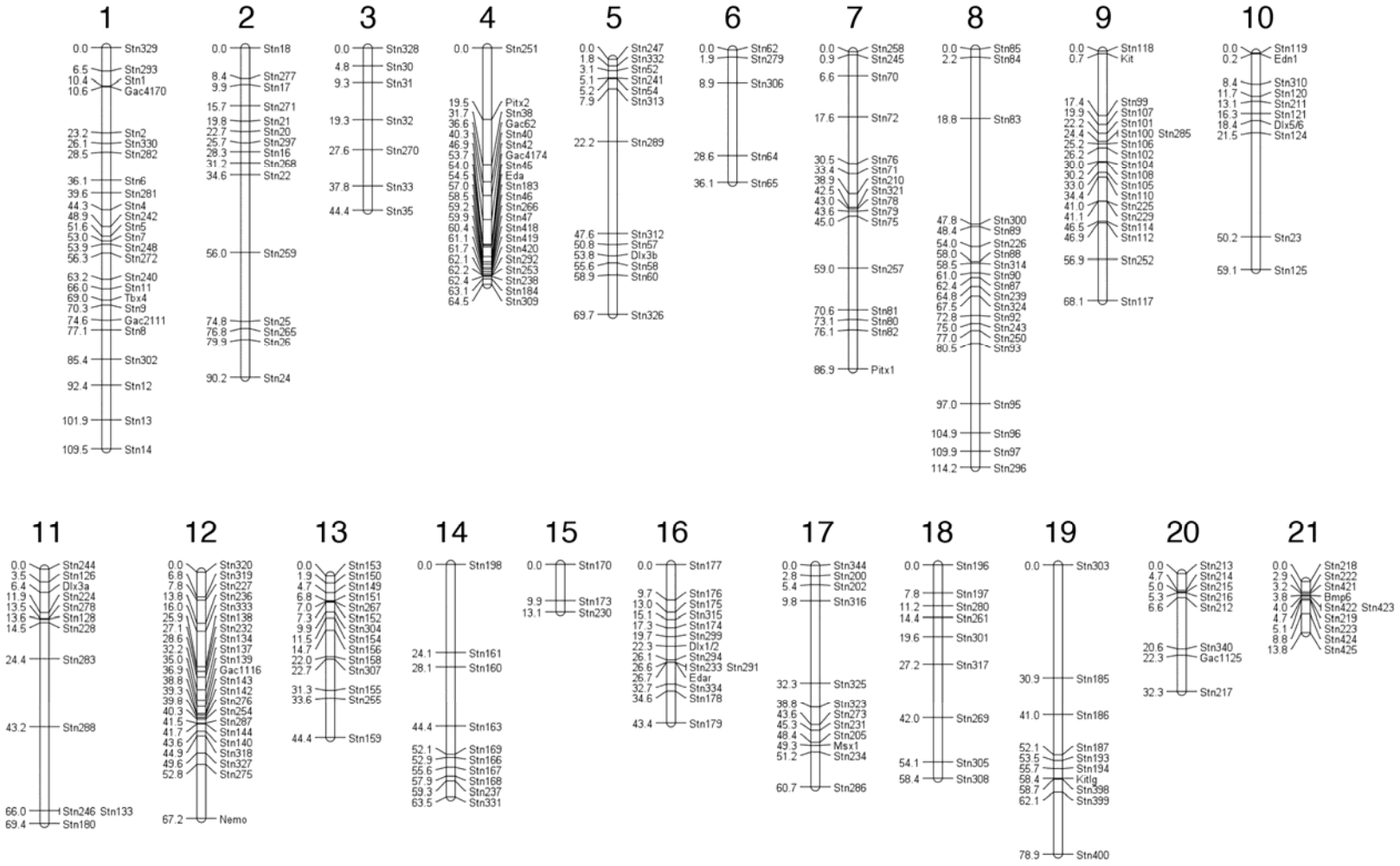

Figure S1 Genetic linkage map. The markers labeled on the map with gene names use the following nearby previously published (COLOSIMO *et al.* 2005; KNECHT *et al.* 2007a; MILLER *et al.* 2007; SHAPIRO *et al.* 2004) microsatellite markers: *Tbx4* = Stn221, *Pitx2*= Stn220, *Eda* = Stn365, *Pitx1*= Stn336, *Nemo* = Stn394, *Edar* = Stn337, *Kitlg* = Stn191 (since *Kitlg* does not recombine from Stn191 in this family). New markers labeled on the map with gene names use the following Stn markers and are described in Table S1 (*Bmp6* = Stn483, *Dlx1/2* = Stn339, *Dlx3a* = Stn430, *Dlx3b* = Stn427, *Dlx5/6* = Stn338, *Edn1* = Stn429, *Kit* = Stn428, *Msx1* = Stn343).

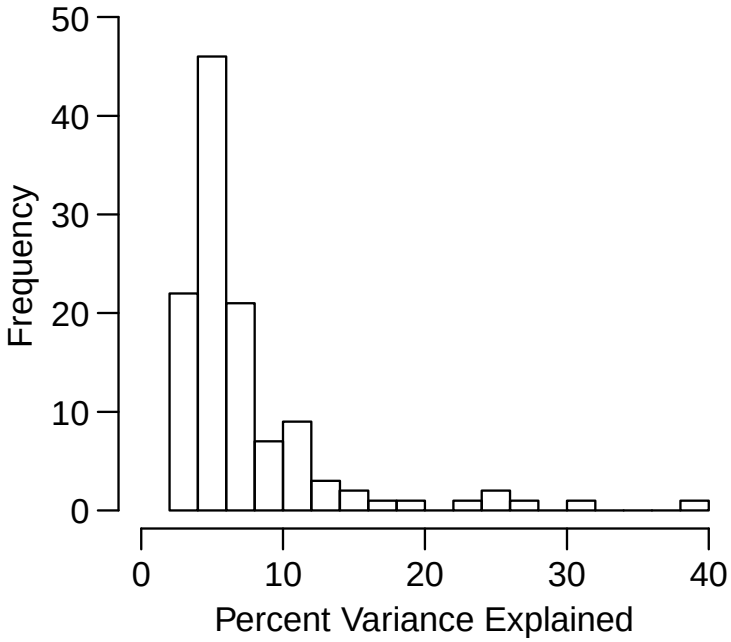

Figure S2 Distribution of percent variance explained (PVE). Histogram of PVE for the 118 filtered QTL. There are many QTL of small effect and few QTL of large effect.

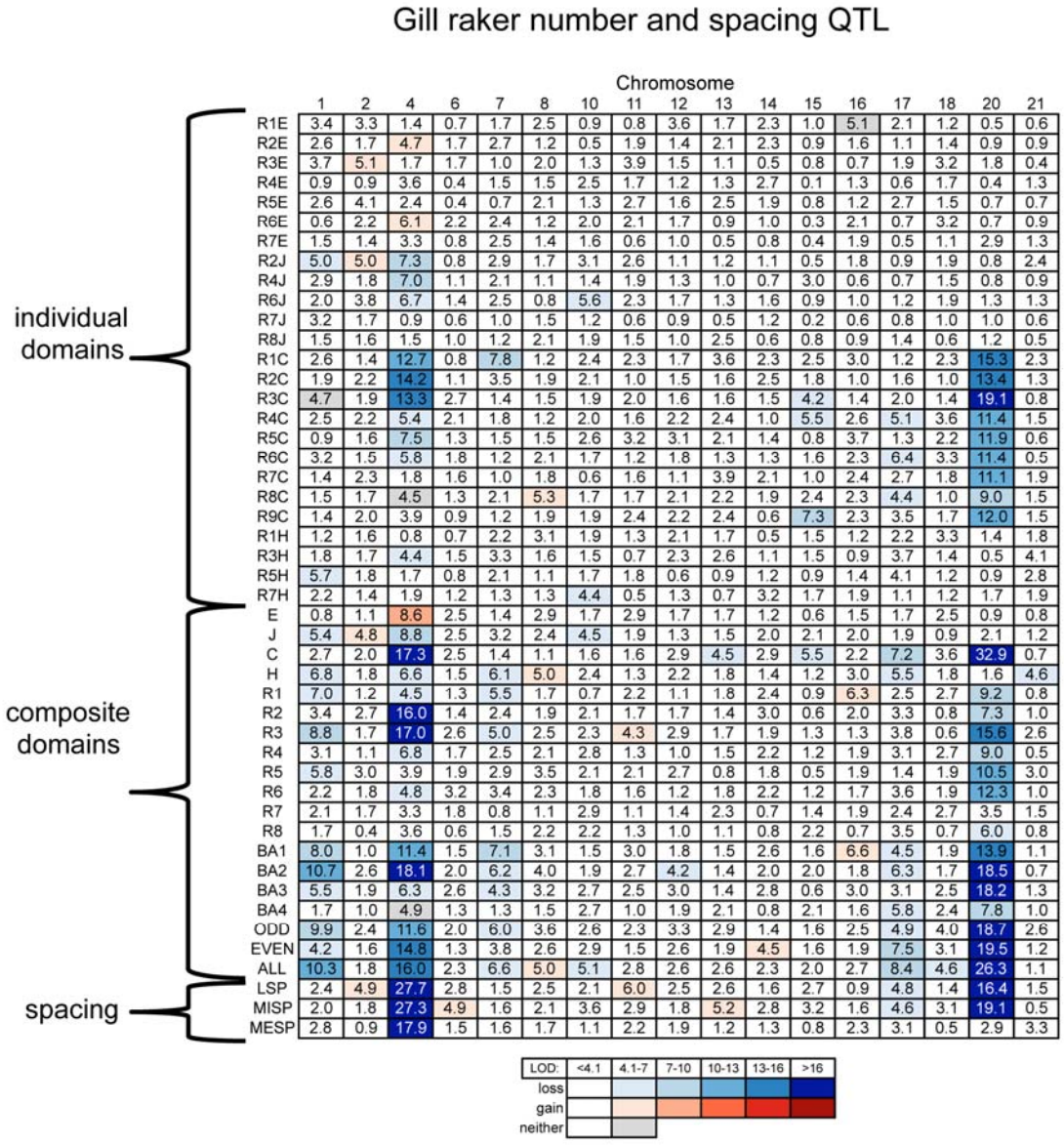

Figure S3 Heat map of gill raker QTL. Summary of LOD scores by phenotype for gill raker number and spacing QTL. Traits (abbreviations in Table S2) are listed to the left. Chromosomes with significant QTL detected are shown as columns. For each trait, the highest LOD score of any marker on each chromosome is shown, with LOD scores colored with the heat map shown at the bottom, with "gain" traits (where benthic allele confers more or bigger bones) colored red and "loss" traits (where benthic allele confers fewer or smaller bones) colored blue. Heterotic QTL (where homozygous marine and benthic F2 fish do not differ significantly in phenotype by two-tailed t-test) are shaded gray.

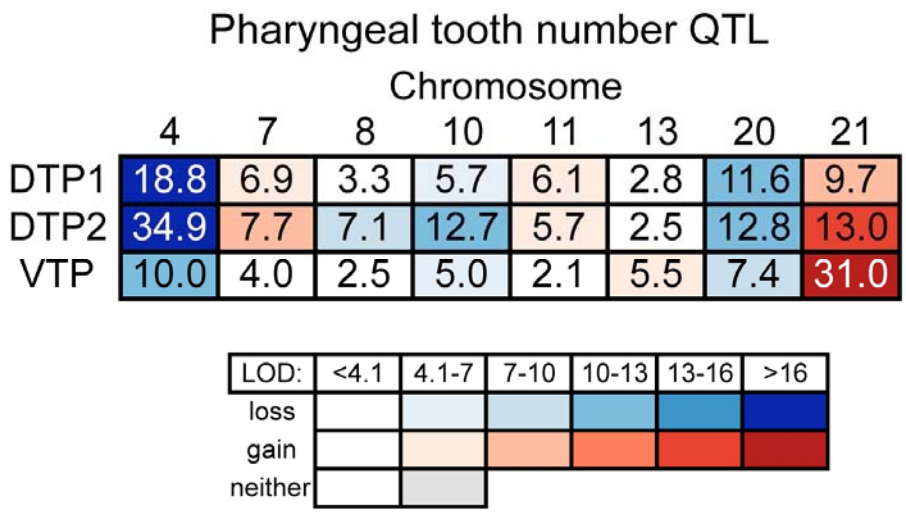

Figure S4 Heat map of pharyngeal tooth number QTL. Summary of LOD scores by phenotype for pharyngeal tooth number. Traits (abbreviations in Table S2) are listed to the left. Chromosomes with significant QTL detected are shown as columns. For each trait, the highest LOD score of any marker on each chromosome is shown, with LOD scores colored with the heat map shown at the bottom, with "gain" traits (where benthic allele confers more or bigger bones) colored red and "loss" traits (where benthic allele confers fewer or smaller bones) colored blue. Heterotic QTL (where homozygous marine and benthic F2 fish do not differ significantly in phenotype by two-tailed t-test) are shaded gray.

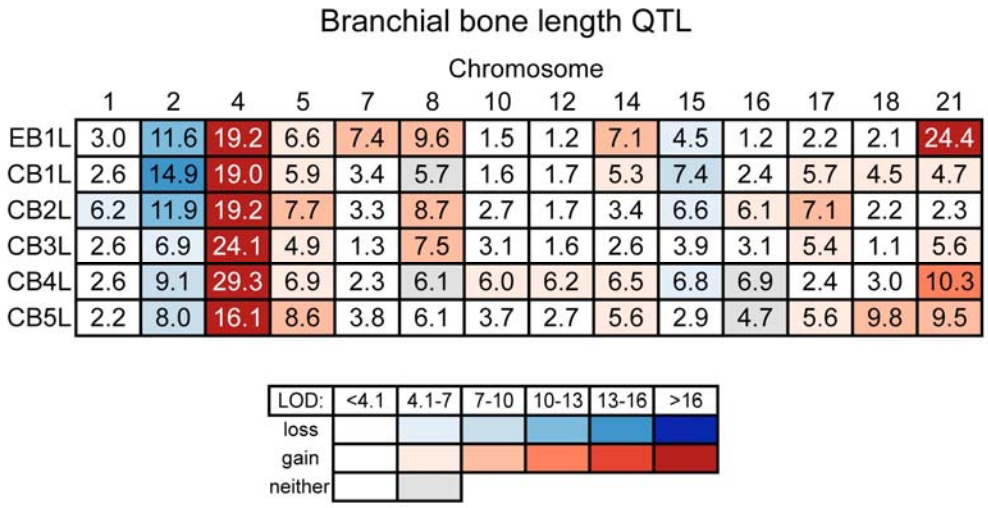

Figure S5 Heat map of branchial bone length QTL. Summary of LOD scores by phenotype for branchial bone length QTL. Traits (abbreviations in Table S2) are listed to the left. Chromosomes with significant QTL detected are shown as columns. For each trait, the highest LOD score of any marker on each chromosome is shown, with LOD scores colored with the heat map shown at the bottom, with "gain" traits (where benthic allele confers more or bigger bones) colored red and "loss" traits (where benthic allele confers fewer or smaller bones) colored blue. Heterotic QTL (where homozygous marine and benthic F2 fish do not differ significantly in phenotype by two-tailed t-test) are shaded gray.

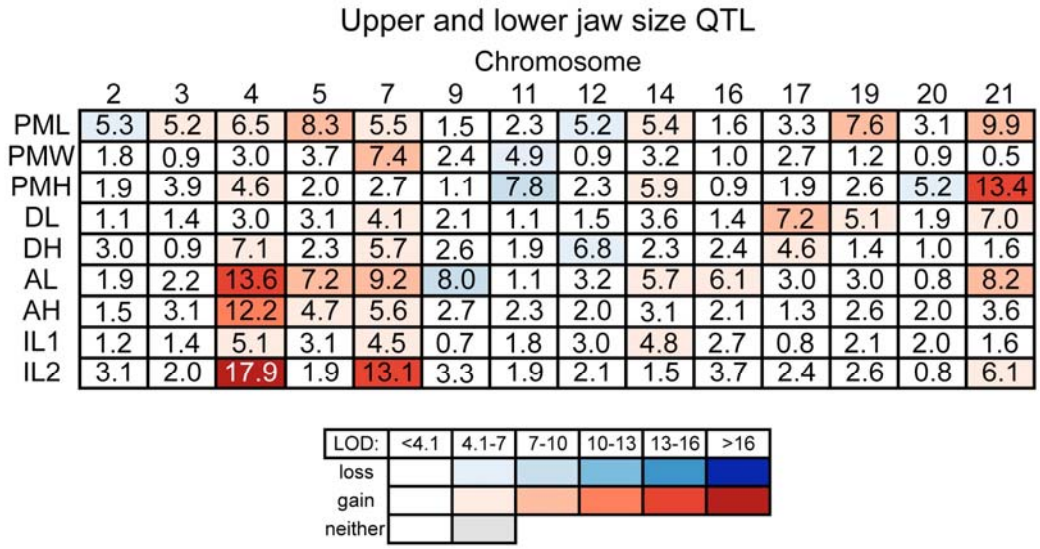

Figure S6 Heat map of jaw size QTL. Summary of LOD scores by phenotype for upper and lower jaw size QTL. Traits (abbreviations in Table S2) are listed to the left. Chromosomes with significant QTL detected are shown as columns. For each trait, the highest LOD score of any marker on each chromosome is shown, with LOD scores colored with the heat map shown at the bottom, with "gain" traits (where benthic allele confers more or bigger bones) colored red and "loss" traits (where benthic allele confers fewer or smaller bones) colored blue. Heterotic QTL (where homozygous marine and benthic F2 fish do not differ significantly in phenotype by two-tailed t-test) are shaded gray.

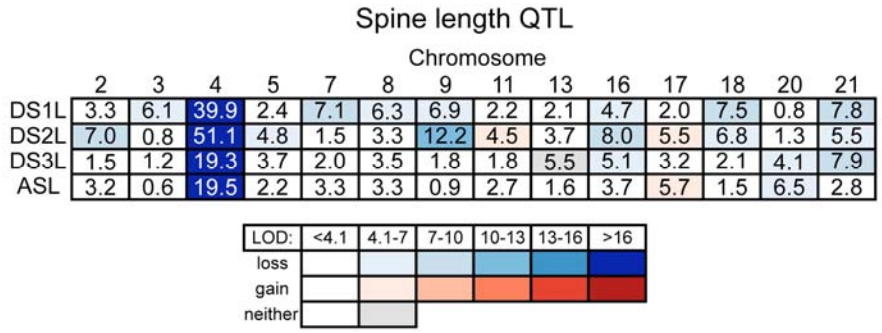

Figure S7 Heat map of spine length QTL. Summary of LOD scores by phenotype for spine length QTL. Traits (abbreviations in Table S2) are listed to the left. Chromosomes with significant QTL detected are shown as columns. For each trait, the highest LOD score of any marker on each chromosome is shown, with LOD scores colored with the heat map shown at the bottom, with "gain" traits (where benthic allele confers more or bigger bones) colored red and "loss" traits (where benthic allele confers fewer or smaller bones) colored blue. Heterotic QTL (where homozygous marine and benthic F2 fish do not differ significantly in phenotype by two-tailed t-test) are shaded gray.

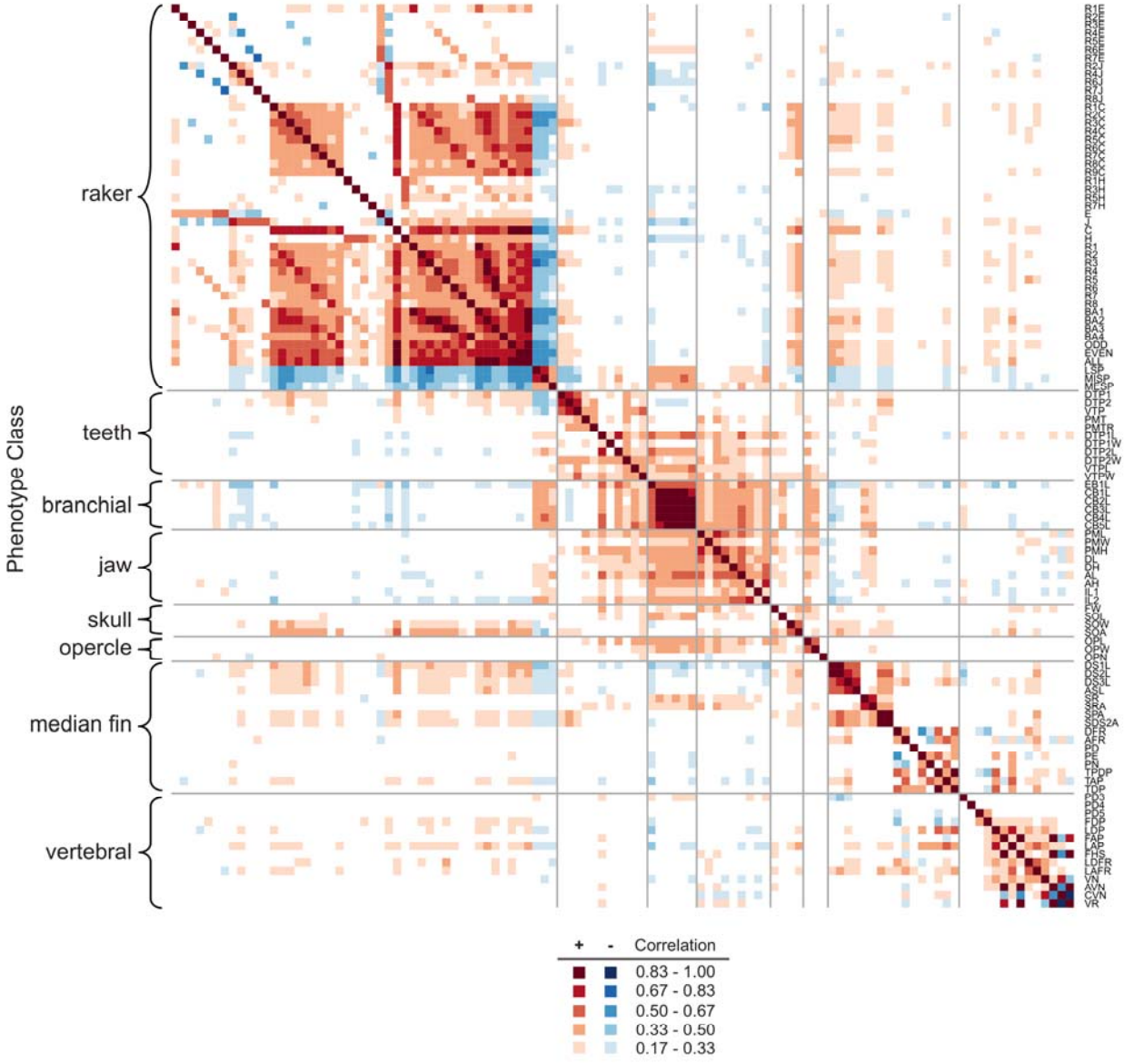

Figure S8 Trait covariance heat map. Classes of traits are grouped on the left, and abbreviations (defined in Table S2) of individual traits are listed on the right. For each pair of traits, the covariance of Z-scored phenotypes (correlation) is indicated by the heat map shown at bottom, with positive covariances colored red and negative covariances colored blue.

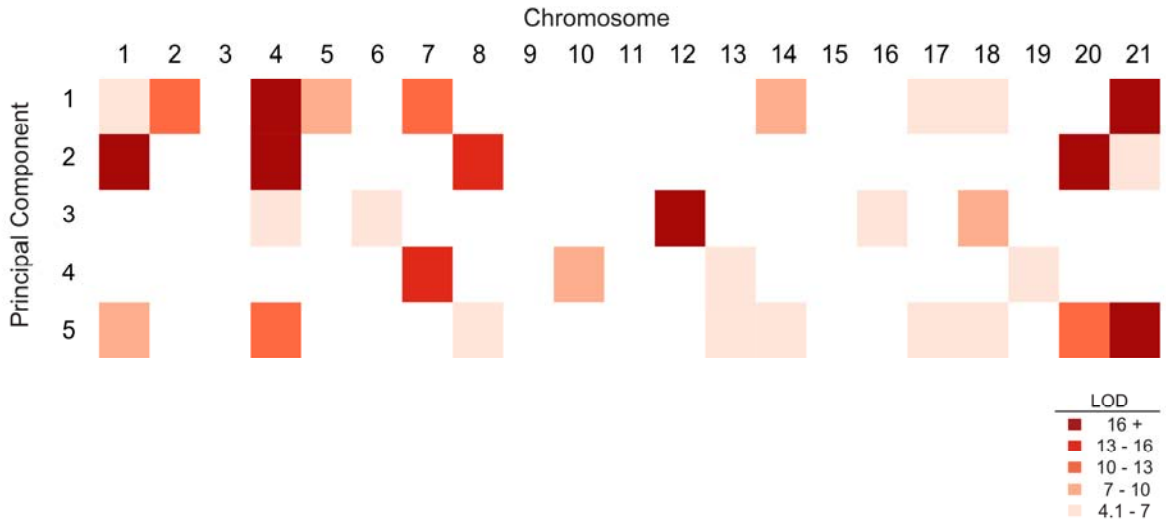

Figure S9 Genome-wide overview of principal component QTL. For each of the top five principal components, the LOD score for each significant QTL is indicated by the heat map shown in the bottom right. Further details of the QTL are presented in File S4.

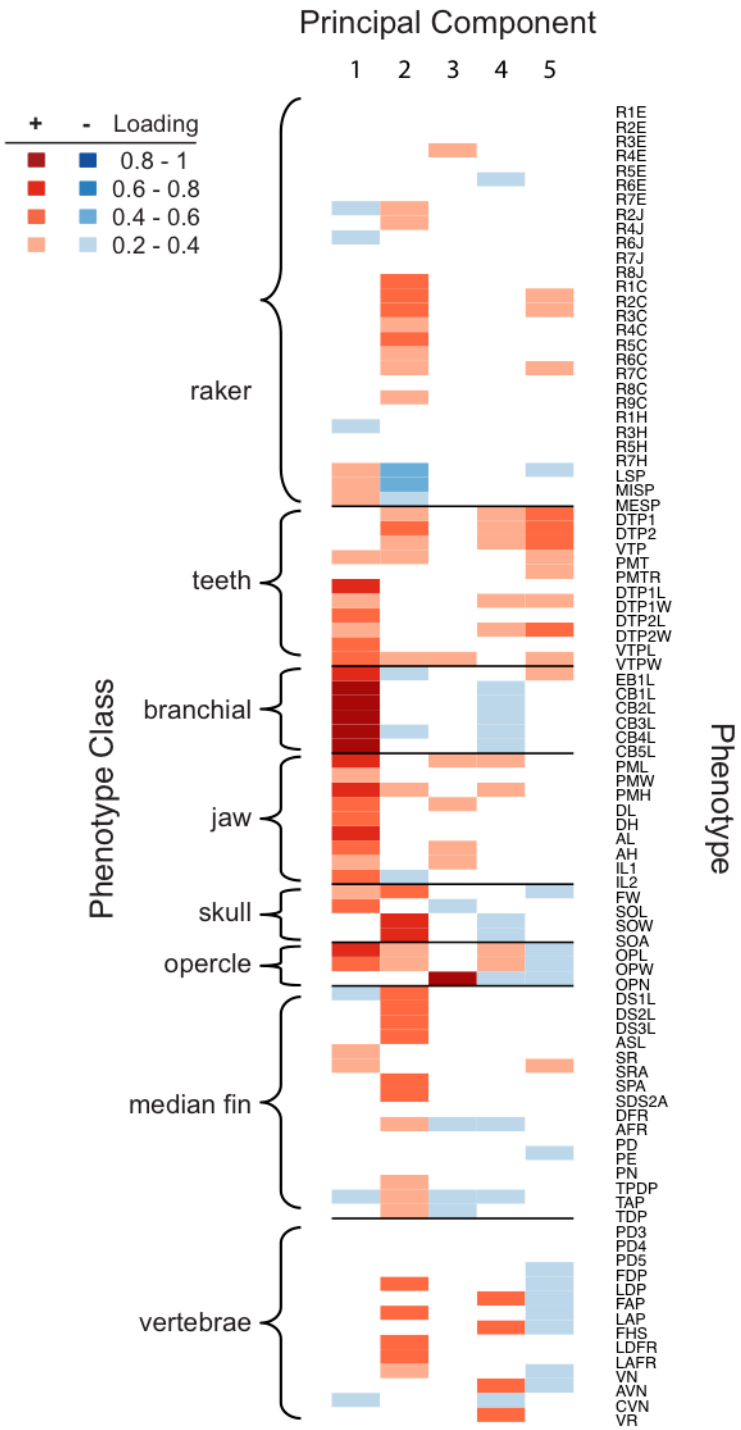

Figure S10 Trait loadings for top five principal components. Classes of traits are grouped on the left, and abbreviations (defined in Table S2) of individual traits are listed on the right. For each principal component, the loading for each trait is indicated by the heat map shown in the upper left, with positive loadings colored red and negative loadings colored blue.

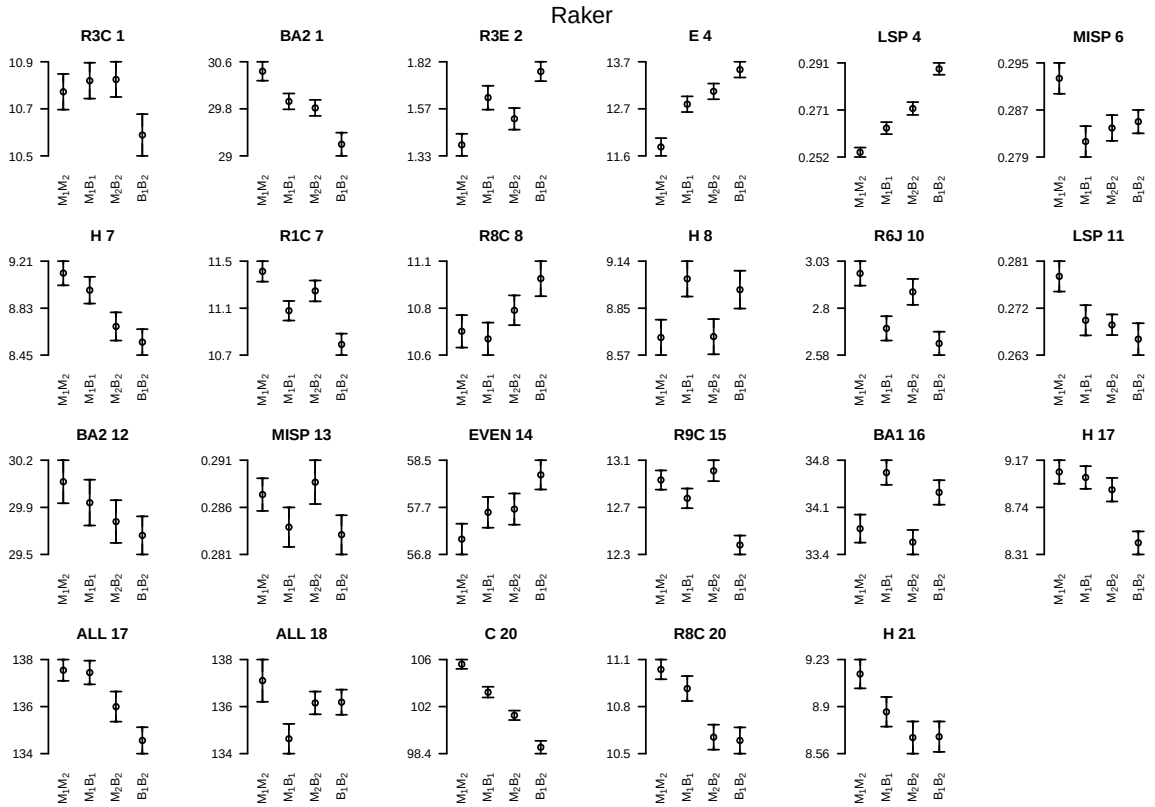

Figure S11 Mean trait phenotypes for different genotypes at peak marker for individual gill raker QTL. Each plot shows the mean size and sex corrected phenotype, if appropriate (back-transformed to a fish of 40 mm), and standard error of the mean for each genotypic class of F2 fish. See Table S2 for list of trait abbreviations, and Table S4 for peak markers used to define genotypic classes at corresponding QTL. Genotype abbreviations: M_1M_2 = homozygous marine, M_1B_1 and M_2B_2 = heterozygous marine/benthic, B_1B_2 = homozygous benthic.

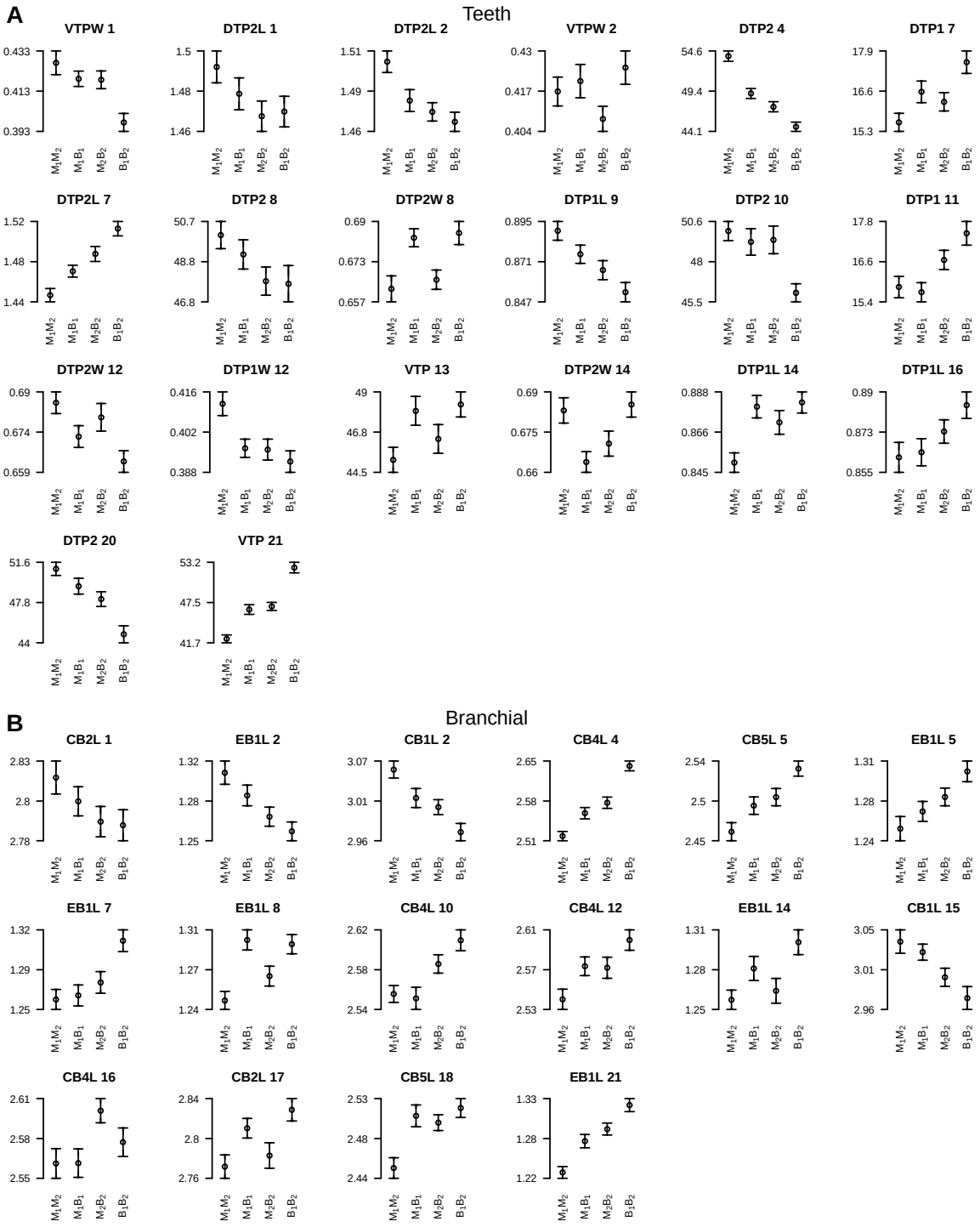

Figure S12 Mean trait phenotypes for different genotypes at peak marker for individual teeth (A) and branchial bone (B) QTL. Each plot shows the mean size and sex corrected phenotype, if appropriate (back-transformed to a fish of 40 mm), and standard error of the mean for each genotypic class of F2 fish. See Table S2 for list of trait abbreviations, and Table S4 for peak markers used to define genotypic classes at corresponding QTL. Genotype abbreviations: M_1M_2 = homozygous marine, M_1B_1 and M_2B_2 = heterozygous marine/benthic, B_1B_2 = homozygous benthic.

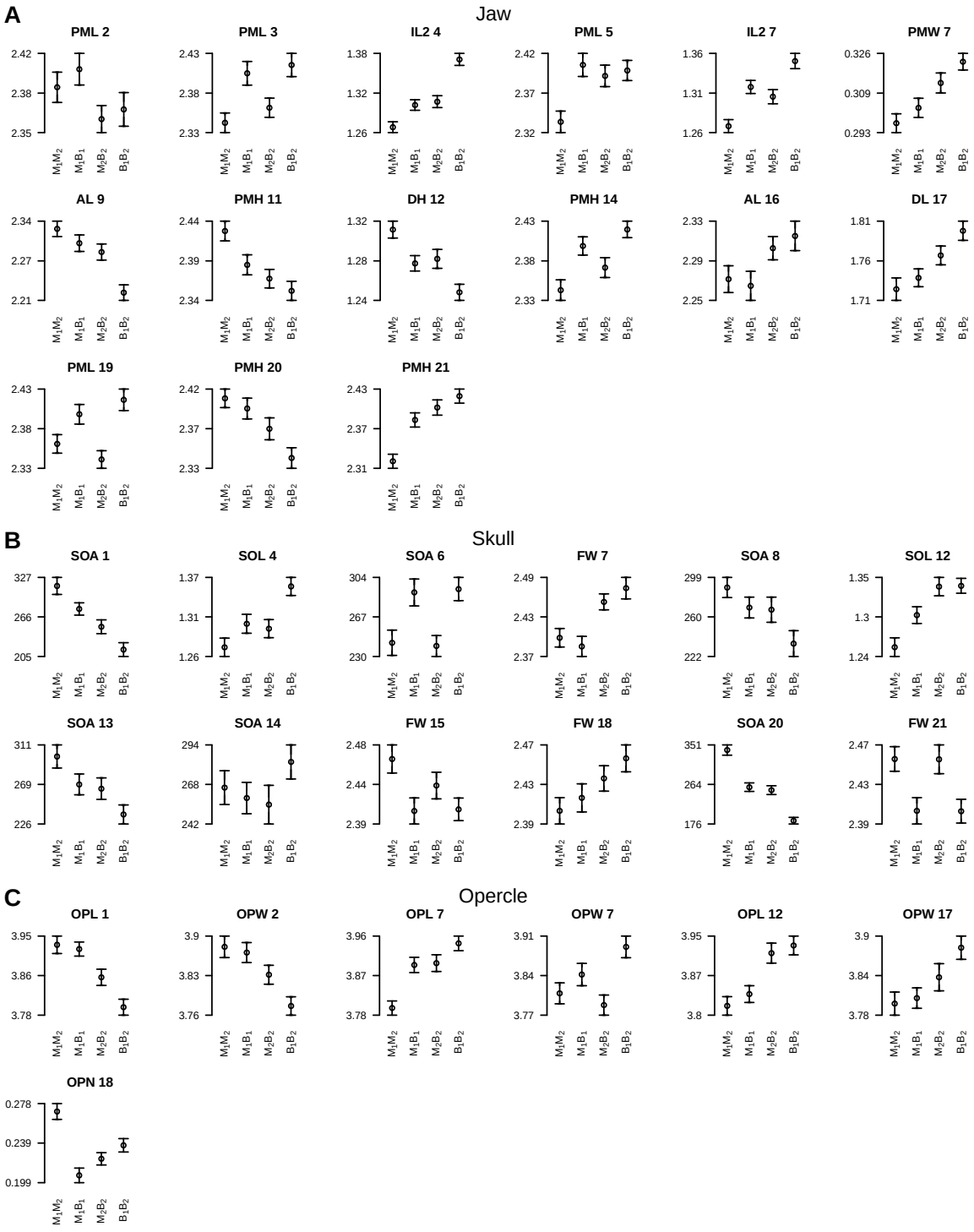

Figure S13 Mean trait phenotypes for different genotypes at peak marker for individual jaw (A), skull (B), and opercle (C) QTL. Each plot shows the mean size and sex corrected phenotype, if appropriate (back-transformed to a fish of 40 mm), and standard error of the mean for each genotypic class of F2 fish. See Table S2 for list of trait abbreviations, and Table S4 for peak markers used to define genotypic classes at corresponding QTL. Genotype abbreviations: M_1M_2 = homozygous marine, M_1B_1 and M_2B_2 = heterozygous marine/benthic, B_1B_2 = homozygous benthic.

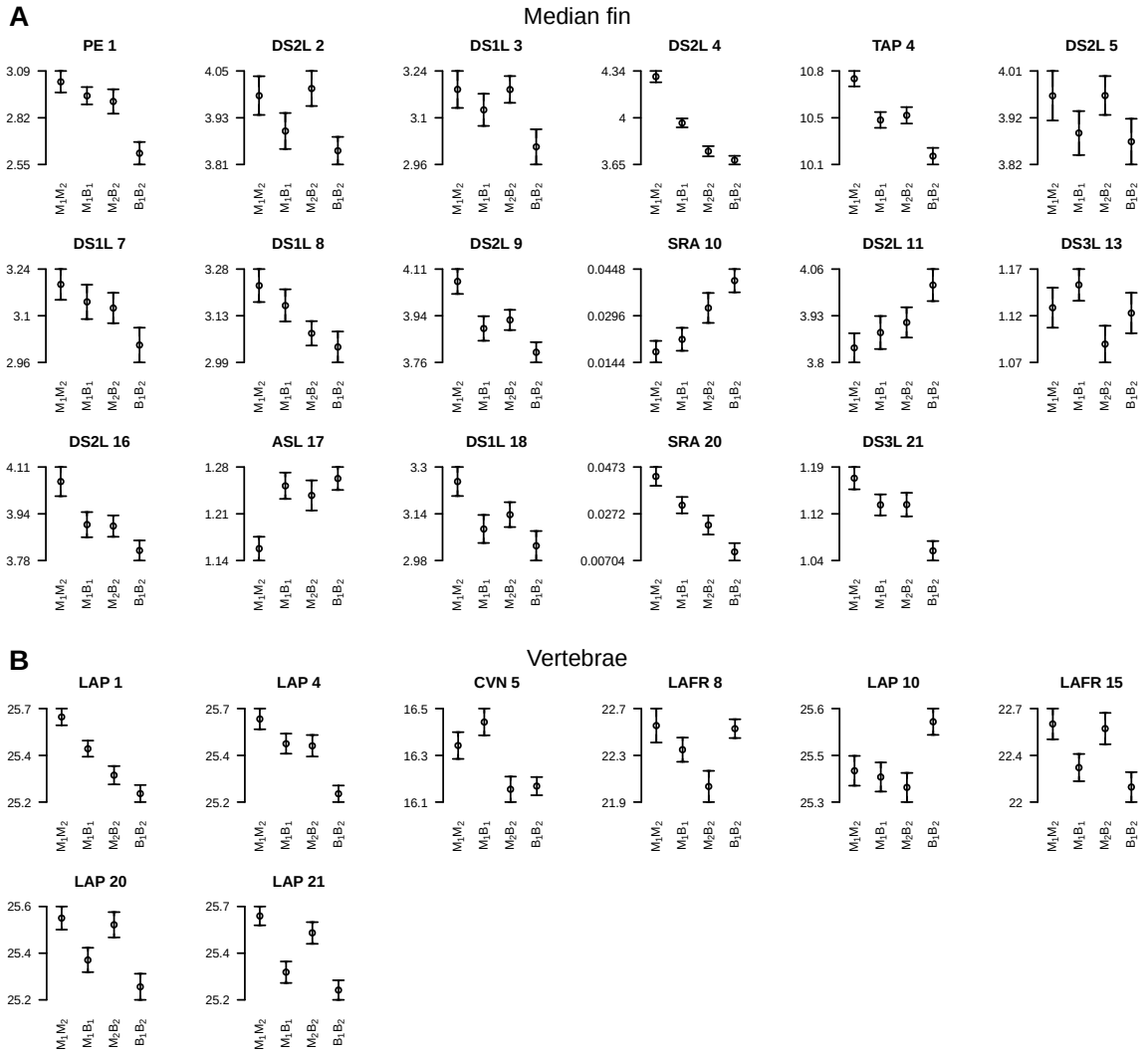

Figure S14 Mean trait phenotypes for different genotypes at peak marker for individual median fin (A) and vertebrae (B) QTL. Each plot shows the mean size and sex corrected phenotype, if appropriate (back-transformed to a fish of 40 mm), and standard error of the mean for each genotypic class of F2 fish. See Table S2 for list of trait abbreviations, and Table S4 for peak markers used to define genotypic classes at corresponding QTL. Genotype abbreviations: M_1M_2 = homozygous marine, M_1B_1 and M_2B_2 = heterozygous marine/benthic, B_1B_2 = homozygous benthic.

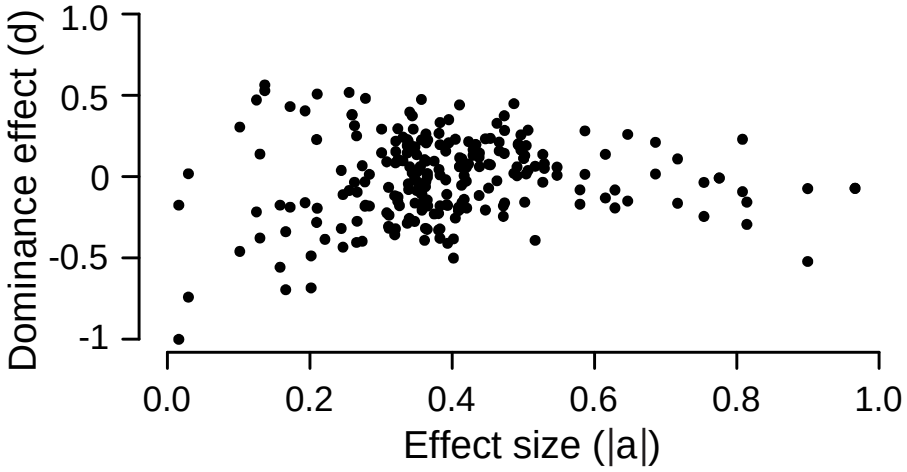

Figure S15 Relation between dominance (*d*, y-axis) and absolute value of *a,* the additive coefficient (x-axis). The range of observed *d* values appears greater with smaller effect sizes.

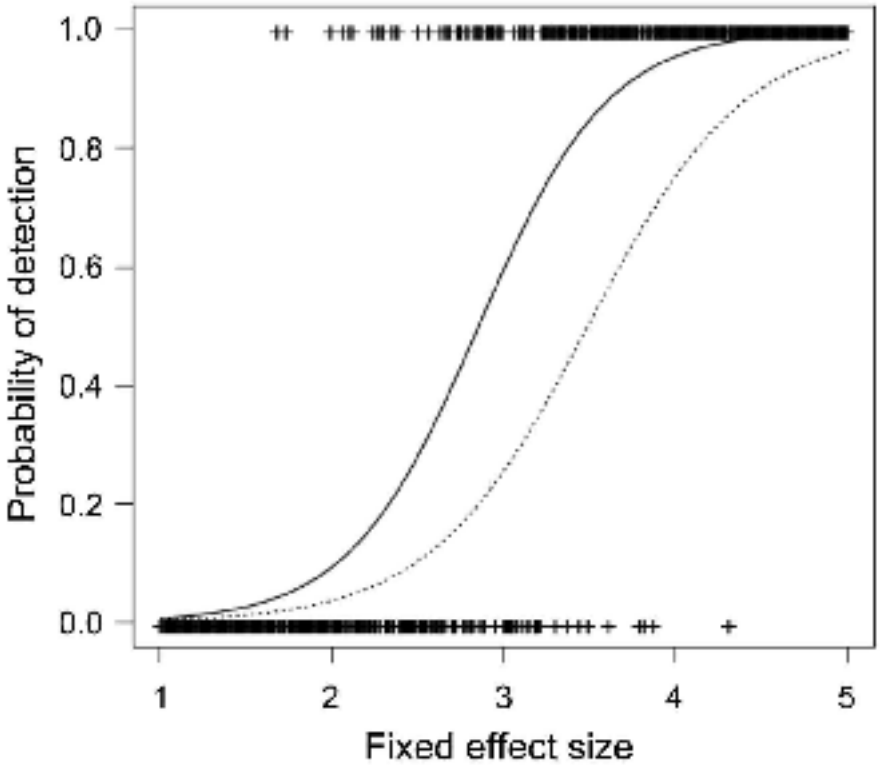

Figure S16 Probability of detection of QTL for simulated varying effect sizes. Logistic regressions fitted to the 400 data points on detection (0 = no, 1 = yes), showing probability of detection for QTL with dominance (*d/a*) of 1 (dominant, solid curve) or 0 (additive; dashed curve). Additive QTL are less likely to be detected.

File S1

Supplemental Materials and Methods

Grandparental population phenotyping

Skeletal morphologies of Japanese marine and Paxton benthic adult wild fish were compared by micro-computerized tomography using a Scanco uCT 40 scanned at 55kvp, 145 uA, at high resolution averaging four frames.

Phenotyping skeletal traits in F2 fish

We phenotyped 110 skeletal traits using a variety of methods described below. All traits were quantified on the left side, except for (1) premaxilla height and length which were quantified on the right side, and (2) premaxilla width, frontal width, supraoccipital traits, median fin and vertebral position traits, which are bilateral or midline measurements (see Figure 2). All linear measurements were quantified using an eye reticule on a Nikon SMZ1500 dissecting microscope unless noted otherwise.

Dissection method for branchial trait phenotyping

We developed a method to dissect out the entire branchial skeleton and mount it flat on a coverslip (Figure 2A). Briefly, under a Zeiss STEMI 2000 dissecting microscope with watchmaker's forceps, eyes were removed, and four cuts were made with iris or vannas scissors: two bilateral cuts dorsal to the opercle and hyomandibula through to the eye sockets, a cut across the frontal bone through the eye sockets, and a cut through the midline parasphenoid bone. Ventrally, the ceratohyals were disarticulated from the basihyal, and the urohyal removed. Next, the entire facial skeleton was removed, exposing the branchial skeleton. The epibranchials were detached from the neurocranium and the branchial skeleton removed by pulling the gut tube away from the rest of the fish. Soft tissue including the gut was removed and a single midline incision was made between the dorsal tooth plates to allow mounting the branchial skeletons flat on bridged coverslips as in Figure 2A. This method enables visualization of the entire branchial skeletal pattern from a dorsal view, as well as previously described variation in the pigmentation of the gill filaments from a ventral view (MILLER *et al.* 2007).

Gill raker traits

Along the anterior/posterior axis, gill rakers are distributed across nine rows projecting from both the anterior and posterior faces of all five branchial segments, except for the fifth branchial segment, which has only an anterior row (Figure 2A). Using the edge of Alizarin-positive branchial bone staining, we defined four dorsal-ventral raker domains as follows: (1) hypo (all rakers medial to the ceratobranchial), (2) cerato (bounded by the edges of the ceratobranchial bones), (3) joint (between

epibranchial and ceratobranchial), and (4) epi (dorsal to the epibranchial) (Figure 2B-E). If a raker spanned these bone landmarks, the center of the raker base was used to assign each raker to a domain. We recorded raker number in each of these 25 anterior-posterior and dorsal-ventral domains using a Zeiss STEMI 2000 dissecting microscope. We also combined the individual domain phenotypes into 19 composite phenotypes in the following possible developmental modules: rows, segments (branchial arches), odd rows, even rows, all, and dorsal/ventral domains (hypo, cerato, joint, and epi).

In addition to gill raker number, we directly measured the inter-raker spacing distance at three positions (lateral, middle, and medial, Figure 2F) along row 2 rakers. Lateral spacing was measured between the second and third raker from the ceratobranchial-epibranchial joint, middle spacing was measured between two rakers in the middle of the ceratobranchial, and medial spacing was measured between the second and third raker from the hypobranchial-ceratobranchial joint. All three spacing measurements were made between the center of the base of the two rakers being measured. For all three spacing measurements, if an atypical raker spacing was present following the above landmarks, an adjacent raker space was recorded if it appeared more typical of the spacing within the row.

We phenotyped gill raker length (from raker tip to ceratobranchial bone of the third raker from the ceratobranchial/epibranchial joint in rows 1 and 2), but after no significant genetic effect was detected after scoring 92 F2 males, we did not pursue this trait further.

Pharyngeal dentition

We quantified pharyngeal tooth number on all three pharyngeal toothplates: the two dorsal toothplates (DTP1 and DTP2) attached to the pharyngobranchials (ANKER 1974), and the one ventral pharyngeal toothplate (VTP) attached to the fifth ceratobranchial (Figure 2G). Teeth were counted using a Zeiss Axiophot compound microscope with DIC optics. Baby teeth that were visible under DIC but did not stain with Alizarin red were not counted. In addition, we measured the lengths and widths of all three toothplates (Figure 2H) by recording the longest and widest point-to-point measurements between Alizarin-positive toothplate bone.

Branchial bones

Along the dorsal-ventral axis, the branchial skeleton consists of: four epibranchials (EBs, dorsal bones in the roof of the buccal cavity); five ceratobranchials (CBs, long ventral bones in the floor of the buccal cavity), and three hypobranchials (HBs, short ventral bones in between the ceratobranchials and the midline). We measured the lengths of all five ceratobranchials and the first epibranchial using the two anterior corners of Alizarin-positive bone as landmarks (see Figure 2I). The lengths of the highly

three-dimensional epibranchials 2-4 and the widths of all ceratobranchials and epibranchials were not measured due to marked variation in mounting angles.

Jaw traits

Premaxillas were manually removed then soaked for several minutes in a dilute 2.5% bleach solution to remove soft tissue before measuring height, width, and length as in Figure 2J. Lower jaw measurements were quantified by dissecting out and separating the left dentary and articular as in Figure 2K, acquiring digitized images with an Evolution MP camera using ImageProPlus on a Leica MZFLIII microscope, then using ImageProPlus software to make linear measurements as in Figure 2K,L.

Skull and opercle traits

We quantified four skull traits: the linear measurement of frontal width or interorbital distance (Figure 2M), and three measurements of the supraoccipital crest (Figure 2N). Supraoccipital traits were quantified from digital images of the dorsal view of the skull taken with an Evolution MP camera on a Leica MZFLIII microscope and analyzed with ImageProPlus software. Three measurements of opercle size and shape were made: the length and width of the opercle, and a measurement of the width of the neck of the opercle (Figure 2O).

Median fin and vertebral traits

Spine serrations were scored from digital images of the second dorsal spine acquired with a Nikon D1X camera fixed to a Nikon SMZ-U microscope. Area of the anterior surface of the spine was calculated by counting the number of pixels in Photoshop (Adobe) and converting to square millimeters. The serration area (SRA) was calculated by subtracting a digitally smoothened dorsal spine area (i.e., a spine without serrations, SDSA) from the total spine area (SPA, Figure 2P). Pterygiophore and fin ray number, and anal spine lengths were quantified under a Leica S8APO microscope with an eye reticule. For all vertebral traits, animals were first X-rayed (Figure 2Q) at 5x magnification for 15-20 seconds at 20 kV in a Micro–50 cabinet specimen radiography machine (Faxitron). Positions of bones in the median skeleton were assigned a numerical value corresponding to the closest vertebra as described (Ahn and Gibson 1999). The position of the last dorsal and anal fin ray was determined based on the position of the pterygiophore that supported the fin ray. On occasion, the element was judged to be equidistant from two vertebrae and was assigned a value that was an average of the two vertebrae.

Genome-wide linkage map

Linkage map construction

A set of 275 microsatellites was genotyped in a single full-sibling family ("Family 4") of 370 fish from a Japanese marine (JAMA) by Paxton benthic (PAXB) freshwater F2 cross (COLOSIMO *et al.* 2004). These markers consisted of previously described sets of genome-wide microsatellites (ALBERT *et al.* 2008; COLOSIMO *et al.* 2004; PEICHEL *et al.* 2001) and markers near previously mapped genes (COLOSIMO *et al.* 2005; KNECHT *et al.* 2007b; MILLER *et al.* 2007; SHAPIRO *et al.* 2004). In addition, we added 16 new markers to the genetic map by genotyping new microsatellites near candidate genes with important roles in pharyngeal arch patterning in other vertebrates (*Dlx1/2*, *Dlx5/6*, *Dlx3*, *Msx1*, *Edn1*) as well as new positional markers. New markers were identified using a variety of methods including degenerate PCR, bacterial artificial chromosome (BAC) screening by radioactively labeled overgo hybridization, BAC end sequencing, physical map information, and publicly available previously sequenced BAC ends, as described in Supplemental Tables S1 and below. A linkage map (Figure S1) was constructed with JoinMap 3.0 (Kyazma), using previously described settings (PEICHEL *et al.* 2001) but by accepting more conservative LOD 6 groupings. The total map length is 1287.8 cM over 21 linkage groups, resulting in an average marker spacing of 5.1 cM. For each linkage group, proper phase was determined from the grandparental genotypes.

Cloning Dlx and Msx genes

Intergenic (*Dlx5/*6) or genic (*Msx1*, *Dlx3a*, and *Dlx3b*) regions of new genes added to map were amplified by PCR using the following primers (all sequences 5' to 3'). For *Dlx5/6,* PCR primers GGTGGGAAAGTGTTTGCACACC and CTGAGACAATCCGCATTCCTGTGG were designed to conserved intergenic sequences (ZERUCHA *et al.* 2000) which were found to flank Stn339 in intervening genomic sequence. For *Dlx3a* and *Dlx3b*, portions of two stickleback *Dlx3* genes were amplified and sequenced using a common forward degenerate primer (GGGTGAAGATHTGGTTYCARAA) and a reverse degenerate primer for either *Dlx3a* (CGGGCTGRTACCARTTYTGRTG) or *Dlx3b* (CGCCCTGYTGRTACCARTGRTT). The resulting *Dlx3* sequences were used to design two gene specific overgoes (see below) for BAC screening. Both *Dlx5/6* and *Dlx3* PCRs used Little Campbell marine genomic DNA as a template. For *Msx1,* degenerate RT-PCR primers CCGTTCAGCGTCGARGCNCTNATGGC and GGGGTGRTACATRCTRTANCC were used with oligo-dT reverse primed cDNA harvested from a 1 cM long Little Campbell marine fry. The resulting RT-PCR amplicon sequence was used to design overgoes (see below) for BAC screening.

Overgo screening, BAC end sequencing, and genotyping

Overgo screening was performed as described at www.chori.org/bacpac/overgohyb.htm. *Dlx1/2* overgoes were directly designed to conserved intergenic sequence (GHANEM *et al.* 2003). Forward and reverse overgo sequences (5' to 3') for each marker or gene were: *Msx1*:
CGGTAGTCTGGATACTTCAGTTCC and GCCCATCGATAAAGCAGGAACTGA; Stn207: TTTCAGCAGGTGCAACGTTTCCAC and AACTAAGAAGGCGAGCGTGGAAAC; *Dlx1/2:* ACCAAGATCTCGAGTGCACAATGT and CCTCATTACGCTGATGACATTGTG; *Dlx3a*: GGCGGCAGTATTAAGAGTAATGCG and CGGTGGGATCCACAAGCGCATTAC; *Dlx3b*: CCGACGCACAGCTCGTCGCCGCCA and TATAATCCTCCAGGTATGGCGGCG; Stn48: GTGCCAGAAAACTTGCATTCCAGG and ATCCCCTCACGTCACACCTGGAAT; EaccMgtg: GCAGGGTGATTGAATGTCTTCACT and GTCCTTAGGAAGATGCAGTGAAGA; 48B15.t7: AACAGTGTTGAGCGCTGAAATGCC and ACCTGTATGCACACACGGCATTTC; Stn292:
AAGATACGGGCTGATGAGCAGTGA and TTCTTACTACGCCTCCTCACTGCT; Stn222: TCGCACTTCAGACACTAAGCCTTG and TGAAGGGTGTCCAAACCAAGGCTT; Bmp6: TGTGACGTTGACCTCAGCTAGACT and GAGGATTTAAACCGGGAGTCTAGC.
For overgo screening, three pairs of labeled overgoes were combined in one hybridization bottle containing four filters, and positive BACs subsequently identified using a combination of the physical map (KINGSLEY *et al.* 2004) and PCR screening. BAC ends were sequenced using ABI3730xl manufacturer's suggestions, using 8 uL of ABI BigDye per 20uL sequencing reaction. Genotypes were generated essentially as previously described (MILLER *et al.* 2007; PEICHEL *et al.* 2001).

QTL mapping and analyses

Trait transformations

Trait processing and analysis was performed in R (http://www.R-project.org/). A custom pipeline was made to correct each trait for sex and/or size-dependence, log-transform if appropriate, and to remove phenotypic outliers as follows. First each trait was tested for size dependence by linear regression vs. standard length (SL), for sex dependence by a one-way ANOVA using sex as a factor, and for sex and size dependence using SL as a covariate and sex as a main effect in a General Linear Model (GLM) ANOVA. If the trait was neither sex nor size dependent, raw trait values were used for QTL mapping. If there was SL-dependence but no sex-dependence, traits were regressed against SL to obtain residuals. If there was sex-dependence but not size dependence, sex was corrected for using the residuals of a one-way ANOVA with sex as a factor. If traits were significantly dependent upon both sex and size, the residuals of the GLM ANOVA were used for QTL mapping. Outliers (defined as fish that had trait values greater than four standard deviations from the mean trait value) were removed and ANOVAs, regressions, and GLM ANOVAs were redone without outliers. Outliers were rare and consisted of only 35 values for 17 total traits (AH, DH, DL, DS1L, DS2L, FDP, IL1, IL2, OPL, OPN, PD4, PML, PMW, SDS2A, SOL, SPA, and SRA). Traits were log-transformed when the

transformation equalized variances (in sextiles ranked by standard length) by Levene's test for equality of variances, and/or normalized the residuals by an Anderson-Darling test of normality.

QTL mapping

QTL mapping was performed in R/qtl (BROMAN and SEN 2009). Initial QTL mapping was performed with *scanone* with Haley-Knott regressions (hk). For each phenotype, ten thousand permutations were performed to determine a LOD threshold at which alpha equals 0.05. The average of these trait-specific thresholds was 4.1; thus this value was used as the QTL significance threshold for all traits. All significant QTL by *scanone* were also identified by *stepwise* mapping, so the larger *stepwise* set of QTL are presented here. The *stepwise* algorithm was performed by an automated forward-backward stepwise search for QTL using *stepwiseqtl* with a main penalty of 4.1, which was the average penalty from 100 *scantwo* permutations for each trait. QTL peak markers and LOD scores were calculated using *refineqtl* and percent variances explained were calculated with *fitqtl*. For a small number of traits (n=11), the *stepwiseqtl* output included markers with a LOD less than 4.1. These markers were conservatively removed. In 10 cases, the *stepwiseqtl* output included two markers on the same chromosome. Only cases where both peak markers had LODs greater than 4.1 and also had non-overlapping 1.5 LOD intervals were considered as two QTL. In cases where the two linked markers had overlapping 1.5 LOD intervals, only the peak marker with the highest LOD was considered a QTL. LOD scores for QTL on chromosomes that did not have significant effects were determined with *addqtl*, adjusting for QTL that were identified from the stepwise search. Additional QTL were included from *addqtl* if they surpassed a 4.1 LOD score threshold and LODs were recalculated as above. This *addqtl/refineqtl/fitqtl* process was iteratively repeated for three rounds and all QTL that had a LOD score above 4.1 in the final *fitqtl* model were included in the final QTL set. LOD scores for phenotypes with no significant QTL were determined by *scanone* with Haley-Knott regressions. Heat maps in Figures 3 and S2-S6 use color schemes from http://colorbrewer2.org/.

Anatomical specificity of QTL

For investigating the anatomical specificity of QTL (Figure 4), the subset of QTL with clearly or likely serially homologous domains (QTL in the raker, teeth, branchial, jaw, and spine classes) were considered. QTL controlling raker spacing were excluded because this phenotype was only quantified on one segment, and QTL controlling toothplate size and tooth number were analyzed separately.

Principal Components Analysis

To determine the major axes of skeletal variation in the dataset, we performed Principal Components Analysis (PCA) using the *FactoMineR* package in R. Phenotypes were size/sex/log-adjusted as necessary (see Table S2) and Z-scored. Missing data were imputed using the *imputePCA* command, then weighted PCA was performed using phenotype weights such that the total weight for each phenotype class was equal. We performed PCA on all phenotypes, excluding composite phenotypes where the non-composite phenotypes comprising the composite phenotype were also present. The first five principal components explained 18.4, 9.4, 4.9, 4.6, and 4.4 percent of the phenotypic variance, respectively. The coordinates for each fish for the five largest principal components were extracted and QTL were mapped as described above.

Investigating biases in dominance

For simulations investigating QTL detection biases for dominance, two cases of QTL were compared: dominant QTL (d/a=1; heterozygotes have the same mean phenotype as the benthic B_1B_2 genotype) and additive QTL (d/a=0; heterozygous mean phenotype equals the mean of the M_1M_2 and B_1B_2 homozygous phenotypes). 400 samples for each value of dominance were used. Effect sizes span the boundaries of detection. Quantities in the simulation were based on the results of the analysis of the trait "DTP2," using Haley-Knott regression and a step size of 5 and a LOD threshold of 4.5. The simulations model a normally distributed trait, with QTL effect sizes ranging from 0 to 5, and a constant residual variance of 30 within each genotypic class, and assume no genotyping errors and no missing values. After detecting four QTL, all QTL were entered into a linear model in R/qtl. Obtained effect sizes for the four QTL ranged from LODs of 5 to 8, with a residual variance of about 28. Exploration with these numbers showed that effect sizes between 0 and 5 led to probabilities of detection ranging from about 0 to about 1.

Overlap with marine-freshwater divergent regions

The number of marine-freshwater divergent genomic regions that show evidence of repeated selection [the HMM or CSS signals of selection from (JONES *et al.* 2012)] within the 1.5 LOD interval of each QTL was determined. To test for enrichment of signals of selection within various groups of QTL, the mean number of overlaps of the QTL group was divided by the mean number of overlaps from 1000 simulations of random placement of signals of selection across the genome. P values were calculated by comparing the mean number of signal of selection-QTL overlaps to a null distribution of simulated placements of signals of selection. For determining the number of signals of selection overlapping the three trait clusters, the following coordinates were used: 2.34-28.56 Mb, 1.71-14.68 Mb, and 0-8.94 Mb for chromosomes 4, 20, and 21, respectively. These physical coordinates correspond to the genetic range on each chromosome that spans all of the clustered QTL shown in Figure 7, based upon markers flanking the 1.5-LOD interval listed in File S3. These coordinates were also used to identify putative

developmental regulatory genes within the trait clusters with Gene Ontology (GO) terms of "multicellular organismal development," "growth factor activity," or "regulation of transcription, DNA-dependent."

Files S2-S4

Available for download as Excel files at http://www.genetics.org/lookup/suppl/doi:10.1534/genetics.114.162420/-/DC1

File S2 Genotype and Phenotype data

All raw phenotype, adjusted phenotype (see Table S2) and genotype data used for QTL mapping. Raw genotypes were coded as follows: A and C are the marine grandparental alleles, B and D are the freshwater grandparental alleles. Genotypes of F2 fish were coded as follows: NA = missing, 1 = AC, 2 = BC, 3 = AD, 4 = BD, 5 = A = AC or AD, 6 = B = BC or BD, 7 = C = AC or BC, 8 = D = AD or BD, 10 = AD or BC.

File S3 Summary of all trait QTL

All detected significant QTL affecting skeletal traits are shown. QTL statistics are displayed in two ways: 1) allowing interpolated markers calculated every cM to be the peak markers or boundaries of the 1.5 LOD intervals or 2) allowing only real markers to be the peak markers or boundaries of the 1.5 LOD intervals. Mean phenotypes are displayed for Z scored phenotypes after size adjustment, sex adjustment, and log transformation, as necessary. For each QTL, one additive effect (half the difference between the two homozygous classes) and two dominance effects (difference between a heterozygous class and the mean of the two homozygous classes) is shown, as well as two dominance values (*d/a).* QTL in raker, opercle, median fin, and vertebrae classes that had expected directions of evolutionary change were determined to be concordant or antagonistic to the direction of evolutionary change.

File S4 Summary of principal component QTL

All detected significant QTL for the five largest principal components (PC1-5) are shown. QTL statistics are displayed in two ways: 1) allowing interpolated markers calculated every cM to be the peak markers or boundaries of the 1.5 LOD intervals or 2) allowing only real markers to be the peak markers or boundaries of the 1.5 LOD intervals.

Table S1 New microsatellites added to stickleback genetic linkage map

Stn marker	Nearby gene or marker	Forward primer sequence (5' to 3')	Reverse primer sequence (5' to 3')	BAC	Methods (see legend)	Accession # of BAC end sequence	Accession # of genetic marker
Stn338	***Dlx5/6***	CACCGCTAGTGTGTGTCTGC	CGCTCTCAAGACCACTCAGG		1		Pr031952730
Stn339	***Dlx1/2***	CAGCAATAGACACACACAGACG	CTGGGCTAAATATGATCCGTTC	14L21.SP6	2,3	KG777549	Pr031952731
Stn340	Stn207	CTAGAAGTCTGAAGAGCTCA	GCAATGATGAGGTCACCAG	75L11.SP6	2,3	KG777550	Pr031952732
Stn343	***Msx1***	TTACAATGGCTGGAGAGACG	CTCAGGCTATTTCTGAGACTCG	40L14.T7	2,3,4,5	KG777551	Pr031952733
Stn418*	EaccMgtg	TGCTGTCTTCAAGCCGTTTTC	GATAATAAGGACTCAAATAATTCAG	187B17.T7	2,5,6,7	CL648612	Pr031952734
Stn419^	Stn48	AGGAAGCTGCAGAGTTCAGG	TGACACCGACAGGCTTCC	49M10	2,3	KG777552	Pr031952735
Stn420	Stn292	CCCTGCTGTTGCACAATG	CTCAGCTGTTGGGAATTATGG	281G07.T7	2,3,5	KG777553	Pr031952736
Stn421	Stn222	CACTCCAGATGGAATCTCTGC	CCTCGACACACACAGATAAACC	168B20.T7	2,5,6	CL648236	Pr031952737
Stn422	*Bmp6*	CTGCCTCATATGGCATGAAG	CCCAGTTGTTGAGTTGGTTG	28D13.T7	2,5,6	CL642350	Pr031952738
Stn423	Stn422	CCTCCAGGACGAATTCAAAG	CTGCATCTCGGCTGTGTGG	258J06.T7	2,5,6,7	CL649886	Pr031952739
Stn424	*Zic1*	AGGTCTCGGTTCGATTACCA	TTGTGCGCTTGCATATGCAT		8		Pr031952740
Stn425	*Rnf32*	CGATTCAACCGACCCAACAC	ACACAGTCCAAACCGTCTCT		8		Pr031952741
Stn427	***Dlx3b***	ACACACACGCACAACACAGC	CCAGAGACGCAACGTGTAGG	72B08.SP6	2,3,4,5	KG777554	Pr031952742
Stn428	***Kit***	CCTGCGCAGAAATAGAGAGG	CGTATTCGGTAGCAGTCACC		8		Pr031952743
Stn429	***Edn1***	CACCCTTACAGGCGATTCAG	CATGTGTTGCATCATGCGTC		8		Pr031952744
Stn430	***Dlx3a***	CGGTCAGATGTGACGAGTG	CGTTGCTGATTCCTCTTGCG	69L16.SP6	2,3,4,5	KG777555	Pr031952745
Stn483	***Bmp6***	CCCGGTTTAAATCCTCATCC	AGGAGGTGATTGACAGCTCG		8		Pr031952746

For each marker, Stn number is listed, as well as nearby gene or genomic region. Markers that appear on the map (Fig. S1) as a gene have the gene name listed in bold. Markers that were discovered from sequence from marine BACs (CHORI 213 BAC library) have the BAC coordinate listed, and when microsatellite was found from BAC end sequence, that BAC end (T7 or SP6) is listed. For genotyping, all forward primers were 5' FAM labeled (Integrated DNA Technologies). In some cases, the first nucleotide of the forward primer was changed from G to C to prevent quenching of FAM. Methods used to identify new markers: 1= PCR amplicon sequencing, 2= BAC screening with overgoes, 3= BAC (end or internal) sequencing, 4= degenerate RT-PCR to find sequence for overgoes, 5= physical map information used (KINGSLEY *et al.* 2004), 6= publicly available BAC end sequences, 7= sequence homology with publicly available BAC end sequences, 8= genome assembly (JONES *et al.* 2012). Primer and overgo sequences used in marker discovery are listed in Supplemental Methods Text S1. *EaccMgtg was an AFLP linked to the plates locus (COLOSIMO *et al.* 2005). The sequence used to design Stn418 is highly repetitive in the stickleback genome and although this marker worked in this cross, it is not recommended. ^ For Stn419, BAC 49M10 was internally sequenced with Stn48 forward primer (PEICHEL *et al.* 2001).

References

COLOSIMO, P. F., K. E. HOSEMANN, S. BALABHADRA, G. VILLARREAL, JR., M. DICKSON *et al.*, 2005 Widespread parallel evolution in sticklebacks by repeated fixation of *Ectodysplasin* alleles. Science **307:** 1928-1933.

JONES, F. C., M. G. GRABHERR, Y. F. CHAN, P. RUSSELL, E. MAUCELI *et al.*, 2012 The genomic basis of adaptive evolution in threespine sticklebacks. Nature **484:** 55-61.

KINGSLEY, D. M., B. L. ZHU, K. OSOEGAWA, P. J. DE JONG, J. SCHEIN *et al.*, 2004 New genomic tools for molecular studies of evolutionary change in threespine sticklebacks. Behaviour **141:** 1331-1344.

PEICHEL, C. L., K. S. NERENG, K. A. OHGI, B. L. COLE, P. F. COLOSIMO *et al.*, 2001 The genetic architecture of divergence between threespine stickleback species. Nature **414:** 901-905.

Table S2 Trait descriptions and transformations

Trait	Description	Class	Model	Number of QTL
R1E	Row 1 epi raker number	raker	Raw	1
R2E	Row 2 epi raker number	raker	SL lm	1
R3E	Row 3 epi raker number	raker	Raw	1
R4E	Row 4 epi raker number	raker	Glm	0
R5E	Row 5 epi raker number	raker	Raw	0
R6E	Row 6 epi raker number	raker	Sex lm	1
R7E	Row 7 epi raker number	raker	Raw	0
R2J	Row 2 joint raker number	raker	SL lm	3
R4J	Row 4 joint raker number	raker	SL lm	1
R6J	Row 6 joint raker number	raker	Sex lm	2
R7J	Row 7 joint raker number	raker	Sex lm	0
R8J	Row 8 joint raker number	raker	Sex lm	0
R1C	Row 1 cerato raker number	raker	Glm	3
R2C	Row 2 cerato raker number	raker	Sex lm	2
R3C	Row 3 cerato raker number	raker	Glm	4
R4C	Row 4 cerato raker number	raker	Glm	4
R5C	Row 5 cerato raker number	raker	SL lm	2
R6C	Row 6 cerato raker number	raker	Glm	3
R7C	Row 7 cerato raker number	raker	Glm	1
R8C	Row 8 cerato raker number	raker	Sex lm	4
R9C	Row 9 cerato raker number	raker	SL lm	2
R1H	Row 1 hypo raker number	raker	Glm	0
R3H	Row 3 hypo raker number	raker	Raw	1
R5H	Row 5 hypo raker number	raker	SL lm	1
R7H	Row 7 hypo raker number	raker	Sex lm	1
E	Epi raker number	raker	Glm	1
J	Joint raker number	raker	Glm	4
C	Cerato raker number	raker	Glm	5
H	Hypo raker number	raker	Glm	6
R1	Row 1 raker number	raker	SL lm	5
R2	Row 2 raker number	raker	Sex lm	2
R3	Row 3 raker number	raker	Raw	5
R4	Row 4 raker number	raker	Sex lm	2
R5	Row 5 raker number	raker	Raw	2
R6	Row 6 raker number	raker	SL lm	2
R7	Row 7 raker number	raker	Glm	0
R8	Row 8 raker number	raker	Raw	1
BA1	Branchial arch 1 raker number	raker	Sex lm	6
BA2	Branchial arch 2 raker number	raker	Sex lm	6
BA3	Branchial arch 3 raker number	raker	Glm	4

BA4	Branchial arch 4 raker number	raker	SL lm	4
ODD	Odd row raker number	raker	Glm	5
EVEN	Even row raker number	raker	Sex lm	5
ALL	All raker number	raker	Glm	8
LSP	Lateral raker spacing	raker	SL lm	5
MISP	Middle raker spacing	raker	Glm	5
MESP	Medial raker spacing	raker	SL lm	1
DTP1	Dorsal toothplate 1 tooth number	teeth	Raw	6
DTP2	Dorsal toothplate 2 tooth number	teeth	Raw	7
VTP	Ventral toothplate tooth number	teeth	SL lm	5
PMT	Premaxilla tooth number	teeth	Glm	0
PMTR	Number of tooth rows on premaxilla	teeth	Glm	0
DTP1L	Dorsal toothplate 1 length	teeth	Glm	5
DTP1W	Dorsal toothplate 1 width	teeth	Glm	3
DTP2L	Dorsal toothplate 2 length	teeth	SL lm	6
DTP2W	Dorsal toothplate 2 width	teeth	Glm	5
VTPL	Ventral toothplate length	teeth	SL lm	3
VTPW	Ventral toothplate width	teeth	Glm	5
EB1L	Epibranchial 1 length	branchial	Glm	8
CB1L	Ceratobranchial 1 length	branchial	Glm	9
CB2L	Ceratobranchial 2 length	branchial	Glm	8
CB3L	Ceratobranchial 3 length	branchial	Glm	6
CB4L	Ceratobranchial 4 length	branchial	Glm	10
CB5L	Ceratobranchial 5 length	branchial	Glm	9
PML	Premaxilla length	jaw	Glm	9
PMW	Premaxilla width	jaw	Glm	2
PMH	Premaxilla height	jaw	Glm	5
DL	Dentary length	jaw	Glm	4
DH	Dentary height	jaw	Glm	4
AL	Articular length	jaw	Glm	7
AH	Articular height	jaw	Glm	3
IL1	In-lever 1 of articular length	jaw	Glm	3
IL2	In-lever 2 of articular length	jaw	Glm	3
FW	Frontal width	skull	Glm	7
SOL	Supraoccipital crest length	skull	SL lm	2
SOW	Supraoccipital crest width	skull	SL lm	4
SOA	Supraoccipital crest area	skull	SL lm	6
OPL	Opercle length	opercle	Glm	3
OPW	Opercle width	opercle	Glm	4
OPN	Opercle neck width	opercle	Sex lm	2
DS1L	Dorsal spine 1 length	median fin	SL lm	8
DS2L	Dorsal spine 2 length	median fin	Glm	9
DS3L	Dorsal spine 3 length	median fin	Glm	5

ASL	Anal spine length	median fin	Glm	3
SR	Serration number on dorsal spine 2	median fin	Glm	2
SRA	Serration area on dorsal spine 2	median fin	Glm	2
SPA	Dorsal spine 2 area	median fin	SL lm	2
SDS2A	Smoothened dorsal spine 2 area (SPA-SRA)	median fin	SL lm	1
DFR	Dorsal fin ray number	median fin	Sex lm	1
AFR	Anal fin ray number	median fin	Glm	1
PD	Predorsal pterygiophore number	median fin	Sex lm	0
PE	Non-ray-bearing postdorsal pterygiophore number	median fin	Raw	1
PN	Non-ray-bearing postanal pterygiophore number	median fin	Raw	1
TPDP	Total postdorsal pterygiophore number	median fin	Sex lm	1
TAP	Total postanal pterygiophore number	median fin	Sex lm	2
TDP	Total dorsal pterygiophore number	median fin	Sex lm	1
PD3	Third predorsal pterygiophore position	vertebrae	Raw	2
PD4	Fourth predorsal pterygiophore position	vertebrae	Raw	0
PD5	Fifth predorsal pterygiophore position	vertebrae	Sex lm	0
FDP	First postdorsal pterygiophore position	vertebrae	Sex lm	0
LDP	Last postdorsal pterygiophore position	vertebrae	Raw	4
FAP	First postanal pterygiophore position	vertebrae	Sex lm	0
LAP	Last postanal pterygiophore position	vertebrae	Raw	5
FHS	First hemal spine position	vertebrae	Sex lm	0
LDFR	Last dorsal fin ray position	vertebrae	SL lm	0
LAFR	Last anal fin ray position	vertebrae	Raw	3
VN	Vertebrae number	vertebrae	Sex lm	2
AVN	Abdominal vertebrae number	vertebrae	Sex lm	0
CVN	Caudal vertebrae number	vertebrae	Sex lm	1
VR	Vertebrae ratio (AVN/CVN)	vertebrae	Sex lm	0

Depending on the relationship of phenotype with standard length (SL) and sex, the phenotype used for QTL mapping was unadjusted (raw), residuals from a SL regression (SL lm), residuals from one-way ANOVA using sex as a factor (Sex lm), or residuals from a SL+Sex General Linear Model ANOVA (Glm). Units are meristic counts for number traits, millimeters for linear measurements, millimeters^2 for area traits, vertebrae number for vertebral position traits (see Supplemental Methods Text S1) or unitless for VR. For 92 of 110 traits, at least one QTL was detected.

Table S3 Sexually dimorphic traits

Trait	P-value	Male		Female	
		Mean +/- SE	n	Mean +/- SE	n
R4E*	7.03E-05	0.861 +/- 0.043	168	0.637 +/- 0.038	188
R6E	3.25E-05	1.70 +/- 0.052	168	1.43 +/- 0.041	187
R6J	1.18E-05	2.52 +/- 0.046	168	2.79 +/- 0.040	188
R7J	5.99E-03	1.36 +/- 0.054	168	1.56 +/- 0.051	187
R8J	1.09E-02	1.79 +/- 0.049	168	1.96 +/- 0.045	188
R1C*	3.02E-03	11.4 +/- 0.064	168	11.1 +/- 0.057	188
R2C	1.21E-05	11.4 +/- 0.061	168	11.1 +/- 0.055	188
R3C*	1.30E-02	11.0 +/- 0.069	168	10.8 +/- 0.059	188
R4C*	4.96E-09	11.3 +/- 0.053	168	10.9 +/- 0.043	188
R6C*	2.98E-02	11.8 +/- 0.063	168	11.6 +/- 0.053	188
R7C*	6.69E-10	13.0 +/- 0.065	168	12.5 +/- 0.052	188
R8C	1.47E-03	11.0 +/- 0.058	168	10.8 +/- 0.057	188
R1H*	1.92E-02	2.50 +/- 0.045	167	2.64 +/- 0.037	187
R7H	1.83E-07	0.339 +/- 0.037	168	0.612 +/- 0.036	188
E*	2.98E-03	13.4 +/- 0.15	168	12.8 +/- 0.13	186
J*	1.09E-05	11.4 +/- 0.14	168	12.2 +/- 0.12	187
C*	1.34E-06	105 +/- 0.38	168	103 +/- 0.32	188
H*	1.54E-03	8.49 +/- 0.085	167	8.84 +/- 0.070	187
R2	1.48E-03	14.8 +/- 0.072	168	14.5 +/- 0.066	188
R4	1.68E-11	15.1 +/- 0.065	168	14.5 +/- 0.055	188
R7*	3.05E-02	16.0 +/- 0.070	168	15.8 +/- 0.067	187
BA1	2.69E-02	34.5 +/- 0.15	167	34.0 +/- 0.13	186
BA2	1.95E-05	30.5 +/- 0.12	168	29.8 +/- 0.10	188
BA3*	4.62E-02	31.7 +/- 0.12	168	31.4 +/- 0.10	187
ODD*	4.55E-02	79.6 +/- 0.27	167	78.9 +/- 0.24	185
EVEN	6.85E-05	58.8 +/- 0.21	168	57.7 +/- 0.18	187
ALL*	1.24E-03	138 +/- 0.46	167	136 +/- 0.39	185
MISP*	1.85E-02	0.291 +/- 0.0017	167	0.286 +/- 0.0015	188
PMT*	1.23E-35	26.9 +/- 0.43	172	20.1 +/- 0.29	195
PMTR*	1.34E-33	2.64 +/- 0.034	172	2.11 +/- 0.024	195
DTP1L*^	6.49E-04	0.891 +/- 0.0039	168	0.872 +/- 0.0043	187
DTP1W*	1.91E-10	0.373 +/- 0.0026	168	0.397 +/- 0.0028	188
DTP2W*	1.01E-08	0.648 +/- 0.0033	168	0.674 +/- 0.0031	188
VTPW*^	8.16E-05	0.436 +/- 0.0038	168	0.417 +/- 0.0030	188
EB1L*^	3.28E-19	1.37 +/- 0.0069	168	1.28 +/- 0.0062	188
CB1L*^	1.14E-18	3.12 +/- 0.0083	168	3.01 +/- 0.0084	188
CB2L*^	8.56E-18	2.91 +/- 0.0080	168	2.80 +/- 0.0080	188
CB3L*	4.11E-14	2.71 +/- 0.0074	168	2.63 +/- 0.0074	188
CB4L*^	2.01E-13	2.65 +/- 0.0075	168	2.57 +/- 0.0073	188

CB5L*^	4.07E-07	2.55 +/- 0.0071	168	2.50 +/- 0.0072	188
PML*^	5.16E-63	2.66 +/- 0.011	172	2.39 +/- 0.0085	194
PMW*^	2.30E-31	0.361 +/- 0.0030	172	0.310 +/- 0.0027	194
PMH*	4.29E-14	2.48 +/- 0.0083	172	2.39 +/- 0.0085	195
DL*	5.13E-24	1.90 +/- 0.0094	165	1.77 +/- 0.0085	186
DH*	2.17E-31	1.39 +/- 0.0063	166	1.28 +/- 0.0063	188
AL*^	2.92E-45	2.52 +/- 0.011	169	2.29 +/- 0.0097	189
AH*^	7.86E-20	0.965 +/- 0.0077	168	0.867 +/- 0.0068	187
IL1*^	2.21E-02	0.859 +/- 0.0061	168	0.840 +/- 0.0053	188
IL2*	3.93E-21	1.41 +/- 0.0069	168	1.31 +/- 0.0066	187
FW*	3.33E-09	2.52 +/- 0.010	172	2.43 +/- 0.010	195
OPL*^	6.31E-21	4.06 +/- 0.013	171	3.88 +/- 0.012	194
OPW*^	3.53E-35	4.09 +/- 0.014	170	3.84 +/- 0.012	192
OPN	1.93E-11	0.288 +/- 0.0072	171	0.236 +/- 0.0031	195
DS2L*^	7.55E-03	3.80 +/- 0.033	167	3.92 +/- 0.029	195
DS3L*^	3.84E-17	0.958 +/- 0.012	168	1.12 +/- 0.015	194
ASL*	5.29E-27	0.994 +/- 0.015	150	1.22 +/- 0.013	178
SR*	7.55E-06	4.55 +/- 0.21	169	3.29 +/- 0.19	193
SRA*	2.58E-14	0.0613 +/- 0.0036	167	0.0292 +/- 0.0022	192
DFR	2.06E-02	10.9 +/- 0.047	168	10.7 +/- 0.042	189
AFR*	1.70E-08	7.88 +/- 0.046	168	7.53 +/- 0.043	189
PD	6.87E-03	6.02 +/- 0.022	169	6.11 +/- 0.023	190
TPDP	9.14E-05	13.8 +/- 0.046	168	13.6 +/- 0.044	189
TAP	7.82E-10	10.9 +/- 0.050	168	10.5 +/- 0.043	189
TDP	1.89E-02	19.9 +/- 0.050	168	19.7 +/- 0.048	189
PD5	9.09E-06	9.91 +/- 0.021	170	10.1 +/- 0.022	195
FDP	2.92E-08	11.7 +/- 0.034	170	11.9 +/- 0.023	193
FAP	2.09E-19	15.6 +/- 0.038	167	16.0 +/- 0.019	193
FHS	1.27E-19	15.5 +/- 0.038	170	16.0 +/- 0.021	194
VN	1.77E-11	31.5 +/- 0.039	162	31.2 +/- 0.031	190
AVN	1.27E-19	14.5 +/- 0.038	170	15.0 +/- 0.021	194
CVN	4.69E-31	17.0 +/- 0.048	162	16.2 +/- 0.035	189
VR	1.78E-31	0.859 +/- 0.0042	162	0.922 +/- 0.0027	189

Mean and standard error of phenotypes within males and females are shown for traits that were significantly sexually dimorphic by two-tailed Student's t test. *Trait was corrected for body size and standardized to 40 mm length. ^Trait was log-adjusted.

Table S4 Summary of filtered QTL

Trait	Class	LG	Marker	LOD	PVE	Mean +/- Standard Error (n)			
						M_1M_2	M_1B_1	M_2B_2	B_1B_2
R3C	raker	1	Stn2	4.7	3.8	10.8 +/- 0.085	10.85 +/- 0.086	10.85 +/- 0.084	10.59 +/- 0.1
BA2	raker	1	Stn5	10.7	7.5	30.4 +/- 0.15	29.9 +/- 0.13	29.8 +/- 0.13	29.2 +/- 0.19
R3E	raker	2	Stn17	5.1	6.4	1.387 +/- 0.057	1.63 +/- 0.061	1.521 +/- 0.056	1.765 +/- 0.05
E	raker	4	Stn38	8.6	10.6	11.83 +/- 0.2	12.78 +/- 0.17	13.06 +/- 0.17	13.55 +/- 0.17
LSP	raker	4	Stn47	27.7	22.6	0.254 +/- 0.0019	0.264 +/- 0.0025	0.2721 +/- 0.0026	0.2885 +/- 0.0024
MISP	raker	6	Stn62	4.9	3.4	0.2921 +/- 0.0025	0.282 +/- 0.0025	0.2841 +/- 0.0021	0.2851 +/- 0.0019
H	raker	7	Stn258	6.1	5.7	9.113 +/- 0.097	8.975 +/- 0.11	8.682 +/- 0.11	8.555 +/- 0.11
R1C	raker	7	Stn75	7.8	7.0	11.39 +/- 0.082	11.07 +/- 0.078	11.23 +/- 0.083	10.8 +/- 0.085
R8C	raker	8	Stn300	5.3	5.5	10.71 +/- 0.081	10.68 +/- 0.081	10.82 +/- 0.074	10.98 +/- 0.087
H	raker	8	Stn95	5.0	4.6	8.679 +/- 0.11	9.03 +/- 0.11	8.684 +/- 0.11	8.965 +/- 0.11
R6J	raker	10	Stn124	5.6	6.4	2.968 +/- 0.059	2.704 +/- 0.058	2.879 +/- 0.062	2.632 +/- 0.056
LSP	raker	11	Stn244	6.0	4.2	0.278 +/- 0.003	0.2694 +/- 0.003	0.2685 +/- 0.002	0.2656 +/- 0.0031
BA2	raker	12	Nemo	4.2	2.8	30.06 +/- 0.16	29.91 +/- 0.17	29.77 +/- 0.16	29.67 +/- 0.14
MISP	raker	13	Stn155	5.2	3.6	0.2873 +/- 0.0018	0.2837 +/- 0.0022	0.2887 +/- 0.0024	0.2828 +/- 0.0022
EVEN	raker	14	Stn166	4.5	3.4	57.11 +/- 0.28	57.6 +/- 0.28	57.66 +/- 0.28	58.28 +/- 0.27
R9C	raker	15	Stn230	7.3	7.8	12.98 +/- 0.081	12.82 +/- 0.083	13.05 +/- 0.089	12.42 +/- 0.079
BA1	raker	16	Stn176	6.6	5.0	33.75 +/- 0.21	34.6 +/- 0.19	33.55 +/- 0.18	34.3 +/- 0.19
H	raker	17	Stn323	5.5	5.1	9.067 +/- 0.11	9.017 +/- 0.1	8.905 +/- 0.11	8.419 +/- 0.11
ALL	raker	17	Stn205	8.4	5.1	137.7 +/- 0.49	137.5 +/- 0.54	136 +/- 0.69	134.4 +/- 0.61
ALL	raker	18	Stn305	4.6	2.8	137.6 +/- 0.9	135.1 +/- 0.63	136.6 +/- 0.49	136.7 +/- 0.54
C	raker	20	Stn215	32.9	25.3	105.6 +/- 0.37	103.4 +/- 0.44	101.5 +/- 0.39	98.88 +/- 0.52
R8C	raker	20	Gac1125	9.0	9.5	11.03 +/- 0.065	10.9 +/- 0.083	10.58 +/- 0.083	10.56 +/- 0.087
H	raker	21	Stn223	4.6	4.2	9.128 +/- 0.1	8.858 +/- 0.11	8.676 +/- 0.11	8.682 +/- 0.11
VTPW	teeth	1	Stn272	6.3	4.8	0.4276 +/- 0.0059	0.4197 +/- 0.0038	0.4191 +/- 0.0044	0.398 +/- 0.0045
DTP2L	teeth	1	Stn13	4.5	3.7	1.493 +/- 0.0077	1.48 +/- 0.0077	1.469 +/- 0.0074	1.471 +/- 0.0074
DTP2L	teeth	2	Stn259	7.8	6.7	1.507 +/- 0.0079	1.478 +/- 0.008	1.47 +/- 0.0068	1.463 +/- 0.0071
VTPW	teeth	2	Stn24	6.5	5.0	0.4169 +/- 0.0046	0.4202 +/- 0.0053	0.4082 +/- 0.004	0.4245 +/- 0.0053

DTP2	teeth	4	Eda	34.9	24.2	53.96 +/- 0.68	49.06 +/- 0.66	47.3 +/- 0.66	44.68 +/- 0.61
DTP1	teeth	7	Stn72	6.9	5.1	15.63 +/- 0.29	16.59 +/- 0.34	16.27 +/- 0.29	17.53 +/- 0.35
DTP2L	teeth	7	Stn75	15.2	13.7	1.444 +/- 0.0071	1.47 +/- 0.0062	1.488 +/- 0.0079	1.515 +/- 0.0076
DTP2	teeth	8	Stn300	7.1	4.1	50.06 +/- 0.67	49.11 +/- 0.71	47.8 +/- 0.69	47.67 +/- 0.89
DTP2W	teeth	8	Stn95	5.1	4.2	0.662 +/- 0.0054	0.6832 +/- 0.0037	0.6658 +/- 0.004	0.6852 +/- 0.0048
DTP1L	teeth	9	Stn102	5.6	4.7	0.8897 +/- 0.0056	0.8756 +/- 0.0055	0.866 +/- 0.0057	0.8527 +/- 0.0058
DTP2	teeth	10	Stn211	12.7	7.6	49.97 +/- 0.61	49.28 +/- 0.84	49.41 +/- 0.88	46.03 +/- 0.58
DTP1	teeth	11	Dlx3a	6.1	4.5	15.82 +/- 0.32	15.67 +/- 0.29	16.63 +/- 0.29	17.43 +/- 0.35
DTP2W	teeth	12	Stn232	5.4	4.4	0.6858 +/- 0.0042	0.6727 +/- 0.0042	0.6802 +/- 0.0053	0.6631 +/- 0.0042
DTP1W	teeth	12	Stn142	4.7	5.2	0.4122 +/- 0.0043	0.3963 +/- 0.0033	0.3958 +/- 0.0037	0.3915 +/- 0.0039
VTP	teeth	13	Stn153	5.5	3.9	45.24 +/- 0.7	47.98 +/- 0.81	46.41 +/- 0.8	48.34 +/- 0.7
DTP2W	teeth	14	Stn198	7.0	5.8	0.6828 +/- 0.0047	0.6637 +/- 0.0038	0.6706 +/- 0.0047	0.685 +/- 0.0047
DTP1L	teeth	14	Stn237	6.6	5.6	0.8505 +/- 0.0051	0.8798 +/- 0.0059	0.8716 +/- 0.0062	0.882 +/- 0.0055
DTP1L	teeth	16	Stn178	7.4	6.4	0.8617 +/- 0.0065	0.8639 +/- 0.0059	0.873 +/- 0.0051	0.8844 +/- 0.0058
DTP2	teeth	20	Stn215	12.8	7.6	50.99 +/- 0.61	49.35 +/- 0.74	48.14 +/- 0.7	44.82 +/- 0.8
VTP	teeth	21	Stn422	31.0	26.2	42.28 +/- 0.56	46.48 +/- 0.69	46.93 +/- 0.58	52.48 +/- 0.76
CB2L	branchial	1	Stn248	6.2	4.2	2.821 +/- 0.012	2.804 +/- 0.011	2.789 +/- 0.011	2.786 +/- 0.011
EB1L	branchial	2	Stn21	11.6	6.7	1.308 +/- 0.01	1.288 +/- 0.0091	1.269 +/- 0.0085	1.257 +/- 0.0083
CB1L	branchial	2	Stn268	14.9	10.4	3.056 +/- 0.011	3.019 +/- 0.013	3.007 +/- 0.01	2.973 +/- 0.012
CB4L	branchial	4	Stn45	29.3	19.1	2.514 +/- 0.0084	2.555 +/- 0.01	2.574 +/- 0.01	2.64 +/- 0.0087
CB5L	branchial	5	Stn52	8.6	5.9	2.46 +/- 0.01	2.49 +/- 0.01	2.5 +/- 0.01	2.533 +/- 0.0087
EB1L	branchial	5	Stn312	6.6	3.7	1.254 +/- 0.011	1.269 +/- 0.0087	1.281 +/- 0.0077	1.303 +/- 0.0089
EB1L	branchial	7	Stn71	7.4	4.2	1.262 +/- 0.0085	1.265 +/- 0.0089	1.276 +/- 0.0091	1.312 +/- 0.0092
EB1L	branchial	8	Stn239	9.6	5.5	1.244 +/- 0.0083	1.3 +/- 0.0092	1.267 +/- 0.0092	1.296 +/- 0.0088
CB4L	branchial	10	Edn1	6.0	3.3	2.551 +/- 0.0088	2.547 +/- 0.012	2.583 +/- 0.0096	2.607 +/- 0.011
CB4L	branchial	12	Stn287	6.2	3.5	2.54 +/- 0.01	2.574 +/- 0.0095	2.572 +/- 0.011	2.6 +/- 0.01
EB1L	branchial	14	Stn163	7.1	4.0	1.259 +/- 0.0075	1.283 +/- 0.0093	1.266 +/- 0.0096	1.303 +/- 0.0096
CB1L	branchial	15	Stn173	7.4	4.9	3.04 +/- 0.014	3.027 +/- 0.0094	2.998 +/- 0.011	2.973 +/- 0.013
CB4L	branchial	16	Edar	6.9	3.9	2.558 +/- 0.011	2.558 +/- 0.011	2.597 +/- 0.009	2.574 +/- 0.011
CB2L	branchial	17	Stn325	7.1	4.9	2.773 +/- 0.012	2.811 +/- 0.0097	2.783 +/- 0.013	2.829 +/- 0.011
CB5L	branchial	18	Stn280	9.8	6.7	2.454 +/- 0.011	2.508 +/- 0.011	2.501 +/- 0.0083	2.517 +/- 0.0097

EB1L	branchial	21	Stn219	24.4	15.5	1.231 +/- 0.0079	1.273 +/- 0.009	1.289 +/- 0.0081	1.322 +/- 0.0088
PML	jaw	2	Stn24	5.3	3.7	2.39 +/- 0.013	2.405 +/- 0.014	2.361 +/- 0.012	2.37 +/- 0.015
PML	jaw	3	Stn31	5.2	3.7	2.344 +/- 0.012	2.405 +/- 0.015	2.363 +/- 0.012	2.415 +/- 0.014
IL2	jaw	4	Stn45	17.9	16.9	1.264 +/- 0.0082	1.297 +/- 0.008	1.302 +/- 0.009	1.366 +/- 0.0091
PML	jaw	5	Stn52	8.3	6.0	2.333 +/- 0.013	2.403 +/- 0.014	2.389 +/- 0.013	2.396 +/- 0.013
IL2	jaw	7	Stn75	13.1	11.9	1.267 +/- 0.0084	1.318 +/- 0.0085	1.305 +/- 0.0091	1.351 +/- 0.0099
PMW	jaw	7	Stn257	7.4	8.3	0.2965 +/- 0.0039	0.3029 +/- 0.004	0.3133 +/- 0.0042	0.3222 +/- 0.0035
AL	jaw	9	Stn102	8.0	5.6	2.329 +/- 0.013	2.304 +/- 0.014	2.289 +/- 0.014	2.22 +/- 0.013
PMH	jaw	11	Stn224	7.8	6.9	2.427 +/- 0.012	2.387 +/- 0.012	2.37 +/- 0.011	2.355 +/- 0.011
DH	jaw	12	Stn318	6.8	6.9	1.313 +/- 0.0085	1.279 +/- 0.0078	1.283 +/- 0.0096	1.249 +/- 0.0083
PMH	jaw	14	Stn331	5.9	5.2	2.345 +/- 0.013	2.399 +/- 0.011	2.372 +/- 0.012	2.419 +/- 0.01
AL	jaw	16	Dlx1/2	6.1	4.3	2.267 +/- 0.014	2.26 +/- 0.015	2.299 +/- 0.012	2.312 +/- 0.015
DL	jaw	17	Stn325	7.2	7.5	1.729 +/- 0.014	1.743 +/- 0.011	1.771 +/- 0.012	1.802 +/- 0.012
PML	jaw	19	Stn194	7.6	5.4	2.358 +/- 0.012	2.398 +/- 0.013	2.338 +/- 0.012	2.417 +/- 0.014
PMH	jaw	20	Stn216	5.2	4.5	2.408 +/- 0.011	2.396 +/- 0.012	2.373 +/- 0.012	2.34 +/- 0.012
PMH	jaw	21	Stn422	13.4	12.3	2.322 +/- 0.011	2.386 +/- 0.011	2.406 +/- 0.012	2.424 +/- 0.011
SOA	skull	1	Stn272	17.7	10.5	313.6 +/- 13	278.2 +/- 9.5	250.9 +/- 11	215.9 +/- 11
SOL	skull	4	Stn253	4.9	5.6	1.272 +/- 0.012	1.304 +/- 0.013	1.297 +/- 0.012	1.354 +/- 0.012
SOA	skull	6	Stn279	8.4	4.7	242.8 +/- 12	290.1 +/- 13	239.8 +/- 9.9	293.2 +/- 11
FW	skull	7	Stn72	6.8	5.4	2.4 +/- 0.014	2.387 +/- 0.015	2.453 +/- 0.012	2.474 +/- 0.016
SOA	skull	8	Stn88	6.3	3.5	289.3 +/- 9.9	269.6 +/- 10	267.5 +/- 12	234.2 +/- 13
SOL	skull	12	Stn318	7.8	9.0	1.253 +/- 0.013	1.298 +/- 0.012	1.339 +/- 0.013	1.34 +/- 0.011
SOA	skull	13	Stn156	8.3	4.7	298.9 +/- 12	268.9 +/- 11	264.3 +/- 12	236.7 +/- 10
SOA	skull	14	Stn167	6.2	3.4	265.8 +/- 11	258.9 +/- 10	254.5 +/- 13	282.9 +/- 11
FW	skull	15	Stn230	7.0	5.6	2.465 +/- 0.015	2.408 +/- 0.014	2.436 +/- 0.015	2.41 +/- 0.012
FW	skull	18	Stn280	4.8	3.8	2.4 +/- 0.014	2.414 +/- 0.015	2.435 +/- 0.014	2.457 +/- 0.014
SOA	skull	20	Stn216	43.0	30.4	340.2 +/- 11	257.6 +/- 9.4	251.1 +/- 9.6	183.2 +/- 7.2
FW	skull	21	Stn223	6.2	4.9	2.457 +/- 0.014	2.4 +/- 0.014	2.457 +/- 0.016	2.4 +/- 0.013
OPL	opercle	1	Stn272	11.4	10.9	3.928 +/- 0.019	3.919 +/- 0.015	3.858 +/- 0.017	3.794 +/- 0.017
OPW	opercle	2	Stn297	7.3	7.5	3.879 +/- 0.02	3.869 +/- 0.018	3.829 +/- 0.017	3.772 +/- 0.017
OPL	opercle	7	Stn79	11.6	11.1	3.797 +/- 0.016	3.893 +/- 0.017	3.897 +/- 0.019	3.942 +/- 0.016

OPW	opercle	7	Stn81	5.3	5.4	3.81 +/- 0.018	3.842 +/- 0.019	3.79 +/- 0.017	3.888 +/- 0.018
OPL	opercle	12	Stn275	9.6	9.1	3.818 +/- 0.017	3.839 +/- 0.016	3.915 +/- 0.018	3.929 +/- 0.017
OPW	opercle	17	Stn231	6.8	7.0	3.8 +/- 0.018	3.808 +/- 0.016	3.84 +/- 0.021	3.887 +/- 0.018
OPN	opercle	18	Stn196	8.5	9.2	0.2704 +/- 0.008	0.2063 +/- 0.0073	0.2229 +/- 0.0063	0.2364 +/- 0.0067
PE	median fin	1	Stn248	4.5	5.5	3.023 +/- 0.062	2.943 +/- 0.05	2.911 +/- 0.07	2.615 +/- 0.064
DS2L	median fin	2	Stn21	7.0	3.9	3.982 +/- 0.05	3.892 +/- 0.046	4.001 +/- 0.045	3.841 +/- 0.035
DS1L	median fin	3	Stn33	6.1	3.8	3.182 +/- 0.054	3.122 +/- 0.047	3.182 +/- 0.039	3.013 +/- 0.052
DS2L	median fin	4	Eda	51.1	38.2	4.302 +/- 0.042	3.96 +/- 0.033	3.751 +/- 0.038	3.685 +/- 0.032
TAP	median fin	4	Stn420	9.7	11.0	10.79 +/- 0.059	10.47 +/- 0.061	10.51 +/- 0.063	10.2 +/- 0.064
DS2L	median fin	5	Stn326	4.8	2.6	3.959 +/- 0.049	3.886 +/- 0.043	3.96 +/- 0.038	3.869 +/- 0.045
DS1L	median fin	7	Stn76	7.1	4.5	3.195 +/- 0.046	3.143 +/- 0.051	3.125 +/- 0.045	3.015 +/- 0.052
DS1L	median fin	8	Stn92	6.3	4.0	3.226 +/- 0.052	3.164 +/- 0.05	3.077 +/- 0.038	3.034 +/- 0.048
DS2L	median fin	9	Stn102	12.2	7.0	4.067 +/- 0.047	3.89 +/- 0.046	3.922 +/- 0.038	3.8 +/- 0.038
SRA	median fin	10	Stn121	6.0	6.7	0.01785 +/- 0.0035	0.02191 +/- 0.0037	0.03213 +/- 0.0049	0.04105 +/- 0.0038
DS2L	median fin	11	Stn224	4.5	2.5	3.845 +/- 0.04	3.887 +/- 0.045	3.915 +/- 0.042	4.018 +/- 0.044
DS3L	median fin	13	Stn155	5.5	4.6	1.127 +/- 0.02	1.15 +/- 0.016	1.09 +/- 0.018	1.121 +/- 0.02
DS2L	median fin	16	Stn299	8.0	4.5	4.059 +/- 0.051	3.906 +/- 0.045	3.902 +/- 0.038	3.815 +/- 0.036
ASL	median fin	17	Stn286	5.7	5.5	1.158 +/- 0.018	1.251 +/- 0.019	1.237 +/- 0.022	1.262 +/- 0.017
DS1L	median fin	18	Stn196	7.5	4.8	3.247 +/- 0.049	3.085 +/- 0.047	3.134 +/- 0.042	3.028 +/- 0.05
SRA	median fin	20	Stn212	7.9	9.0	0.04322 +/- 0.004	0.03082 +/- 0.0036	0.02228 +/- 0.0041	0.01077 +/- 0.0037
DS3L	median fin	21	Stn421	7.9	6.7	1.175 +/- 0.019	1.13 +/- 0.018	1.131 +/- 0.02	1.054 +/- 0.016
LAP	vertebrae	1	Stn240	13.1	10.9	25.68 +/- 0.05	25.49 +/- 0.049	25.33 +/- 0.056	25.21 +/- 0.051
LAP	vertebrae	4	Stn419	10.4	8.5	25.61 +/- 0.055	25.48 +/- 0.053	25.46 +/- 0.057	25.21 +/- 0.044
CVN	vertebrae	5	Stn58	5.0	6.4	16.32 +/- 0.062	16.43 +/- 0.062	16.12 +/- 0.059	16.13 +/- 0.042
LAFR	vertebrae	8	Stn87	5.9	14.9	22.55 +/- 0.15	22.33 +/- 0.11	22 +/- 0.14	22.52 +/- 0.085
LAP	vertebrae	10	Stn120	5.5	4.4	25.4 +/- 0.056	25.38 +/- 0.055	25.34 +/- 0.055	25.58 +/- 0.049
LAFR	vertebrae	15	Stn170	4.3	10.5	22.61 +/- 0.12	22.26 +/- 0.11	22.57 +/- 0.12	22.11 +/- 0.12
LAP	vertebrae	20	Stn340	8.3	6.7	25.55 +/- 0.05	25.37 +/- 0.052	25.52 +/- 0.055	25.25 +/- 0.057
LAP	vertebrae	21	Stn223	14.6	12.3	25.62 +/- 0.048	25.33 +/- 0.055	25.53 +/- 0.056	25.24 +/- 0.05

Only the non-overlapping QTL with highest LOD score within each trait class are shown. Phenotypes are presented as phenotype of a fish of 40 mm SL, with residuals added to each genotypic class (M_1M_2 is homozygous marine, B_1B_2 homozygous benthic, and MB classes the heterozygotes). For traits that were only size corrected, the linear regression equation was used, for traits both size and sex corrected, the GLM equation was used.

Table S5 Regional or global QTL controlling serially homologous skeletal elements

Category of homologous skeletal elements	Number and description of anatomical domains	Regional QTL (controlling subset of domains)	Global QTL (controlling all domains)
Gill raker number	25 domains in 9 anterior/posterior and 4 dorsal/ventral regions	10	0
Pharyngeal tooth number	2 dorsal, 1 ventral toothplate	4	4
Branchial bone length	1 dorsal, 5 ventral bones	10	4
Jaw size	1 dorsal, 1 ventral bone	7	5
Spine length	3 dorsal, 1 anal spine	13	1
Total	--	44	14

For each set of likely serially homologous skeletal elements, QTL controlling these elements were classified as controlling only a subset of the domains (anatomically regional) or controlling all the domains (global). Most QTL are anatomically regional, and this trend holds broadly across different trait classes.

Table S6 Dominance of QTL by phenotypic class

Class	Under-dominant	Recessive	Partially recessive	Additive	Partially dominant	Dominant	Over-dominant
raker	0.09	0.15	0.26	0.17	0.15	0.04	0.13
teeth	0.08	0.05	0.20	0.35	0.30	0.00	0.02
branchial	0.03	0.16	0.09	0.41	0.25	0.03	0.03
jaw	0.03	0.10	0.27	0.17	0.33	0.07	0.03
skull	0.04	0.00	0.25	0.50	0.12	0.08	0.00
opercle	0.07	0.21	0.21	0.21	0.14	0.00	0.14
median fin	0.09	0.12	0.24	0.29	0.15	0.06	0.06
vertebrae	0.06	0.12	0.31	0.06	0.19	0.12	0.12
gain	0.07	0.16	0.17	0.29	0.23	0.05	0.04
loss	0.06	0.07	0.27	0.27	0.20	0.05	0.08
all	0.06	0.11	0.22	0.28	0.21	0.05	0.06

Dominance (*d/a*) ranges for different dominance classes follow cut-offs of (BURKE *et al.* 2002): < -1.25 for underdominant, -1.25 to -0.75 for recessive, -0.75 to -0.25 for partially recessive, -0.25 to 0.25 for additive, 0.25-0.75 for partially dominant, 0.75-1.25 for dominant and >1.25 for overdominant. For each dominance class, the proportion of filtered QTL that have dominance values within that range are listed. A tendency towards additive and partially additive QTL is seen broadly across trait classes. Constructive (gain) QTL and regressive (loss) QTL also show a trend towards additivity.

Table S7 Trait clustering *P* values

Chromosome	All QTL			Large effect QTL		
	Genetic	Physical	Gene number	Genetic	Physical	Gene number
1	0.59	0.39	0.33	0.16	0.09	0.07
2	0.78	0.58	0.36	0.90	0.83	0.75
3	0.99	0.99	1.00	1.00	1.00	1.00
4	0.22	0.50	0.37	**0.00**	**0.01**	**0.00**
5	0.97	0.64	0.80	1.00	1.00	1.00
6	0.98	1.00	0.99	1.00	1.00	1.00
7	0.41	0.37	0.36	0.27	0.27	0.27
8	0.90	0.41	0.38	0.94	0.77	0.76
9	1.00	0.99	0.99	0.81	0.78	0.80
10	0.76	0.56	0.62	0.76	0.70	0.73
11	0.97	0.85	0.95	1.00	1.00	1.00
12	0.57	0.38	0.49	0.80	0.75	0.81
13	0.81	0.93	0.93	1.00	1.00	1.00
14	0.80	0.53	0.55	1.00	1.00	1.00
15	0.08	0.83	0.83	1.00	1.00	1.00
16	0.51	0.68	0.60	1.00	1.00	1.00
17	0.78	0.49	0.50	1.00	1.00	1.00
18	0.75	0.59	0.56	0.75	0.71	0.70
20	0.09	0.43	0.42	**0.03**	0.14	0.14
21	**0.00**	**0.02**	**0.01**	**0.00**	**0.01**	**0.00**

P values for enrichment of QTL on each chromosome for all QTL or large effect QTL were calculated by comparing the actual number of QTL per chromosome to the distribution from 1000 simulated placements of QTL. Simulations were ran assuming QTL were randomly placed in proportion to the 1) the genetic length of the chromosome, 2) the physical length of the chromosome, or 3) the number of Ensembl-predicted genes on the chromosome. *P* values less than 0.05 are in bold. Relative to simulated QTL placed in proportion to the genetic length of each chromosome, large effect QTL (the top quartile of QTL by LOD) are significantly enriched on chromosomes 4, 20, and 21.

LITERATURE CITED

AHN, D. G., and G. GIBSON, 1999 Axial variation in the three-spine stickleback: genetic and environmental factors. Evol Dev **1:** 100-112.

ALBERT, A. Y., S. SAWAYA, T. H. VINES, A. K. KNECHT, C. T. MILLER *et al.*, 2008 The genetics of adaptive shape shift in stickleback: pleiotropy and effect size. Evolution **62:** 76-85.

ANKER, G. C., 1974 Morphology and kinetics of the head of the stickleback, *Gasterosteus aculeatus*. Trans. Zool. Soc. Lond. **32:** 311-416.

BROMAN, K. W., and S. SEN, 2009 *A guide to QTL mapping with R/qtl*. Springer, Dordrecht.

BURKE, J. M., S. TANG, S. J. KNAPP and L. H. RIESEBERG, 2002 Genetic analysis of sunflower domestication. Genetics **161:** 1257-1267.

COLOSIMO, P. F., K. E. HOSEMANN, S. BALABHADRA, G. VILLARREAL, JR., M. DICKSON *et al.*, 2005 Widespread parallel evolution in sticklebacks by repeated fixation of *Ectodysplasin* alleles. Science **307:** 1928-1933.

COLOSIMO, P. F., C. L. PEICHEL, K. NERENG, B. K. BLACKMAN, M. D. SHAPIRO *et al.*, 2004 The genetic architecture of parallel armor plate reduction in threespine sticklebacks. PLoS Biol **2:** e109.

GHANEM, N., O. JARINOVA, A. AMORES, Q. LONG, G. HATCH *et al.*, 2003 Regulatory roles of conserved intergenic domains in vertebrate *Dlx* bigene clusters. Genome Res **13:** 533-543.

JONES, F. C., M. G. GRABHERR, Y. F. CHAN, P. RUSSELL, E. MAUCELI *et al.*, 2012 The genomic basis of adaptive evolution in threespine sticklebacks. Nature **484:** 55-61.

KINGSLEY, D. M., B. L. ZHU, K. OSOEGAWA, P. J. DE JONG, J. SCHEIN *et al.*, 2004 New genomic tools for molecular studies of evolutionary change in threespine sticklebacks. Behaviour **141:** 1331-1344.

KNECHT, A. K., K. E. HOSEMANN and D. M. KINGSLEY, 2007a Constraints on utilization of the EDA-signaling pathway in threespine stickleback evolution. Evolution & Development **9:** 141-154.

KNECHT, A. K., K. E. HOSEMANN and D. M. KINGSLEY, 2007b Constraints on utilization of the EDA-signaling pathway in threespine stickleback evolution. Evol Dev **9:** 141-154.

MILLER, C. T., S. BELEZA, A. A. POLLEN, D. SCHLUTER, R. A. KITTLES *et al.*, 2007 *cis*-Regulatory changes in *Kit ligand* expression and parallel evolution of pigmentation in sticklebacks and humans. Cell **131:** 1179-1189.

PEICHEL, C. L., K. S. NERENG, K. A. OHGI, B. L. COLE, P. F. COLOSIMO *et al.*, 2001 The genetic architecture of divergence between threespine stickleback species. Nature **414:** 901-905.

SHAPIRO, M. D., M. E. MARKS, C. L. PEICHEL, B. K. BLACKMAN, K. S. NERENG *et al.*, 2004 Genetic and developmental basis of evolutionary pelvic reduction in threespine sticklebacks. Nature **428:** 717-723.

ZERUCHA, T., T. STUHMER, G. HATCH, B. K. PARK, Q. LONG *et al.*, 2000 A highly conserved enhancer in the *Dlx5/Dlx6* intergenic region is the site of cross-regulatory interactions between *Dlx* genes in the embryonic forebrain. J Neurosci **20:** 709-721.